Biomolecular nanolayers on synthetic organic films: their structure and properties for biosensor applications

KAMIL AWSIUK

Thesis for Ph.D. degree
under the supervision of
Prof. dr hab. Andrzej Budkowski

Department of Advanced Materials Engineering
Institute of Physics
Jagiellonian University

Kraków 2013

Overview

The study object of this Thesis are biomolecular (proteins, oligonucleotide) nanolayers formed on synthetic organic (silane) films that modify model silicon (SiO_2, Si_3N_4) surfaces identical to these used in biosensor transducers. The aim of this Thesis is micro- and spectro-scopic analysis of the structure and properties of biomolecular nanolayers relevant for biosensor applications. In particular, the issue of silicon-transducer functionalization with different sensing biomolecules (proteins, oligonucleotides) is extremely important to increase biosensor specificity, selectivity and sensitivity.

Biosensors become very popular and important research field concerning fabrication of devices to diagnose early onset of human diseases, paving the way for advances in personalized health care. Brief description of biosensors and different methods of biomolecules immobilization is presented in **Chapter 1**.

The process of biosensors surface preparation is mostly a multistep procedure exploiting different reagents and biomolecules. Variety of used materials influence not only biosensor specificity but can also decrease nonspecific interactions, responsible for false positive results. Therefore, exact surface analysis is important to understand biomolecular immobilization and subsequent biomolecular detection. To this end different scanning probe microscopic methods such as Atomic Force Microscopy (AFM), Near-field Scanning Optical Microscopy (NSOM) and spectroscopic methods - Time-of-Flight Secondary Ion Mass Spectrometry (ToF-SIMS), X-ray Photoelectron Spectroscopy (XPS) and Angle Resolved XPS (ARXPS) have been implemented to analyse a model biosensor surface. Detailed experimental background of this Thesis is specified in **Chapter 2**.

Initial step to prepare biosensor surface typically involves modification of silicon-based transducer to increase biomolecules immobilization. The most common method to obtain suitable interface between biomolecules and silicon surface is silanization. The results presented in **Chapter 3** compare surface modification with two different silanes, namely (3-Aminopropyl)triethoxysilane (APTES) and (3-Glycidoxypropyl)trimethoxysilane (GOPS). Different end groups of synthetic organic films formed by GOPS and APTES silane enhance chemisorption or physical adsorption, respectively, of biomolecules to the silanized silicone surface.

Silicon-based model biosensors surfaces with protein/amino-organosilane/silicon structure have been examined after each step of preparation: a) modification with APTES; b) functionalization with rabbit gamma globulins (IgG); c) blocking the free sites with bovine serum albumin (BSA) as well as after immunoreaction with antibody. Obtained microscopic (surface features) and spectroscopic (surface protein density) results as well as systematic analysis of multicomponent biosensor surfaces are described in **Chapter 4**.

Changes in both the size of surface features and amount of immobilized proteins observed after immunoreaction (presented in **Chapter 4**) motivated an extension of these studies to model immunoassay described in **Chapter 5**. The biosensors surface was functionalized with two different (rabbit or mouse) gamma globulins and after blocking procedure (with BSA) reacted with complementary ani-IgG at various concentrations ranged from 0.3 to 330 nM.

Finally, several micro(spectro)scopic methods have been applied to assist with the optimization of immobilization protocols used to attach indirectly oligonucleotide probes to biosensor surfaces with the

usage of biotin-streptavidin system. In particular, four different approaches to immobilize oligonucleotides on silicon surfaces (SiO_2 silanized with APTES) have been examined. Implemented experimental methods not only pointed to the most effective protocols to immobilize oligonucleotide probes but also allowed for an insight into multi-molecular overlayer composition. These studies are described in details in **Chapter 6**.

The results presented in this Thesis correspond to biomolecular nanolayers on synthetic organic films that have been used in universal bioanalytical lab-on-chip platform PYTHIA, fabricated within the FP7 project (2008-2012) “Monolithically integrated interferometric biochiPs for label-free earlY deTection of Human dIseAses”.

Contents

Results and discussion

Chapter 1

Introduction

1.1 Biosensors: principles and properties

Recently, the demand for fast and accurate measurements using small volumes of biochemical samples has been a driving force for construction of biosensor. Biosensor is a device which transforms biological or chemical information into a usable output signal. The basic concept of a biosensor, which combines biochemical components with a physical element, is similar for all constructions (Figure 1.1). Each construction consists of two major elements.

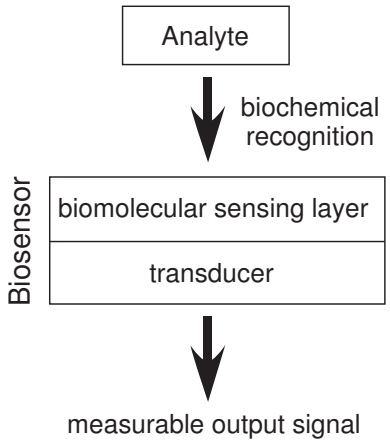

Figure 1.1: Schema presenting the basic concept of a biosensor.

The first element is a layer of biomolecules which recognizes and detects the presence or activity of target analyte in tested sample. As a recognition element proteins (for example enzyme or antibody), oligonucleotides or even living cells are used. Biomolecules in sensing layer define what kind of molecules will be detected. Therefore, biosensors are widely exploited in such areas as life sciences, medical diagnostics and food, environmental or drug screening. They also have been used for military applications for the detection of harmful and dangerous substances [1]. What is more, preparation of a biomolecular layer is the crucial step for selectivity and specificity of biosensor.

The second element is a transducer responsible for the conversion of biochemical recognition event into measurable output signal. Biochemical interaction in sensing layer influences transducer physical prop-

erties, for example refractive index, conductivity or mass. Therefore, depending on transducer properties an optical, electrical or mechanical output signal can be measured.

In some classes of biosensors molecules have to be labelled to enable their detection. To this end e.g. fluorescence or radioactive tags are attached to the target molecules. Unfortunately, during labelling procedure target molecule can be modified and its activity might be changed. Therefore, very important class of biosensors is label-free sensors. Label-free sensors not only detect unmodified molecules but also enable real-time detection.

Constant research in biosensor field focuses on the fabrication of small and portable devices capable of detecting "on-line" small amount of analyte in the sample. Moreover, further miniaturization leads to construction of fully integrated systems called lab-on-chip. Another important goal is that cheap and user-friendly devices could be applied in every diagnostic centre or even a privately owned praxis. Consequently, it will enable not only fast diagnosis but also a screening of patients to specify their genetic profiles. The most popular constructions of label-free biosensors utilizing different output signals are briefly described below.

Surface plasmon resonance biosensor

Surface plasmon resonance (SPR) is one of the most popular sensing methods applied in biosensors [1–3]. Typical SPR biosensor consists of a metal layer (typically gold) deposited on glass and placed into water. Metal surface immersed in water is functionalized with detecting molecules. The whole system is illuminated through the glass by a laser. The laser beam incident on metal/water interface is reflected and the light intensity is measured. At characteristic angle (resonant angle) intensity of reflected light drops remarkably, what is caused by generation of surface plasmons (electromagnetic waves which propagate along metal/dielectric interface) on the metal/water interface. The resonant angle is a function of the dielectric constant in the region near the interface. Binding events on sensing layers modify the dielectric constant and thereby resonant angle is shifted. By monitoring the intensity of light and changes of resonant angle quantitative information about presence and concentration of detected analyte can be obtained.

Interferometric biosensor

Interferometric biosensor is another example of an optical sensor. In many cases they are based on Mach-Zehender interferometer (MZI) [4, 5].

MZI biosensors consist of optical waveguide divided into two arms which, after a certain distance, merge and form one output optical waveguide. One of the arms is functionalized with sensing molecules (sensing arm) and exposed to the surrounding medium. The second one is a reference arm and is covered with a protective layer. Light beam injected to a waveguide splits into two arms and the interference between light coming from both arms is observed due to phase shift. Part of the light, which travels through the waveguide, extends to the medium and forms so called evanescent field. Biomolecular recognition on sensing arm modulates evanescent field what induces phase shift between light beams traveling in both sensing and reference arms. Measured interference signal enables detection and provides quantitative information about target analyte.

Cantilever biosensor

Cantilever biosensor is an example of a mechanical sensor [6, 7]. It consists of array of cantilevers which have only one side functionalized with recognition molecules. Due to the binding of detected molecules to the sensing surface intermolecular forces arise and induce surface stress. Mechanical stress in the surface leads to a contraction or expansion of the sensing surface. As a result cantilever bends and deflects because the stress acts only on the one side of the cantilever.

In addition, detection method based on changes of resonant frequency of cantilever (resonant-mode) can be applied [8]. Cantilever which can be treated as a harmonic oscillator is excited close to its resonance frequency. Resonant frequency of harmonic oscillator depends only on spring constant and effective mass. During binding target molecule mass and its distribution along the cantilever changes and as a result resonant frequency is shifted to lower values.

Bending or oscillation frequency changes of the cantilever can be measured using an optical beam deflection similar as in AFM technique (see 2.2.1) and yield information about presence of analyte in measured sample.

Field effect transistors biosensor

Biosensors based on field effect transistors (FET) are an example of electrochemical sensors [9, 10]. Especially organic thin film transistors (OTFT) are promising for application in chemical and biological sensing. OTFT consists of three metal electrodes (gate, drain and source), a thin film of organic semiconducting material and an insulator layer. Different geometries can be utilized in biosensor. In OTFT with bottom-gated geometry (an insulator layer separates gate from organic thin film) organic layer [11] or source and drain electrodes can be used as sensitive layer [12]. Changes observed in voltage-current characteristics of OTFT show effective detection of biomolecules.

1.2 Modification of silicone based biosensor transducer with organic films

Silicon-based materials like glass, silicon nitride or pure silicon have been widely exploited in fabrication of biosensors. Many different architectures including nanowire [9, 10], microcavity [13] or cantilevers [6] have been implemented in construction of different types of biosensor.

The interface between biomolecules and biosensor transducer is of critical importance in developing effective diagnostic tool. In many label-free biosensors sensing layer has to be in close vicinity of transducer surface, because small changes of physicochemical properties, due to biorecognition event, can be detected only within a few nanometers. In addition, the surface of biosensor transducer has to be biocompatible. Therefore, surface of silicon-based transducer is mostly modified with synthetic organic films to provide a suitable interface between transducer and immobilized biomolecules. Such films incorporate specific groups and change the physicochemical properties of surface to promote immobilization of biomolecules via physical adsorption, covalent bonding or specific binding (see Section 1.3). Moreover, intermediate organic layer acts as a spacer and reduces steric hindrance of detecting molecules. Consequently, modification with synthetic organic films also has a great impact on stability and functionality of biomolecular sensing layer as well as increase of signal to noise ratio.

Organo-silanes

Silanization is one of the most common ways to incorporate chemically well defined functional groups on surface of silicone-based substrates. Various protocols for silanization have been presented including deposition from: aqueous solution, organic solution or gas phase.

Organo-silanes can bind strongly to a silicone-based surface through siloxane bonds. The most popular reagents are trialkoxysilanes of general structure $(RO)_3Si(CH_2)_nX$ (where X is functional group). Alkoxy groups attached to Si are lost in the presence of water. Consequently, silanols condensate with each other, or with surface silanol groups forming siloxane bonds. As a result mechanically and chemically markedly stable overlayer is created in which functional groups are oriented away from the underlying silicone-based surface. An excess of water leads to undue polymerization, while insufficient amount of water results in incomplete monolayer formation [14, 15].

A large variety of suitable functional groups, through the choice of an organic functionality, can be introduced on the surface. The most popular organo-silanes incorporate: amino, epoxy, carboxy or thiol group.

Organo-silane layer is not only used to introduce chemical functional groups able to immobilize biomolecules [16]. It is also a suitable platform to introduce appropriate chemical linkers or dendrimers [17, 18] where the biomolecules can be attached. Consequently, silanization is the most widely adapted technique for modification of silicone-based transducer in biosensing applications.

Dendrimers

Dendrimers are monodispersed globular macromolecules with branched chemical structure constructed around a central core. A range of functional groups can be incorporated (e.g. aldehyde) to multiple branch ends to enable immobilization of biomolecules. Due to high functional group density they create on the surface large modified areas. Dendrimer layer can be prepared by Langmuir-Blodgett or spin-casting techniques, however, the most popular involve covalent attachment to the pre-silanized surface.

Dendrimers are mostly applied in DNA and protein microarrays [17–19]. Especially poly(amidoamine) (PAMAM) is the most popular dendrimer in biomedical application due to a number of surface amino functional groups.

1.3 Biomolecules immobilization: structure and properties

Biomolecules are molecules of biological origin including proteins, nucleic acids or polysaccharides. Many of these molecules possess special properties to carry out specific biological processes. In biosensor application ability to detection of complementary biomolecules via specific binding or hybridization is widely exploited.

Biomolecules after immobilization might change their conformation what consequently affects their properties and activity. Therefore, choice of the strategy adopted for biomolecules immobilization is extremely important in preparation step of biosensor surface.

Below there are presented and described different methods and approaches commonly used to immobilize proteins and nucleic acids on the surface.

1.3.1 Protein immobilization

Proteins are biomacromolecules responsible for biochemical reactions of catalysis (e.g. enzymes) and immune responses. They have also structural and mechanical functions as well as play an important role in cell signalling.

Proteins are biopolymers built of hundreds to hundreds of thousands repeating monomeric units. Twenty different monomeric units called amino acids are incorporated in proteins. Each amino acid consists of α carbon, carboxyl group, amino group, side group and hydrogen. Amino acids are covalently linked by the peptide bond formed by the condensation reaction between carboxyl and amino group. The side group different for each amino acids might be polar or nonpolar, electrostatically charged or not. Therefore, these side groups determine the shape and properties of the protein. The sequence of linked amino acids is the primary structure of protein and is defined by the genetic code.

The secondary structure of protein is formed when the protein folds up into a defined shape. The two major secondary structures are α helix and β sheet. α helix appears when a linear hydrogen bond is formed between every amide hydrogen and carbonyl oxygen four residues further along in the sequence. The result is a cylindrical structure where the wall of the cylinder is formed by the hydrogen-bonded polypeptide backbone, and side groups are pointing outwards. β sheets consist of a few beta strands (different segments of the amino acid sequence in polypeptide chain) arranged side by side and connected with hydrogen bonds between backbone groups. The beta strands can run parallel or antiparallel to one another forming pleated sheet where side groups alternately point upward and downward away from the sheet.

Polypeptide chain folds spontaneously into a more compact structure forming tertiary structure which determines biological functions of protein. Tertiary structure is stabilized by a large number of (mostly weak) interactions. The most important interactions involved in the stabilization are:

- charged interactions
- hydrogen bonding
- disulphide bonding
- van der Waals interaction
- hydrophobic interaction

Many proteins consist of more than one polypeptide chain (subunit) and are called oligomers. Depending on the number of subunits such complex are known as dimers, trimers, tetramers and so on. The structure of associated subunits is stabilized by the same weak interactions as tertiary structure and quaternary structure of proteins is formed.

Proteins are very complex molecules. Therefore, many different strategies, utilizing chemical and physical properties of proteins, have been applied to immobilize them into the solid surface. All these strategies can be classified into three categories (Figure 1.2): physical adsorption, covalent bonding and specific binding.

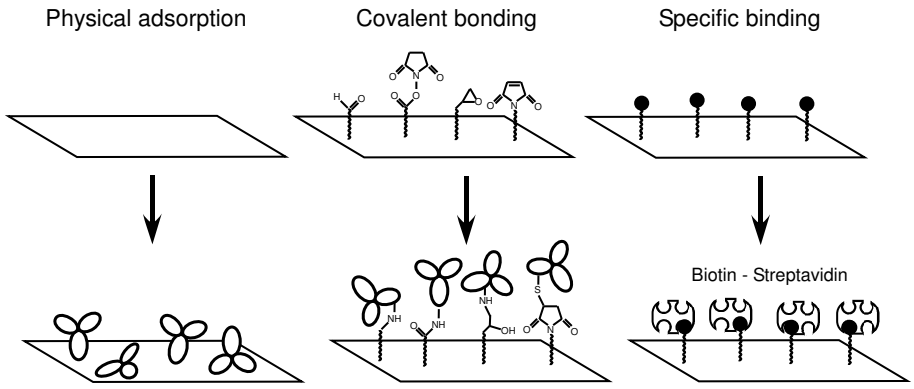

Figure 1.2: Three categories of protein immobilization.

1.3.1.1 Physical adsorption

Protein molecules can adsorb on almost all kinds of interfaces. Therefore, protein adsorption phenomenon has been discussed by many authors [20–22]. Most of them point to complexity of this process and describe many different mechanisms and forces acting between protein and surface, including hydrophobic, electrostatic and van der Waals forces, responsible for protein adsorption. In addition, temperature, the ionic strength and pH of the buffer as well as properties of the surface and protein - protein interaction are also important parameters. Regardless this, protein adsorption phenomenon can take place only if the Gibbs energy of the system decreases. For spontaneous adsorption at constant pressure p and temperature T the change of the Gibbs energy ΔG is described with:

$$\Delta G = \Delta H - T\Delta S < 0 \tag{1.1}$$

where ΔH and ΔS refer to change of the enthalpy and the entropy of the system, respectively [23].

Another very important aspect is orientation of molecules adsorbed onto the surface. Proteins are typically asymmetric molecules and only in exceptional cases they exhibit a spherical shape. Therefore, due to the different shapes they could adsorb with different orientation. The model example can be Immunoglobulin G (IgG) which is Y-shaped molecule. Alternatively, globular IgG molecule is commonly presented as ellipsoid (see 2.1.2.1). Figure 1.3 presents different possible orientations of IgG on the surface. Cause IgG possesses two binding sites on their "arms"(F_{ab} regions) the orientation of adsorbed molecule has a great impact on its activity.

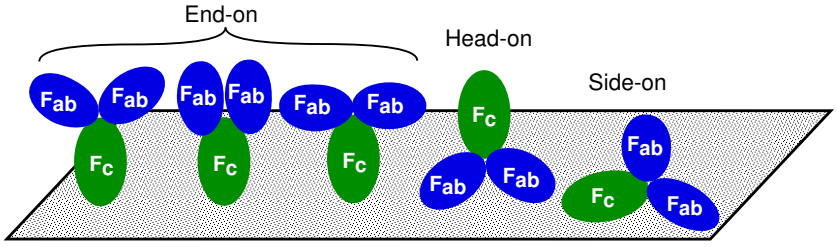

Figure 1.3: Different orientations of adsorbed IgG molecules [24].

Additionally, proteins can undergo conformational changes and unfold due to different forces acting during the adsorption process. Taking into account the three dimensional structure stability the pro-

teins can be divided into two groups “soft” and “hard” [25]. So-called “hard” proteins such as lysozyme, β-lactoglobulin or α-chymotrypsin upon adsorption maintain their structure as they have in the dissolved state. On the other hand, “soft” proteins such as bovine serum albumin (BSA), immunoglobulin G (IgG), fibrinogen or α-lactoglobulin have low structural stability and upon adsorption can spread on the surface.

There are presented and described below a few major parameters that influence protein adsorption.

pH

pH is one of the major parameters which determines electrostatic state of proteins. If pH of buffer is close to the isoelectric point (pI) of a protein the negative and positive charges cancel out and the net charge is almost zero. For higher pH condition (pH>pI) proteins are negatively charged whereas for pH<pI molecules are positively charged. Therefore, pH condition has an impact on electrostatic interaction between surface and protein molecule. This causes an increase or a decrease in Gibbs energy depending on whether it is a repulsive or an attractive interaction, respectively.

Despite the fact that by changing pH attractive electrostatic interaction between proteins and surface can appear, the maximum of adsorption is generally observed near the pI. Matsumoto et al. and Bremer et al. show that the pH curves for BSA and IgG adsorption have a bell-shape with the maximum close to the pI [26, 27]. Such a behavior suggests that electrostatic interaction driven by pH condition cannot be the main force responsible for protein adsorption.

Ionic strength

Not only pH but also ionic strength of the solution influences electrostatic protein-surface interaction. The range and the strength of electrostatic potential can be modified by the ions dissolved in the buffer. The counter-ions form diffusive double layer close to the charged molecule or surface immersed in an electrolyte solution. Such a layer damps electric potential what means that the higher ionic strength the shorter electrostatic interaction between charged entities is.

Jones et al. present for BSA adsorbed to negatively charged membrane that higher ionic strength results in less adsorption at the pI and at pH below it but greater adsorption at pH above pI [28]. Similar results were obtained by Bremer et al. for IgG adsorbed to positively and negatively charged substrates. Lower salt concentration decreases or increases relative initial adsorption rate when protein molecules and surface were like-charged or opposite charged, respectively [27]. In addition, protein-protein repulsive electrostatic interaction affects the inner structure of adsorbed protein layer. For pH$\neq$pI protein assemble into a loosely packed layer whereas if pH=pI molecules tend to form a more densely packed layer [29]. This suggests that overall adsorption depends on the combination of both protein-protein and protein-surface electrostatic interactions. Increased ionic strength reduces electrostatic repulsion between like charged molecules and like charged protein and surface but also decreases attractive interaction between opposite charged protein molecule and surface.

Surface properties

Surface properties such as hydrophobicity and roughness have a great impact on protein adsorption. Generally proteins prefer to adsorb onto hydrophobic surfaces rather than hydrophilic ones [30, 31]. Due to

the entropic increase, which is caused by the release of water dipoles from hydrophobic surface to the bulk solution during protein adsorption, the adhesion of proteins is enhanced on the hydrophobic surfaces [32]. In addition, the steady-state adsorption of proteins on hydrophilic surface is strongly dependent on the protein concentration [27,33]. In turn to hydrophobic ones for which this dependence is absent [33]. Protein concentration influences the initial adsorption rate. For high initial rate the filling time is short, consequently, molecules have little time to undergo conformation changes and spread. Consequently, molecules have no time to take larger area per molecule (molecular footprint). This results in higher adsorption saturation as more molecules can occupy the same surface area. Such differences in the steady-state adsorption as a function of protein concentration reveal that protein molecules undergo any conformation changes faster and spread on hydrophobic surfaces rather than on hydrophilic ones [31, 33].

Moreover, Norde et al. claim that "soft" proteins tend to adsorb onto various surfaces in contrast to "hard" proteins which can adsorb onto hydrophilic surfaces only when electrostatic attraction between protein molecules and surface exists (Table 1.1) [25]. Still, adsorption of negatively charged β-lactoglobulin to hydrophilic negatively charged silicone surface is reported by Marsh et al. [31]. Such an exception might point to the existence of additional protein-surface interaction and complexity of protein adsorption phenomenon.

Table 1.1: Scheme predicting occurrence of protein adsorption, dependent on charge (+/-) and other protein and surface properties [25].

			surface			
			hydrophobic		hydrophilic	
			+	-	+	-
Protein	hard	+	yes	yes	no	yes
		-	yes	yes	yes	no
	soft	+	yes	yes	yes	yes
		-	yes	yes	yes	yes

Hydrophobicity of the surface also impacts on the secondary structure of protein. Sethurman et al. report that for a hydrophobic surface the amount of α helixes decreases and they are partly transited to β sheet. Moreover, for a hydrophilic surface secondary structural content was close to that in free solution [34].

Denis et al. indicate that not only hydrophobicity has an impact on protein adsorption but also surface roughness. Result obtained for collagen adsorbed to the surfaces with different properties confirmed that larger amounts are adsorbed to the hydrophobic surfaces compared to the hydrophilic ones. What is more, atomic force microscopic measurements reveal that morphology of protein layer depends on both hydrophobicity and roughness. On smooth surfaces collagen forms elongated supramolecular assemblages with small or high (attributed to collagen aggregates) surface features on hydrophilic or hydrophobic surface, respectively. Such structures are not observed on rough substrata [35].

1.3.1.2 Covalent bonding

Covalent bonds are mostly formed between the groups of amino acids side chains and suitable complementary groups from the surface. There are many different functional groups which might be introduced to the surface (with methods described in Section 1.2) to enable immobilization of proteins. The most popular compatible chemical groups are presented in Table 1.2 and described below.

Table 1.2: Commonly applied functional groups for covalent protein immobilization [36, 37].

Surface functional groups	Protein side groups	amino acids
aldehyde	-NH_2	Lys
NHS ester	-NH_2	Lys
epoxy	-NH_2, -SH or -OH	Lys, Cys, Ser, Thr
maleimide	-SH	Cys

Aldehyde

One of the most common strategy to immobilize proteins to the surface employs an aldehyde group (Figure 1.4a). Aldehyde group forms imine bonds with amine group of lysine (common to almost every protein) - so called Schiff base. Immobilization via a Schiff base is reversible, however, carbon-nitrogen double bond can be reduced by using some reagents (for example sodium cyanoborohydride) to stable secondary amine linkage.

Aldehyde group is mostly incorporated by glutaraldehyde reagent to the previously aminated surface [38, 39]. However, glutaraldehyde in aqueous solution might possess different structures what influences reactivity. Betanacor et al. studied mechanism of enzyme immobilization to the support activated with dimer or monomer glutaraldehyde form [38]. Presented results suggest that dimer yields fast protein immobilization, whereas monomer activation leads to low immobilization rate. In addition, in a low ionic strength immobilization proceed via first ionic exchange with amino group of the support, followed by the covalent attachment. If high ionic strength is used enzyme is directly immobilized by covalent bonding but the process is slower.

NHS ester

N-Hydroxysuccinimide (NHS) ester (Figure 1.4b) readily reacts with amine group of lysine forming stable amide bonds. Unfortunately, NHS ester is unstable in aqueous conditions and ester hydrolysis competes with protein attachments.

Parker et al. proposed using a dry organic solvent to avoid ester hydrolysis. Organic solvents can dissolve significant amounts of protein and results for catalase dissolved in 2,2,2-trifluoroethanol demonstrate effective protein immobilization to the gold surface modified with NHS ester [40, 41].

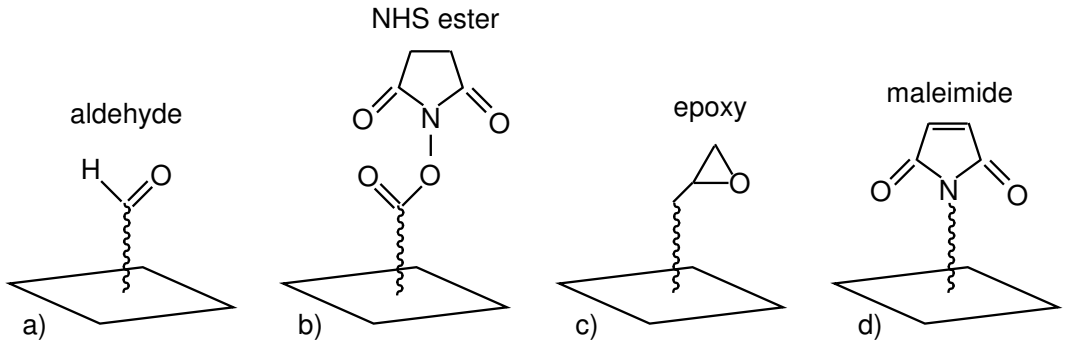

Figure 1.4: Chemical structure of functional groups: a) aldehyde; b) NHS ester; c) epoxy; d) maleimide; used for covalent protein immobilization [36, 37].

Yet, according to Wagner et al. hydrolysis of the NHS ester presented on the surface is very slow at pH 7.5 and 8.5 [42]. Additionally, hydrolysis was not complete even after 37.5h, whereas, NHS derivatives in solution at pH 8.0 have a half-life of 1 h. This suggests that monolayer arrangement decreases the reactivity and application of NHS ester in aqueous conditions is possible. Notwithstanding, optimization of parameters like pH, concentration or ionic strength is necessary.

Epoxy

Immobilization of protein to epoxy (Figure 1.4c) modified substrate takes place through a two step mechanism. Firstly, protein adsorption is promoted and secondly, covalent reaction between amino acid side groups (amino, thiol or hydroxyl) and epoxy group occurs.

Epoxy groups are very stable in neutral pH and under aqueous reaction conditions. However, to promote physical adsorption the use of high ionic strength is recommended [43]. Unfortunately, such a condition can be too harsh for some kinds of proteins for example enzymes. Therefore, many attempts focus on developing other methods to increase protein adsorption, mostly based on incorporation of additional chemical groups.

Mateo et al. proposed preparation of different multifunctional epoxy supports by modifying a 10-20% of the epoxy groups with additional groups which promote physical adsorption of proteins [43]. To modify epoxy groups Aminated, Iminodiacetic Acid, Copper-Iminodiacetic Acid and Boronate Supports were implemented. Presented results reveal that initial immobilization could be carried out at low ionic strength conditions and into hydrophilic supports. Additional, results for immobilized enzymes show that for some supports enzymes preserved 75-100% of their activity (corresponding to the soluble enzymes used for immobilization).

Mateo et al. also examined the amino-epoxy support consisting of epoxy groups over a layer of ethylenediamine that is covalently bound to the support [44]. Such an approach does not reduce epoxy groups at the surface and the ratio of amino to epoxy groups (promoted physical adsorption) is 1:1. Incorporation of the layer of amino groups improves protein immobilization rates as well as enables immobilization of enzyme at low ionic strength and provides better stability of the enzymes.

Maleimide

Maleimide group (Figure 1.4d) can react with the thiol side chain in cysteine and as a result forms stable thioether bond. The reaction is rapid and specific at a physiological pH (6.5-7.5). However, protein possesses very few cysteine residues on the surface. Therefore, site-selective immobilization is possible by modification of protein molecules.

Ferrero et al. modified protein in such a way that only one cysteine residue was exposed on the surface [45]. Presented results for wild type and mutant cytochrome P450 from Bacillus megaterium reveal that highly exposed unique cysteine residue is capable to form covalent linkage to the different spacers with maleimide group.

Other method has been presented by Ichihara et al. who suggest incorporating oligocysteine tag [46]. Due to the problem with purification of enhanced green fluorescent protein (EGFP) with an N-terminal tag consisting of five tandem cysteine repeats an additional histidine tag has to be incorporated. The best results, taking into account production, purification, and immobilization, were obtained for recombinant EGFP with an N-terminal His-tag and a C-terminal Cys-tag.

1.3.1.3 Specific binding

Proteins possess on their surface binding sites which can interact with ligand or binding sites presented on the surface of a complementary protein. Protein-protein or protein-ligand specific binding is one of the methods which offers oriented immobilization of proteins. The specific binding occurs by non-covalent intermolecular forces, such as van der Waals forces and ionic or hydrogen bonds.

However, to utilize specific binding for protein immobilization its ligand or complementary protein has to be previously deposited on the surface. To this end many different approaches have been applied using physical adsorption and covalent bonding.

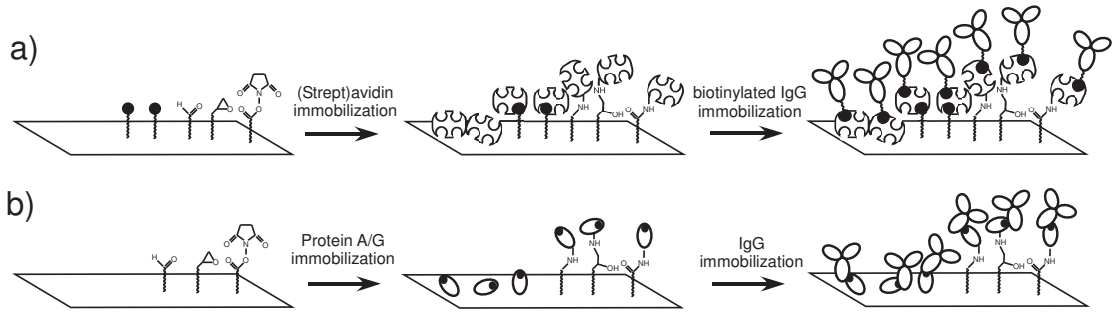

Figure 1.5: Protein immobilization via specific binding using a) biotin-(strept)avidin and b) Protein A/G-IgG system.

(Strept)avidin-biotin system

(Strept)avidin-biotin is a model system of ligand-receptor interactions due to high specificity and affinity. It is also one of the strongest non-covalent bonding with dissociation constant $K_d = 4\times10^{-14}$ M and $K_d = 0.6\times10^{-15}$ M for streptavidin (see Section 2.1.2.3) and avidin, respectively.

Biotin, also called vitamin H or B7, consists of tetrahydroimidizalone ring fused with a tetrahydrothiophene ring to which valeric acid is attached. Only the bicyclic ring is important in specific binding with one of the four binding sites presented on the surface of streptavidin or avidin. The valeric acid chain can be modified to generate biotinylated reagents [47]. Such reagents can be used to introduce biotin as a functional group to dendrimers [48], thiols [49] or pre-silanized surfaces [50, 51].

Moreover, biotin can be also conjugated with proteins [49,52], their fragments [49] or other biomolecules (e.g. estrone) [50]. Since biotin molecules are small (244.3 Da) biotinylation does not affect protein conformation and properties.

Protein immobilization with (strept)avidin-biotin system consist of a few steps during which biomolecular multilayer is formed. Firstly, (strept)avidin is immobilized to the surface via covalent bonding, physical adsorption or specific binding with biotin reagents incorporated to the surface. Finally, biotinylated protein is immobilized to the surface due to (strept)avidin-biotin interaction (Figure 1.5 a) [49, 52].

Interesting results have been presented by Muller et al. who used thiol with desthiobiotin instead of biotin as functional group [49]. Desthiobiotin is biotin analog that has lower binding constant with streptavidin. Therefore, biomolecular multilayer formed on the surface can be washed away by using biotin solution. As a result, procedure of streptavidin and biotynylated protein docking can be repeated several times on the same desthiobiotin modified surface.

Protein A/Protein G - Immunoglobulin G system

Protein A and Protein G are recombinant cell wall components of Staphylococcus aureus and Streptococcal bacteria, respectively. Both of them bind specifically to the F_c region of IgG antibody and as a result binding sites placed on F_{ab} regions are exposed. Many different approaches including: protein thiolation [53], covalent bonding [3, 39, 54] or adsorption (pseudochemisorbtion) [55] have been applied to immobilize Protein A/G to the surface (Figure 1.5 b). Regardless of the approaches, orientation of protein A/G is important to enable specific binding of IgG [53, 55].

Results obtained by Bae et al. as well as Oh et al. show that protein G layer increases formation of antibody-antigen complex compared to direct immobilized IgG to thiolated gold surface [3, 53]. Protein G base layer controls orientation of IgG (with Fab regions exposed to the analyte), whereas, IgG is immobilized with various configurations (end-on, side-on, head-on) to thiolated surface [53].

Moreover, comparative study of different methods to immobilize antibodies against Japanese encephalitis virus (JEV) to silicone surfaces tested by Huy et al. indicates that the method using protein A is the most effective. Compared with other approaches it yields threefold improvement in the detection of JEV antigens [39].

1.3.2 Nucleic acid immobilization

The term nucleic acid is a common name for ribonucleic acid (RNA) and deoxyribonucleic acid (DNA). RNA and DNA are biopolymers consisting of a sequence of units called nucleotides. Each nucleotide is built with a nucleobase (also called base), a pentose sugar and a phosphate group. RNA and DNA consist of the different pentose sugar: ribose and 2'-deoxyribose, respectively. Phosphate groups and

five-carbon sugars are connected through phosphodiester bond and form a backbone of nucleic acids. Five carbon atoms of sugar are counted and phosphate group are attached to the 3' and 5' carbons. As a result in nucleotides string characteristic direction from 3'- to 5'-end can be distinguished. To the 1' carbon of sugar ring nucleobase (heterocylic amine) is attached. There are two different types of nucleobase: purines and pyrimidines. Two purines; adenine and guanine are common for DNA and RNA. On the other hand, two pyrimidines: cytosine and thymine occur in DNA, while in the RNA case thymine is replaced by uracil. The sequence of bases forms primary structure of nucleic acids and stores genetic code or information how to duplicate themselves and guide the synthesis of proteins.

The nucleobase can form complementary base-pairs stabilized by hydrogen bonds which are specified by the structure of the heterocylic amines. Guanine can form three hydrogen bonds with cytosine, whereas adenine can form two hydrogen bonds with thymine (DNA) or uracil (RNA).

RNA is usually single-stranded, but it might form hairpin structures by base pairing of self-complementary regions. Such a structure might be also observed in single-stranded DNA. However, the most popular secondary structure of DNA is double helix. Double-helical three-dimensional structure is made of two complementary right-handed strands in an anti-parallel direction that are coiled about the same axis. Consequently, complementary base-pairs from the two opposite DNA strands are stacked in the interior of the helix.

A short single-strand DNA or RNA is called oligonucleotide. The sequence of oligonucleotides can be specified. Therefore, they are often synthesised in laboratory to match a region where a mutation is known to occur. Consequently, oligonucleotide probes are widely applied in microarrays and biosensors to detect genetic diseases as well as viruses or bacteria.

Mostly all strategies of nucleic acids immobilization to the surface are based on two methods: specific binding or covalent bonding. Both of these methods are based mostly on modification of 5'-end of the RNA, single-strand DNA or oligonucleotide with appropriate chemical group or molecule.

1.3.2.1 Thiol- or amine- terminated nucleic acids

Thiolation (-SH) is one of the most popular method to attach nucleic acids covalently to the surface. -SH group strongly reacts with gold surface and stable brush-like layer is formed. However, to obtain maximum hybridization efficiency the control of surface coverage of nucleic acids is extremely important. To this end Herne et al. proposed to use mixed monolayers of thiolated oligonucleotide and spacer [56]. The described two steps method, where attaching of oligonucleotides from micromolar solution is followed by immersion in spacer milimolar solution, brings two benefits. Firstly, nonspecifically immobilized DNA are mostly removed from the surface. Secondly, surface coverage is controlled and oligonucleotide probes are accessible for specific hybridization.

Moreover, thiol- or amine- (-NH_2) terminated nucleic acids might be immobilized to silicone-based surface but firstly surface modification with organo-silane is required. Organo-silane layer allows to attach terminated oligonucleotides directly [57] or via incorporation of specific linker [58, 59]. Charles et al. show that -SH and -NH_2 terminated oligonucleotides present comparable attachment to silanized surface with an additional cross linker incorporated [58]. However, DNA hybridization was significantly more efficient for

amino- terminated oligonucleotides and decrease of hybridization at higher densities for thiol- terminated probes was observed.

1.3.2.2 Biotinylated nucleic acids

The most popular method to immobilize nucleic acids via specific binding exploits (strept)avidin-biotin system (see Section 1.3.1.3). Biotin is a small molecule which can be attached to the 5'-end of nucleic acid, without interfering with their physiochemical and biological properties. Finally, streptavidin or avidin pre-immmobilized to the surface are used as an anchoring layer. Exploiting biotin-streptavidin system seems to be more complicated than thiolation of nucleic acids, due to the additional step of streptavidin immobilization. However, numerous experiments show many advantages of using the biotin-streptavidin system.

One of the advantages is that streptavidin acts as a bridge between the solid surface and the oligonucleotide probes. Such bridge reduces steric hindrance and keeps the oligonucleotides more accessible for reaction during hybridization as compared to directly immobilized probes. Moreover, Su et al. report that well ordered streptavidin layer formed on biotinylated surface provides a suitable platform for biotin conjugated DNA assembly [60]. Streptavidin layer mediates DNA probe orientation and as a result has an impact on hybridization efficiency. Therefore, ordered streptavidin layer increases hybridization efficiency compared to the dissipative streptavidin film formed through amine coupling.

Another advantage of biotin-streptavidin system was reported by Mir et al. [61]. They compared non-specific binding of nanoparticles to thiolated oligonucleotide (DNA) strands covalently attached to gold and biotinylated oligonucleotide (DNA) assembled on the streptavidin platform after target hybridization. Results of experiments have shown that streptavidin underlayer minimizes the non-specific binding of negatively charged quantum dots as well as streptavidin molecules due to the significant polar hydrophilic repulsion.

Bibliography

[1] Kawaguchi, T., Shankaran, D. R., Kim, S. J., Gobi, K. V., Matsumoto, K., Toko, K., and Miura, N. *Talanta* **72**(2), 554–560 (2007).

[2] Bora, M., Celebi, K., Zuniga, J., Watson, C., Milaninia, K. M., and Baldo, M. A. *Optics Express* **17**(1), 329–336 (2009).

[3] Oh, B.-K., Kim, Y.-K., Park, K. W., Lee, W. H., and Choi, J.-W. *Biosensors and Bioelectronics* **19**(11), 1497–1504 (2004).

[4] Hong, J., Choi, J. S., G.Han, Kang, J. K., Kim, C. M., Kim, T. S., and Yoon, D. *Analytica Chimica Acta* **573-574**, 97–103 (2006).

[5] Prieto, F., Sepúlveda, B., Calle, A., Llobera, A., Domínguez, C., Abad, A., and Lechuga, A. M. L. M. *Nanotechnology* **14**(8), 907–912 (2003).

[6] Fritz, J., Baller, M. K., Lang, H. P., Rothuizen, H., Vettiger, P., Meyer, E., Güntherodt, H. J., Gerber, C., and Gimzewski, J. K. *Science* **288**(5464), 316–318 (2000).

[7] Calleja, M., Nordström, M., Álvarez, M., Tamayo, J., Lechuga, L. M., and Boisen, A. *Ultramicroscopy* **105**(1-4), 215–222 (2005).

[8] Burg, T. P., Godin, M., Knudsen, S. M., Shen, W., Carlson, G., Foster, J. S., Babcock, K., and Manalis, S. R. *Nature* **446**(7139), 1066–1069 (2007).

[9] Gao, A., Lu, N., Wang, Y., Dai, P., Li, T., Gao, X., Wang, Y., and Fan, C. *Nano Letters* **12**(10), 5262–5268 (2012).

[10] Zheng, G., Patolsky, F., Cui, Y., Wang, W., and Lieber, C. *Nature Biotechnology* **23**(10), 1294–1301 (2005).

[11] Zhang, Q. and Subramanian, V. *Biosensors and Bioelectronics* **22**(12), 3182–3187 (2007).

[12] Yan, F., Mok, S. M., Yu, J., Chan, H. L. W., and Yang, M. *Biosensors and Bioelectronics* **24**(5), 1241–1245 (2009).

[13] Armani, A. M., Kulkarni, R. P., Fraser, S. E., Flagan, R. C., and Vahala, K. *Science* **317**(5839), 783–787 (2007).

[14] Wong, A. K. Y. and Krull, U. J. *Analytical and Bioanalytical Chemistry* **383**(2), 187–200 (2005).

[15] Howarter, J. A. and Youngblood, J. P. *Langmuir* **22**(26), 11142–11147 (2006).

[16] Psarouli, A., Bourkoula, A., Petrou, P., Misiakos, K., Chaniotakis, N., and Kakabakos, S. *Procedia Engineering* **25**, 350–353 (2011).

[17] Benters, R., Niemeyer, C. M., Drutschmann, D., Blohm, D., and Wöhrle, D. *Nucleic acids research* **30**(2), E10 (2002).

[18] Le Berre, V., Trévisiol, E., Dagkessamanskaia, A., Sokol, S., , Caminade, A.-M., Majoral, J. P., Meunier, B., and François, J. *Nucleic acids research* **31**(16), E88 (2003).

[19] Ajikumar, P. K., Ng, J. K., Tang, Y. C., Lee, J. Y., Stephanopoulos, G., and Too, H.-P. *Langmuir* **23**(10), 5670–5677 (2007).

[20] Rabe, M., Verdes, D., and Seeger, S. *Advances in Colloid and Interface Science* **162**(1-2), 87–106 (2011).

[21] Vogler, E. *Biomaterials* **33**(5), 1201–1237 (2012).

[22] Tsapikouni, T. and Missirlis, Y. *Materials Science and Engineering B* **152**(1-3), 2–7 (2008).

[23] Norde, W. *Journal of Dispersion Science and Technology* **13**(4), 363–377 (1992).

[24] Buijs, J., Lichtenbelt, J. W. T., Norde, W., and Lyklema, J. *Colloids and Surfaces B: Biointerfaces* **5**(1-2), 11–23 (1995).

[25] Norde, W. and Lyklema, J. *Advances in Colloid and Interface Science* **179-182**, 5–13 (2012).

[26] Matsumoto, H., Koyama, Y., and Tanioka, A. *Journal of Colloid and Interface Science* **264**(1), 82–88 (2003).

[27] Bremer, M., Duval, J., Norde, W., and Lyklema, J. *Colloids and Surfaces A* **250**(1-3), 29–42 (2004).

[28] Jones, K. and O'Melia, C. *Journal of Membrane Science* **165**(1), 31–46 (2000).

[29] Demaneche, S., Chapel, J.-P., Monrozier, L., and Quiquampoix, H. *Colloids and Surfaces B* **70**(2), 226–231 (2009).

[30] Malmsten, M. *Colloids and Surfaces B* **3**(5), 297–308 (1995).

[31] Marsh, R., Jones, R., and Sferrazza, M. *Colloids and Surfaces B* **23**(1), 31–42 (2002).

[32] Sethuraman, A., Han, M., Kane, R. S., and Belfort, G. *Langmuir* **20**(18), 7779–7788 (2004).

[33] van der Veen, M., Stuart, M., and Norde, W. *Colloids and Surfaces B* **54**(2), 136–142 (2007).

[34] Sethuraman, A., Vedantham, G., Imoto, T., Przybycien, T., and Belfort, G. *Proteins: Structure, Function and Genetics* **56**(4), 669–678 (2004).

[35] Denis, F., Hanarp, P., Sutherland, D., Gold, J., Mustin, C., Rouxhet, P., and Dufrene, Y. *Langmuir* **18**(3), 819–828 (2002).

[36] Rusmini, F., Zhong, Z., and Feijen, J. *Biomacromolecules* **8**(6), 1775–1789 (2007).

[37] Wong, L. S., Khan, F., and Micklefield, J. *Chemical Reviews* **109**(9), 4025–4053 (2009).

[38] Betancor, L., López-Gallego, F., Hidalgo, A., Alonso-Morales, N., Mateo, G. D.-O. C., Fernández-Lafuente, R., and Guisán, J. M. *Enzyme and Microbial Technology* **39**(4), 877–882 (2006).

[39] Huy, T. Q., Hanh, N. T. H., Van Chung, P., Anh, D. D., Nga, P. T., and Tuan, M. A. *Applied Surface Science* **257**(16), 7090–7095 (2011).

[40] Parker, M.-C., Patel, N., Davies, M. C., Roberts, C. J., Tendler, S. J. B., and Williams, P. M. *Protein Science* **5**(11), 2329–2332 (1996).

[41] Parker, M.-C., Davies, M. C., and Tendler, S. J. B. *Journal of Physical Chemistry* **99**(43), 16155–16161 (1995).

[42] Wagner, P., Hegner, M., Kernen, P., Zaugg, F., and Semenza, G. *Biophysical Journal* **70**(5), 2052–2066 (1996).

[43] Mateo, C., Fernández-Lorente, G., Abian, O., Fernández-Lafuente, R., and Guisán, J. M. *Biomacromolecules* **1**(4), 739–745 (2000).

[44] Mateo, C., Torres, R., Fernández-Lorente, G., Ortiz, C., Fuentes, M., Hidalgo, A., López-Gallego, F., Abian, O., Palomo, J. M., Betancor, L., Pessela, B. C. C., Guisan, J. M., and Fernández-Lafuente, R. *Biomacromolecules* **4**(3), 772–777 (2003).

[45] Ferrero, V. E. V., Andolfi, L., Di Nardo, G., Sadeghi, S. J., Fantuzzi, A., Cannistraro, S., and Gilardi, G. *Analytical Chemistry* **88**(22), 8438–8446 (2008).

[46] Ichihara, T., Akada, J. K., Kamei, S., Ohshiro, S., Sato, D., Fujimoto, M., Kuramitsu, Y., and Nakamura, K. *Journal of Proteome Research* **5**(9), 2144–2151 (2006).

[47] Smith, C. L., Milea, J. S., and Nguyen, G. H. *Immobilization of nucleic acids using biotin-strept(avidin) systems*, volume 261 of *Topics in Current Chemistry*. (2006).

[48] Kim, Y. P., Hong, M. Y., Shon, H. K., Chegal, W., Cho, H. M., Moon, D. W., Kim, H. S., and Lee, T. G. *Applied Surface Science* **255**(4), 1110–1112 (2008).

[49] Müller, W., Ringsdorf, H., Rump, E., Wildburg, G., Zhang, X., Angermaier, L., Knoll, W., Liley, M., and Spinke, J. *Science* **262**(5140), 1706–1708 (1993).

[50] Birkert, O., Haake, H.-M., Schütz, A., Mack, J., Brecht, A., Jung, G., and Gauglitz, G. *Analytical Biochemistry* **282**(2), 200–208 (2000).

[51] Choi, H. J., Kim, N. H., Chung, B. H., and Seong, G. H. *Analytical Biochemistry* **347**(1), 60–66 (2005).

[52] Kakabakos, S. E. and Khosravi, M. J. *Clinical Chemistry* **38**(5), 725–730 (1992).

[53] Bae, Y. M., Oh, B. K., Lee, W., Lee, W. H., and Choi, J. W. *Biosensors and Bioelectronics* **21**(1), 103–110 (2005).

[54] Zengin, A. and Caykara, T. *Applied Surface Science* **257**(6), 2111–2117 (2011).

[55] Johnson, B. N. and Mutharasan, R. *Biosensors and Bioelectronics* **28**(17), 6928–6934 (2012).

[56] Herne, T. and Tarlov, M. *Journal of the American Chemical Society* **119**(38), 8916–8920 (1997).

[57] Lenigk, R., Carles, M., Ip, N. Y., and Sucher, N. J. *Langmuir* **17**(8), 2497–2501 (2001).

[58] Charles, P. T., Vora, G. J., Andreadis, J. D., Fortney, A. J., Meador, C. E., Dulcey, C. S., and Stenger, D. A. *Langmuir* **19**(5), 1586–1591 (2003).

[59] Shircliff, R. A., Martin, I. T., Pankow, J. W., Fennell, J., Stradins, P., Ghirardi, M. L., Cowley, S. W., and Branz, H. M. *ACS Applied Materials and Interfaces* **3**(9), 3285–3292 (2011).

[60] Su, X., Wu, Y. ., Robelek, R., and Knoll, W. *Langmuir* **21**(1), 348–353 (2005).

[61] Mir, M., Cameron, P. J., Zhong, X., Azzaroni, O., Álvarez, M., and Knoll, W. *Talanta* **78**(3), 1102–1106 (2009).

Chapter 2

Experimental

2.1 Materials

2.1.1 Organo-silanes

Silicon oxide (SiO_2) or silicon nitride (Si_3N_4) were used to prepare model biosensor surface. Silicon surfaces were modified with two different silanes to form a biocompatible synthetic organic layer (see section 1.2). (3-Aminopropyl)triethoxysilane (APTES) and (3-Glycidoxypropyl)trimethoxysilane (GOPS) were used to prepare a suitable interface for protein immobilization via physical adsorption or covalent bonding, respectively.

2.1.1.1 (3-Aminopropyl)triethoxysilane (APTES)

(3-Aminopropyl)triethoxysilane (APTES) is one of the most frequently used organo-silane reagents for the preparation of amino-terminated films on silicon substrates. The structure of APTES molecule is shown in Figure 2.1a. Surface amine (NH_2) groups on APTES thin film promote physical adsorption increasing affinity between silicon surface and biomolecules. Alternatively, covalent bonding of biomolecules is possible after incorporation of an appropriate biofunctional linker [1, 2].

The thickness of APTES overlayer deposited from aqueous solution ranges from 0.8 to 1.3 nm [3].

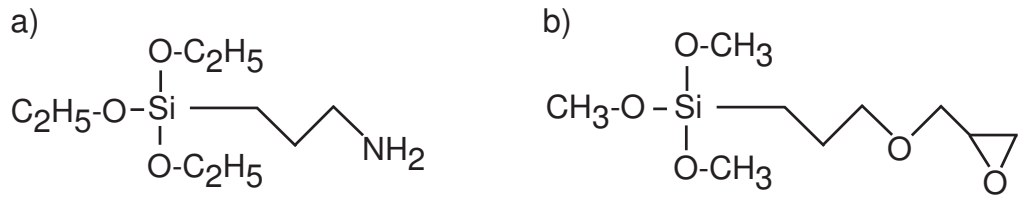

Figure 2.1: Chemical structures of a) APTES and b) GOPS molecules.

2.1.1.2 (3-Glycidoxypropyl)trimethoxysilane (GOPS)

The use of (3-Glycidoxypropyl)trimethoxysilane (GOPS) in surface coatings is intended to enable covalent bonding of biomolecules to silicone-based surfaces. The epoxide ring is reactive toward nucleophiles such as amines, thiols or acids and can be used for subsequent coupling of biomolecules (see Section 1.3.1.2). The structure of GOPS molecule is shown in Figure 2.1b. Literature values of monolayer thickness range from 0.75 to 1.1 nm for GOPS deposited from toluene solutions [4].

2.1.2 Proteins

2.1.2.1 Immunoglobulin G

Immunoglobulin G (IgG) belongs to antigen family which plays a crucial role in the immune system and is responsible for recognition and binding of antigens.

IgG is composed of four peptide chains - two heavy and two light chains. Polypeptide chains are grouped into three regions: one F_c and two F_{ab} which are connected by flexible hinge region. Heavy chains are present in both F_c and F_{ab} regions, whereas light chains are only located in F_{ab} regions. The folding of the chains results in Y shaped molecule whose "arms" are formed by F_{ab} regions and contain biological active antigen binding sites. Molecular weight of IgG molecule is about 156kDa [5] and its nominal dimensions are 14.5 nm $\times$ 8.5 nm $\times$ 4 nm [6]. The pI range for polyclonal rabbit IgG is 6.0-8.0 [5].

2.1.2.2 Bovine Serum Albumin

Bovine Serum Albumin (BSA) is a serum albumin originated from domestic cows. It is a relatively large globular protein with molecular mass 66.3 kDa and dimensions 4 nm $\times$ 4 nm $\times$ 14 nm [7]. Reported isoelectric point of BSA is about 4.6-4.7 [8].

BSA is one of the most commonly used blocking reagent to reduce non-specific interaction (e.g. in biosensors or enzyme-linked immunosorbent assay test (ELISA)) [7].

2.1.2.3 Streptavidin

Streptavidin is homo-tetrameric protein purified from Streptomyces avidinii. It is an ellipsoidal molecule with dimensions 4.5 nm $\times$ 4.5 nm $\times$ 5 nm and molecular weight about 60 kDa [5]. The pI for streptavidin is about 5.0 [9].

Streptavidin is commonly used in immunochemical and diagnostic assays as well as biosensors thanks to the strong non-covalent interaction with biotin (see Section 1.3.1.3). The molecule possesses four biotin binding sites - one for each subunit.

2.2 Experimental techniques

2.2.1 Atomic Force Microscopy

Atomic Force Microscopy is one of the Scanning Probe Microscopy (SPM) techniques which utilize a sharp scanning tip (apex radius at the order of nanometers) to examine surface topography and its local

properties. The idea of AFM is based on interaction between atoms of a scanning tip and a surface. The real interaction has very complex character, however it can be described theoretically by Lenard-Jones potential. The force acting between tip and surface atoms is repulsive in a short tip-surface distance, whereas in a large distance it changes into attractive one (Figure 2.2).

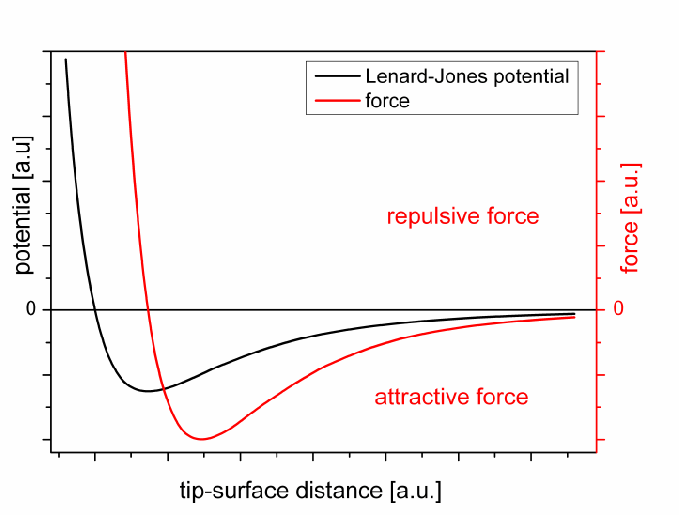

Figure 2.2: Qualitative form of Lennard-Jones potential (left scale, black curve) and force between tip and surface atoms (right scale, red curve).

AFM might work in two different modes depending on a way how the scanning tip interacts with the surface. In contact mode (Figure 2.3b) the tip constantly touches the surface and repulsive force is responsible for interaction. On the other hand, in non-contact mode (Figure 2.3c) the tip oscillates close to the surface and interacts through attractive forces. Intermediate contact mode is a special type of non-contact mode. In this mode the tip oscillates close to the surface but for a short time touches the surface.

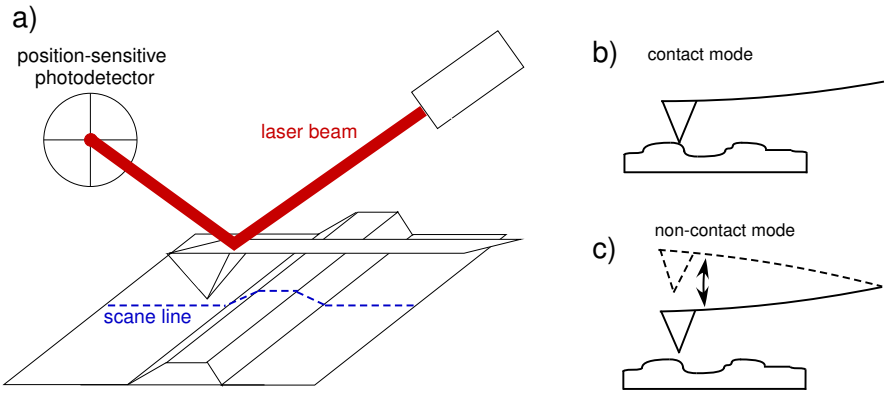

Figure 2.3: Schematic description of (a) AFM measurements with the laser beam deflection system and AFM (b) contact and (c) non-contact modes. The cantilever bending due to the forces acting between tip and surface atoms results in beam deflection which is analysed by position-sensitive photodetector.

The most popular way to detect interaction between the tip and the surface is based on laser beam deflection (Figure 2.3a). Scanning tip is mounted on flexible cantilever the back side of which is illuminated

with a focused laser beam. Reflected laser light falls on the centre of position-sensitive quadrant photodiode. In contact mode cantilever might bend (topography measurements) or twist (lateral force microscopy (LFM)) due to the interaction with the surface. Each cantilever deflection causes dislocations of laser beam from the centre of photodetector. In non-contact mode surface topography or other properties might change the amplitude or phase of tip oscillations measured by photodetector. Electronic feedback system changes the distance between the tip and the sample to maintain deflection (in contact mode), amplitude or phase (in non-contact mode). The changes in the distance reveal the surface topography. Finally, piezoelectric scanner moves the sample or the tip and information from the feedback system is collected point by point, consequently, topographic, phase or friction (LFM) AFM micrographs are created. Phase or friction (LFM) maps provide information about local mechanical properties.

In this thesis all scans were collected in the intermediate contact mode, since protein immobilized to the surface are very soft, sticky and susceptible.

2.2.1.1 Methods of AFM data analysis

The 2 dimensional Fourier transform [10, 11] and autocorrelation function [12] are useful tools to examine more quantitatively surface features observed on topographic maps obtained from AFM measurements (Figure 2.4).

2.2.1.1.1 2-dimensional Fourier transform

Fast Fourier transform (FFT) (one of the algorithms to compute Fourier transform) of AFM micrographs presenting random set of surface features yields an isotropic diffusive ring on (k_x, k_y) plane. Next, radial average of the squared FFT amplitude is used to calculate power spectrum P(k). The reversal of the wave vector ($1/k_{max}$) at the maximum of the spectrum P(k) provides a measure of the distance between the features observed in AFM micrographs.

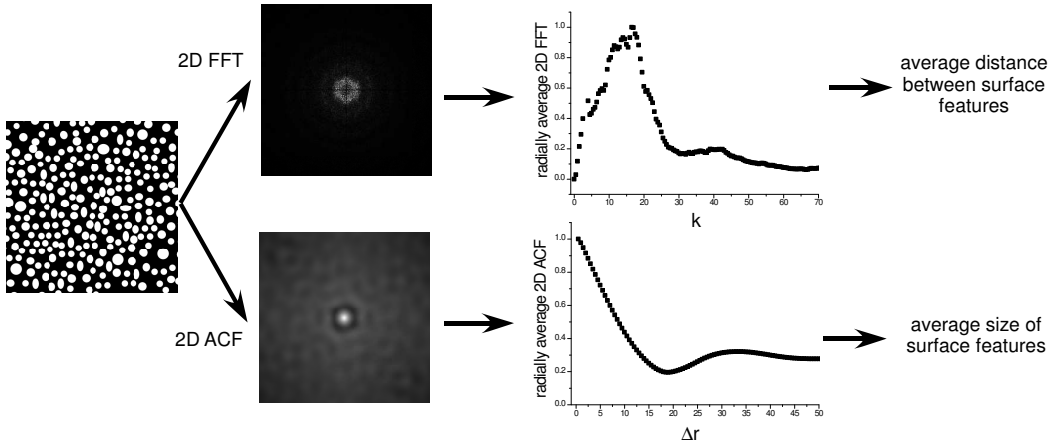

Figure 2.4: Schematic representation of 2D-FFT and 2D-ACF analysis of AFM micograph.

2.2.1.1.2 2-dimensional autocorrelation function

2-dimensional autocorrelation function (ACF) takes the image and the same image shifted by distance Δx and Δy in the X and Y axis with respect to the centre of the image and computes correlation between them. As a result, 2D ACF image (defined on (Δx, Δy) plane) is created with central part containing information about surface features. The doubled value of width-at-half-maximum (2whm) of radially averaged 2D ACF is taken as an average size of surface features observed on AFM topographic micrographs.

2.2.2 Near-field Scanning Optical Microscopy

The near field scanning optical microscopy (NSOM) is a SPM technique recording simultaneously two types of signals, providing information about topography and optical properties of examined surface.

NSOM technique utilises a near-field (evanescent electro-magnetic field) which allows detect structures with sizes below the half of light wavelength, that are not detectable in a far-field where the Abbe criterion is preserved [13]. Evanescent (electro-magnetic) field appears at the end of a tapered optical fibre (with an aperture in the range of 50-100 nm) illuminated by laser light. It forms a scanning tip placed in a close proximity (a few nanometres) to a sample, where near-field interacting with surface it transforms into normal light wave and can be collected in far-field as a transmitted, reflected or fluorescence light, depending on the NSOM configuration (Figure 2.5). The tip-surface distance is controlled in a similar way as in AFM with conventional optical system based on laser beam deflection (see Section 2.2.1) or it involves the usage of a tuning fork (see Figure 2.5) [14].

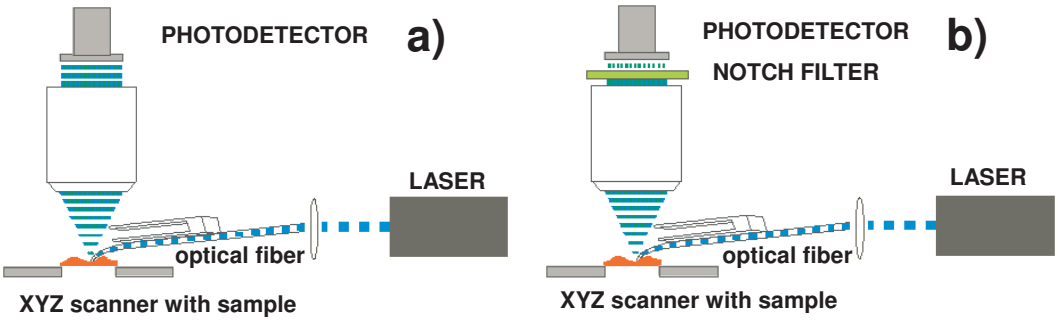

Figure 2.5: NSOM (reflection mode) microscopy set up. The optical fiber tip scans across the sample surface at constant nanometer tip-surface distance (controlled by tuning fork), while the surface is illuminated by a sub-wavelength aperture. The light intensity of the whole reflection spectrum (a) or the filtered fluorescence spectrum (b) is recorded as a function of tip position simultaneously with topographic data.

Thanks to its spatial resolution, better than in traditional optical microscopy, NSOM is a powerful tool to examine biological samples [15–17].

2.2.3 X-ray Photoelectron Spectroscopy and Angle Resolved XPS

2.2.3.1 Principles of X-ray Photoelectron Spectroscopy

The principles of X-ray Photoelectron Spectroscopy (XPS) method are described with equation (2.1). A surface illuminated with hard X-rays of energy $h\nu$ emits electrons (so called photoelectrons) with kinetic

energy (E_k) equal to:

$$E_k = h\nu - E_B - \phi \tag{2.1}$$

where E_B is electron binding energy and ϕ is the work function. Electrons can be ejected from tightly bound core levels or weakly bound valence level. Because photoelectrons strongly interact with the atoms of the substrate only some fraction of them emerges from surface with original E_k. Attenuation length λ is a characteristic distance for escaping electrons which takes into consideration both elastic and inelastic scattering of electrons. Sampling depth (d_{sd}) defines maximal thickness of analysed surface layer for take-off angle $\Theta = 0^\circ$ (with respect to the surface normal). Commonly, the sampling depth is described with equation (2.2). This gives about 8.7 nm for 95% detection of C1s line, excited by Al Kα radiation [18].

$$d_{sd} = 3\lambda \cos\Theta \tag{2.2}$$

If the monochromatic X-ray is used, binding energy can be calculated from the measured kinetic energy. Energy scale is charge referenced to the neutral (C-C) carbon C1s peak at 284.6 eV. Binding energy is unique to each element and sensitive to its chemical state (binding energy shift is so called chemical shift). Consequently, elements composition and their chemical state can be identified.

Typically magnesium (Mg) or aluminium (Al) anodes with their characteristic lines Mg Kα (1253.6 eV) and Al Kα (1486.6 eV) are used as X-ray source. Energy distribution of ejected photoelectrons is measured with analyser (typically concentrating hemispherical analyser) and their intensities by detectors. As a result the photoelectrons intensities are plotted as a function of kinetic energy.

Intensities of photoelectrons (I_i) are described with equation (2.3):

$$I_i = const\ \sigma_i \int_0^\infty Z_i(z) exp\left(\frac{-z}{\lambda_i \cos\Theta}\right) dz = K\ \sigma_i\ \lambda_i\ Z_i\ |_{for\ Z_i(z)=Z_i\ and\ \Theta=0^\circ} \tag{2.3}$$

where $const$ is the instrumental constant, σ_i photoionisation cross-section and Z_i - stoichiometric molar fraction of the element emitting photoelectrons. Analysis of photoelectron intensities allows to determine concentration of elements present in the surface (see Section 2.2.3.3.1).

2.2.3.2 Principles of Angle Resolved XPS

Angle-Resolved XPS is a useful method which allows to collect information from different depths of examined layer. Thickness of evaluated layer is modified by changing the take-off angle Θ (equation (2.2)). The maximal sampling depth ($\Theta = 0^\circ$) can be reduced to one-half ($\Theta = 60^\circ$) and even to around one-third for ($\Theta = 70^\circ$) (Figure 2.6). Therefore, ARXPS can be used as a non-destructive method (without sputtering) to determine chemical composition as a function of depth. In addition, ARXPS measurements enable layer thickness estimation by tracking signals characteristic for substrate and thin ($< d_{sd}$) overlayer (see Section 2.2.3.3.2) [19, 20].

2.2.3.3 Methods of XPS and ARXPS data analysis

2.2.3.3.1 Determination of atomic concentration

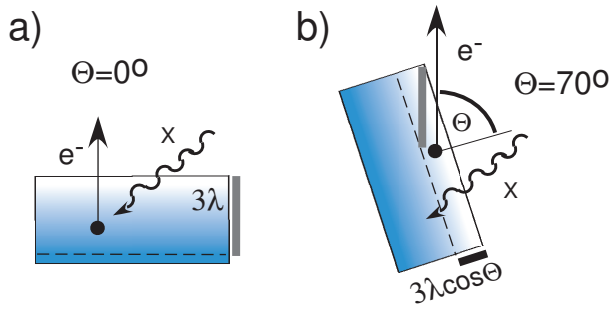

Figure 2.6: Effect of take-off angle Θ on sampling depth. At low take-off angle ($\Theta = 0°$) (a) more electrons are collected from atoms situated deeper in the sample, whereas, at higher take-off angle (b) only atoms near the surface are examined.

The intensities of the ejected photoelectrons are proportional to the concentrations of elements present in the surface. Consequently, XPS technique gives possibility to determine atomic concentrations C_i of every element (ignoring H atoms). For this purpose the following equation (2.4) is used [18, 19]:

$$C_i = \frac{X_i}{\sum_n X_n} \tag{2.4}$$

where n includes all elements presented in the sample and X_i are normalized photoelectron intensities. X_i for element i is defined as a ratio of photoelectron intensity to sensitivity factor S_i, specified by photoionization cross-section σ_i and attenuation length λ_i (see equation (2.5)).

$$X_i = \frac{I_i}{S_i} = \frac{I_i}{\sigma_i \lambda_i} \tag{2.5}$$

2.2.3.3.2 Determination of organic layers thickness and biomolecules surface coverage

Mono- and bilayer models to estimate thicknesses of thin organic layers deposited on semi-infinite substrate were presented in my MSc Thesis [19]. They were applied to describe non-homogeneous protein layers immobilized on silicon substrates coated with organo-silane films. The whole system is characterized by three parameters: thickness D of the bottom organic film, thickness d of the biomolecular (e.g. protein) top layer and surface fractional coverage F with proteins (Figure 2.7) .

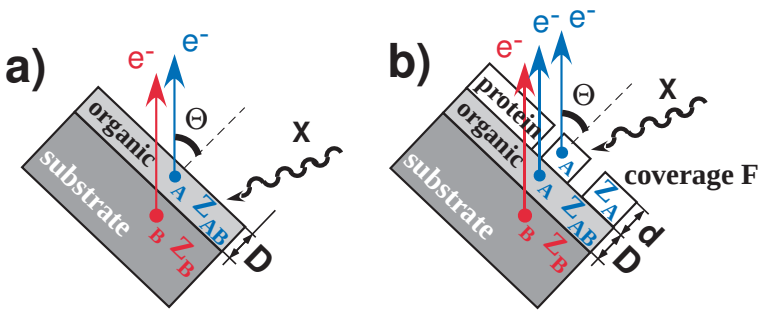

Figure 2.7: Mono- (a) and bilayer (b) model introduced to analyse angle-resolved XPS data. Characteristic photoelectrons are emitted by the element B, characteristic for the substrate (with molar fraction Z_B), and the element A, unique for both the organic film (with molar fraction Z_{AB} and thickness D) and biomolecular (e.g protein) layer (with molar fraction Z_A and thickness d).

Thickness estimation is based on the ratio of normalized intensities (equation (2.5)) of photoelectrons characteristic for the substrate (B) and bilayer (A) at different take-off angles. Taking into account equations (2.3) and (2.5) normalized photoelectron intensities can be written as:

$$X_B(\Theta) = \frac{const}{\lambda_B}(1-F)\int_D^{\infty} Z_B\, exp\left(\frac{-z}{\lambda_B \cos\Theta}\right) dz + \frac{const}{\lambda_B} F \int_{D+d}^{\infty} Z_B\, exp\left(\frac{-z}{\lambda_B \cos\Theta}\right) dz \tag{2.6}$$

$$X_A(\Theta) = \frac{const}{\lambda_A}(1-F)\int_0^{D} Z_{AB}\, exp\left(\frac{-z}{\lambda_A \cos\Theta}\right) dz + \frac{const}{\lambda_A} F \int_0^{d} Z_A\, exp\left(\frac{-z}{\lambda_A \cos\Theta}\right) dz + \frac{const}{\lambda_A} F \int_d^{D+d} Z_{AB}\, exp\left(\frac{-z}{\lambda_A \cos\Theta}\right) dz \tag{2.7}$$

where additional parameters are the stoichiometric molar fractions of the element B (here Si), characteristic for the substrate (Z_B), and the element A , unique for both the bottom organic film (Z_{AB}) and biomolecular layer (Z_A). Procedure to estimate stoichiometric molar fractions is described in Section 2.2.3.3.1. In the model where organic bilayer is deposited on silicon-based surface, C1s and N1s are the characteristic signals for organic layers.

Taking the ratio of the normalized intensities (equations (2.7) and (2.6)) from bilayer and substrate results in:

$$\frac{X_A(\Theta)/Z_A}{X_B(\Theta)/Z_B} = \frac{F\left[1-exp\left(\frac{-d\sec\theta}{\lambda_A}\right)\right] + \left(\frac{Z_{AB}}{Z_A}\right)\left[1-exp\left(\frac{-D\sec\theta}{\lambda_A}\right)\right]\left[1-F+Fexp\left(\frac{-d\sec\theta}{\lambda_A}\right)\right]}{exp\left(\frac{-D\sec\theta}{\lambda_B}\right)\left[1-F+Fexp\left(\frac{-d\sec\theta}{\lambda_B}\right)\right]} \tag{2.8}$$

Surface coverage F can be determined independently from the AFM or NSOM measurements [19]. If biomolecular layer is homogeneous (F=1) equation (2.8) reduces to the simplest form:

$$\frac{X_A(\Theta)/Z_A}{X_B(\Theta)/Z_B} = \frac{\left[1-exp\left(\frac{-d\sec\theta}{\lambda_A}\right)\right] + \left(\frac{Z_{AB}}{Z_A}\right)\left[1-exp\left(\frac{-D\sec\theta}{\lambda_A}\right)\right]\left[exp\left(\frac{-d\sec\theta}{\lambda_A}\right)\right]}{exp\left(\frac{-D\sec\theta}{\lambda_B}\right) exp\left(\frac{-d\sec\theta}{\lambda_B}\right)} \tag{2.9}$$

In monolayer model F= 0 and equation (2.8) can be rewritten to the form:

$$\frac{X_A(\Theta)/Z_{AB}}{X_B(\Theta)/Z_B} = \frac{1-exp\left(\frac{-D\sec\theta}{\lambda_A}\right)}{exp\left(\frac{-D\sec\theta}{\lambda_B}\right)} \tag{2.10}$$

where only D is the fitting parameter. To reduce the number of fitting parameters in the bilayer model the thickness D of bottom organic layer is estimated from the monolayer model applied to separate ARXPS measurements of silicone-based surface modified with organic monolayer.

Parameter d is the XPS thickness of equivalent biomolecular layer with uniformly distributed mass that justifies effective attenuation of electrons. In reality, the mass is localized in molecules distributed over the surface. Therefore better description is obtained with biomolecular surface coverage, which can be obtained by multiplying d with the biomolecular partial specific volume.

2.2.4 Time-of-Flight Secondary Ion Mass Spectrometry

Time of flight secondary ion mass spectrometry (ToF-SIMS) is one of the most popular methods implemented for detailed chemical surface analysis. This is due to its sensitivity, specificity and high mass resolution as well as lateral and depth resolutions. The main idea of ToF-SIMS measurement is to analyse with time of flight mass spectrometer the secondary ions (positively or negatively charged) identified by mass to charge ratio (m/z). These ions are emitted when the surface is bombarded by energetic (keV) primary ions (for example Bi^+, Bi_3^+, Ga^+, C_{60}^+). Depending on the sputtering conditions, two operating regimes in SIMS can be distinguished: dynamic (d-SIMS) and static (s-SIMS) SIMS. In d-SIMS higher ion dose is deposited on the analysed surface, causing surface sputtering, and therefore d-SIMS is used for depth profiling or 3D imaging. In s-SIMS the primary ion dose density must be kept low to prevent each point of the surface area from being hit more than once. This is fulfilled for the primary ion dose density below 10^{13} ions/cm^{-2} [21]. Within available time scale less than 1% of the top surface is damaged [21, 22]. Such working conditions allow to get information on the original composition and chemistry of radiation-sensitive molecular surfaces from the outermost 1-2 nm layer. This makes static SIMS an excellent method to analyse biomolecules on solid interfaces.

2.2.4.1 Methods of ToF-SIMS data analysis

2.2.4.1.1 Single Peak Analysis

Secondary ions (positively or negatively charged), identified by mass to charge ratio (m/z), reflect chemical composition of examined surface. The ToF-SIMS spectra are dominated by lower m/z peaks and present fragments of biomolecules rather than whole molecules. The characteristic signals are chosen based on SIMS studies of amino acid homopolymers [23, 24] and nucleobases, nucleosides and nucleotides [25]. Appearance of these signals in secondary ions spectrum gives evidence of proteins and DNA or RNA presence on the surface. However, composition of biomolecules is remarkably similar and single peak analysis is, therefore, complicated and sometimes cannot allow to distinguish between different biomolecules e. g. two proteins. In addition, single peak analysis might be affected by surface contamination or matrix effect.

2.2.4.1.2 Principal Component Analysis

Principal Component Analysis (PCA) is one of the multivariate analysis techniques which is especially attractive for the analysis of ToF-SIMS spectra of immobilized biomolecules. PCA reduces a large set of highly correlated peak intensities in ToF-SIMS spectra into scores of a smaller number of new variables called Principal Components (PCs). PCs are uncorrelated and are linear combinations of all of the original variables. Therefore they capture more information than any one of the original variables.

PCA analysis allows to differentiate the ToF-SIMS spectra of different biomolecules immobilized to the substrate. Wagner et al. presented that spectra from 13 different proteins immobilized to different substrates could be readily distinguished using PCA [26].

Additionally, it was also observed that the scores on PC are directly related to the amount of immobilized proteins [27, 28]. This observation allows to obtain not only qualitative (detection of molecular

presence on the surface) but also quantitative (protein surface density) results from ToF-SIMS measurements. Moreover, PCA provides more accurate quantitative results than single peak analysis [29].

2.2.4.1.3 Principal Component Regression

Although PCA yields quantitative information about surface properties (e.g. surface protein density), the scores on PC are given in arbitrary units. However, the scores on PC can be given in absolute units, enabling wider comparison with independent measurements. To this end Principal Component Regression (PCR) method is implemented to obtain correlation between the scores on PC and biomolecular surface density determined in absolute units from other techniques.

Kim et al. present that the scores on PC1 correlate very well with streptavidin surface density determined by SPR or ellipsometric measurements [28–30].

Bibliography

[1] Psarouli, A., Bourkoula, A., Petrou, P., Misiakos, K., Chaniotakis, N., and Kakabakos, S. *Procedia Engineering* **25**, 350–353 (2011).

[2] Huy, T. Q., Hanh, N. T. H., Van Chung, P., Anh, D. D., Nga, P. T., and Tuan, M. A. *Applied Surface Science* **257**(16), 7090–7095 (2011).

[3] Kim, J., Seidler, P., Wan, L. S., and Fill, C. *Journal of Colloid and Interface Science* **329**(1), 114–119 (2009).

[4] Luzinov, I., Julthongpiput, D., Liebmann-Vinson, A., Cregger, T., Foster, M. D., and Tsukruk, V. V. *Langmuir* **16**(2), 504–516 (2000).

[5] Kaur, K. and Forrest, J. A. *Langmuir* **28**(5), 2736–2744 (2012).

[6] Lee, K.-B., Park, S.-J., Mirkin, C. A., Smith, J. C., and Mrksich, M. *Science* **295**(5560), 1702–1705 (2002).

[7] Jeyachandran, Y. L., Mielczarski, J., Mielczarski, E., and Rai, B. *Journal of Colloid and Interface Science* **341**(1), 136–142 (2010).

[8] Tang, Q., Xu, C. H., Shi, S. Q., and Zhou, L. M. *Synthetic Metals* **147**(1-3), 247–252 (2004).

[9] Smith, C. L., Milea, J. S., and Nguyen, G. H. *Immobilization of nucleic acids using biotin-strept(avidin) systems*, volume 261 of *Topics in Current Chemistry*. (2006).

[10] Zemła, J., Rysz, J., Budkowski, A., and Awsiuk, K. *Soft Matter* **8**(20), 5550–5560 (2012).

[11] Cyganik, P., Bernasik, A., Budkowski, A., Bergues, B., Kowalski, K., Rysz, J., Lekki, J., Lekka, M., and Postawa, Z. *Vacuum* **63**(1-2), 307–313 (2001).

[12] Fekete, L., Kůsová, K., Petrák, V., and Kratochvílová, I. *Journal of Nanoparticle Research* **14**(8) (2012).

[13] Betzig, E., Trautman, J. K., Harris, T., Weiner, J., and Kostelak, R. *Science* **251**(5000), 1468–1470 (1991).

[14] Otero, J., Banos, R., González, L., Torrents, E., Juárez, A., and Puig-Vidal, M. *Colloids and Surfaces B: Biointerfaces* **102**, 117–123 (2013).

[15] Mooren, O. L., Erickson, E. S., Dickenson, N. E., and Dunn, R. C. *Journal of Laboratory Automation* **11**(4), 268–272 (2006).

[16] Prauzner-Bechcicki, S., Wiltowska-Zuber, J., Budkowski, A., Lekka, M., and Rysz, J. *Acta Physica Polonica A* **121**(2), 533–538 (2012).

[17] Baylis, R. M., Doak, S. H., Holton, M. D., and Dunstan, P. R. *Ultramicroscopy* **4-5**(4), 308–312 (2007).

[18] Briggs, D. *Surface analysis of polymers by XPS and static SIMS*. Cambridge University Press, (1998).

[19] Awsiuk, K., Bernasik, A., Kitsara, M., Budkowski, A., Rysz, J., Haberko, J., Petrou, P., Beltsios, K., and Raczkowska, J. *Colloids and Surfaces B: Biointerfaces* **80**(1), 63–71 (2010).

[20] Ton-That, C., Shard, A. G., and Bradley, R. H. *Langmuir* **16**(5), 2281–2284 (2000).

[21] Vickerman, J. C. and Briggs, D. *ToF-SIMS: surface analysis by mass spectrometry*. IM Publications and Surface Spectra Limited: Chichester and Manchester, (2001).

[22] Walker, A. V. *Analytical Chemistry* **80**(23), 8865–8870 (2008).

[23] Mantus, D. S., Ratner, B. D., Carlson, B. A., and Moulder, J. F. *Analytical Chemistry* **65**(10), 1431–1438 (1993).

[24] Samuel, N. T., Wagner, M. S., Dornfeld, K. D., and Castner, D. G. *Surf.Sci.Spectra* **8**, 163–184 (2001).

[25] May, C. J., Canavan, H. E., and Castner, D. G. *Analytical Chemistry* **76**(4), 1114–1122 (2004).

[26] Wagner, M. S. and Castner, D. G. *Langmuir* **17**(15), 4649–4660 (2001).

[27] Stetsyshyn, Y., Zemła, J., Zolobko, T., Fornal, K., Budkowski, A., Kostruba, A., Donchak, V., Harhay, K., Awsiuk, K., Rysz, J., Bernasik, A., and Voronov, S. *Journal of colloid and interface science* **387**(1), 95–105 (2012).

[28] Kim, Y. P., Hong, M. Y., Shon, H. K., Chegal, W., Cho, H. M., Moon, D. W., Kim, H. S., and Lee, T. G. *Applied Surface Science* **255**(4), 1110–1112 (2008).

[29] Kim, Y. P., Hong, M. Y., Shon, H. K., Moon, D. W., Kim, H. K., and Lee, T. G. *Applied Surface Science* **252**(19), 6801–6804 (2006).

[30] Kim, Y. P., Hong, M. Y., Kim, J., Oh, E., Shon, H. K., Moon, D. W., Kim, H. S., and Lee, T. G. *Analytical Chemistry* **79**(4), 1377–1385 (2007).

Chapter 3

Protein adsorption and covalent bonding to silicon nitride substrate modified with organo-silanes

3.1 Abstract

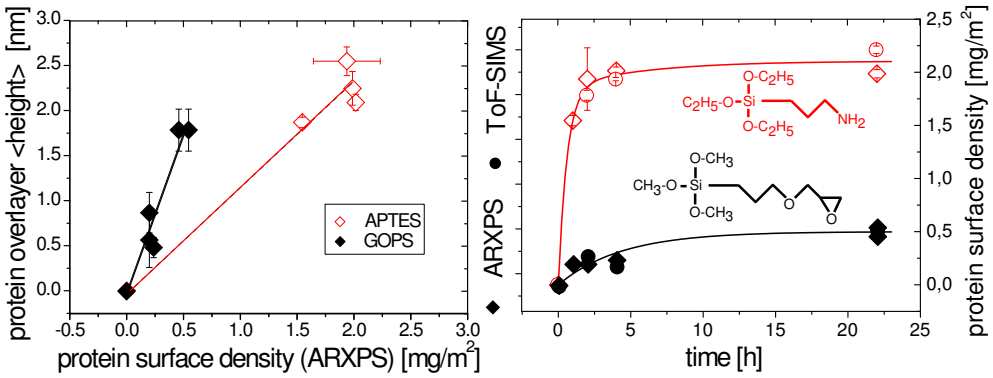

Organo-silanes provide a suitable interface between the silicon-based transducers of various biosensing devices and the sensing proteins, immobilized through physical adsorption, as for (3-aminopropyl)triethoxysilane (APTES), or covalent binding, e.g. via protein amine groups to (3-glycidoxypropyl)trimethoxysilane (GOPS) modified surface. Immobilization of rabbit gamma globulins (IgG) to silicon nitride surfaces, modified either with APTES or GOPS, was examined as a function of incubation time using Atomic Force Microscopy (AFM), Angle-Resolved X-ray Photoelectron Spectroscopy (ARXPS) and Time of Flight Secondary Ion Mass Spectrometry (ToF-SIMS). Multivariate technique of principal component analysis was applied to ToF-SIMS spectra in order to enhance sensitivity of immobilized IgG detection. Principal component regression shows a linear relationship with surface density determined rigorously from ARXPS following an organic bilayer approach, allowing for protein coverage quantification by ToF-SIMS. Taking it overall the surface immobilized amount of IgG is higher and develops faster on the surfaces silanized with APTES rather than with GOPS. Similar, although less distinct, difference is observed between the two surface types concerning the temporal evolution of average AFM height. The average height of protein

overlayer correlates well with ARXPS and ToF-SIMS data expressed in terms of protein surface density. However, determined linear regression coefficients are distinctively higher for the surfaces modified with epoxy- rather than amino-silane, suggesting different surface density and conformation of the proteins immobilized through to covalent binding and physical adsorption.

Highlights

• Protein immobilization compared for Si3N4 modified with amino- and epoxy-silanes. • Correlated ToF-SIMS and angle-resolved XPS data yield protein surface coverage. • Surface coverage is higher and develops faster for adsorption than covalent bonding. • AFM height vs. surface coverage relations reflect distinct packing and conformation.

Keywords

gamma globulins; physical adsorption; covalent bonding; Time-of-Flight Secondary Ion Mass Spectrometry; Principal Component Regression

3.2 Introduction

Biomolecular immobilization is an issue important in various fields of biotechnology, critical for the performance of biomedical implants, biosensors, assay platforms, templates for tissue engineering, etc. Different schemes for surface immobilization of biomolecules have been developed, involving covalent bonding, physical adsorption or specific (bio)molecular interactions depending on the surface to be modified.

Transducers made of silicon are often modified with organo-silanes in order to be functionalized with biomolecules and thus effectively converted to biosensors with high binding activity and specificity [1–3]. The organo-silanes, available with different functional groups, change the physicochemical properties of silicon surfaces and enable biomolecular immobilization by physical adsorption and/or covalent bonding. Amino-silanes, e.g. (3-aminopropyl)triethoxysilane (APTES), increase the affinity between silicon and biomolecules [2, 4] and enable physical adsorption. Alternatively, specific groups present at the surfaces after silanization with either epoxy-silanes, e.g. (3-glycidoxypropyl)trimethoxysilane (GOPS), or APTES allow for the covalent bonding of biomolecules either directly or after an intermediate functionalization step with an appropriate biofunctional linker [2, 3, 5].

To evaluate different immobilization protocols it is also important to understand the underlying phenomena starting from a molecular level. Therefore many studies focus on biomolecules orientation, organisation, conformational changes that have an impact on both the kinetics and the final outcome of immobilization [6–8]. To this end also immunoglobulin adsorption was examined at various solution and surface conditions [9–14], that were found to modify protein orientation [9, 12–16] and hence also antigen binding on model and biosensor surfaces [12, 14]. Overall conformational control of adsorbed IgG can be obtained with different surface chemistry [11–13, 15] or pH varied around the isoelectric point [9].

Different experimental methods were employed to characterize biomolecules immobilized on the surface of various materials. Atomic force microscopy (AFM) working in non-contact mode and in ambient

conditions is a popular method implemented to analyse the 3-D structure of immobilized protein overlayers [17–26]. While reliable imaging is easier with ambient than liquid AFM, molecular shapes obtained with both methods can be quite similar [18]. In addition, when AFM cantilever is not in contact with the surface, its topology can be acquired without any distortion [22]. Therefore ambient non-contact AFM can provide information about characteristic vertical [19–22, 25] and lateral scales [18, 23] of surface features corresponding to immobilized biomolecules (or even their subunits [23]) that can be interpreted based on known biomolecular dimensions. Unfortunately, AFM does not yield biomolecule surface density (except for very low protein coverage). Therefore, many additional spectroscopic techniques have been used to quantify the amount of immobilized molecules [4, 25, 27–31]. In our previous works we have presented a model to determine protein surface density from angle-resolved X-ray photoelectron spectroscopy (ARXPS) measurements. This model, by tracking specific signals from substrate and biomolecular layer as a function of take-off angle, enables quantification of immobilized proteins [4]. Recently, thanks to its high chemical specificity and surface sensitivity, Time of Flight Secondary Ion Mass Spectrometry (ToF-SIMS) has also become an increasingly popular method to examine immobilized biomolecules. As, ToF-SIMS is a very sensitive method so the relative evaluation of molecular concentration based on singular mass signals might be affected by matrix effects or surface contaminations [29]. Therefore, to obtain more accurate results the multivariate ToF-SIMS analysis is used: Principal Component Analysis (PCA) identifies, based on ToF-SIMS spectra, subtle differences in protein coverage between various samples. However, to quantify in absolute units of protein surface density the PCA scores from the ToF-SIMS spectra, they must be correlated with the amount of immobilized biomolecules estimated by other methods like surface plasmon resonance, ellipsometry or isotope-labelling [27, 28, 30, 31]. To this end Principal Component Regression (PCR) has been performed.

In this Chapter, protein immobilization to silicon nitride surfaces modified with two different organosilanes is compared. In particular, rabbit gamma globulins (IgG) have been immobilized by physical adsorption or covalent bonding onto Si_3N_4 surface modified with APTES and GOPS, respectively, and examined as a function of the incubation time. Protein surface density was determined from ARXPS measurements and then correlated with ToF-SIMS data analysed with PCA in order to quantify protein surface coverage with ToF-SIMS. In addition, analysis of ARXPS and ToF-SIMS data revealed differences in the immobilization kinetics between physical adsorption and covalent bonding. Moreover, AFM micrographs not only revealed nanostructure of immobilized IgG molecules but also correlation between average AFM height and protein surface density, determined from ARXPS or ToF-SIMS measurements, were observed. These findings reflect distinct packing and conformation of immobilized protein resulting via physical adsorption or covalent bonding.

3.3 Materials and methods

3.3.1 Materials

Silicon wafers were purchased from Montco Silicon Technologies, Inc. (Spring City, PA, USA). Silicon nitride (Si_3N_4) surfaces were obtained by a two-step process. Firstly, a 1-μm thick silicon diox-

ide layer was fabricated by low pressure chemical vapour deposition and then an additional 150-nm thick silicon nitride layer was deposited on the top. The silanes, 3-aminopropyl(triethoxysilane) (APTES) and (3-glycidyloxypropyl)trimethoxysilane (GOPS), used to modify silicon substrates as well as the rabbit gamma globulins (from rabbit serum, Cohn fraction II, III, 99% electrophoretic purity, product number G0261) were purchased from Sigma Chemical Co. (St. Louis, MO, USA).

3.3.2 Surface modification and protein immobilisation

Si_3N_4 surfaces were cleaned and hydrophilized with oxygen plasma (using a reactive ion etcher) applied for 30 s under pressure of 10 mTorr and power of 400 W. The hydrophilized surfaces were then modified by immersion in a 0.5% (v/v) aqueous APTES solution for 2 min., followed by gentle washing with distilled water, drying under N_2 flow and curing at 120 °C for 20 min. Alternatively, the hydrophilized surfaces were immersed in a 1% (v/v) solution of GOPS in dry toluene and incubated for 18 h at room temperature (RT). After washing with dry toluene and ethanol and treatment in an ultrasonic bath in ethanol for 20 min, the surfaces were dried under N_2 flow. The surfaces modified with APTES and GOPS are expected to have similar negative zeta potential (as determined for silanized glass with identical value of -24mV at physiological pH [32]) that should not induce different behaviour concerning their protein immobilization properties. In turn, in a separate study, surface modified with NH_2-terminated thiols was found to be positively charged [15].

Rabbit gamma globulins, Cohn fraction II, III, derived from non-immunized rabbits serum (molecular weight of about 150 kDa, isoelectric point 7.3($\pm$1.2), diffusion coefficient $D_0 = 3.9\times10^{-11}$ cm^2/s measured at pH 7.4 and 20 °C [33], Stokes-Einstein diameter 2R = 10.4 nm [34]), were immobilized to the silanized silicon substrates through incubation with a 100 μg/mL (0.66 μM) solution in 50 mM phosphate buffer, pH 7.4, at RT. After incubation for 1, 2, 4 or 22 hours, the samples were gently washed with 50 mM phosphate buffer, pH 7.4, and distilled water and dried under N_2 flow to prepare them for AFM and spectroscopic measurements (in air and vacuum, respectively).

3.3.3 Surface characterization

3.3.3.1 AFM

Atomic Force Microscopy (AFM) measurements were performed in non-contact mode using an Agilent 5500 AFM microscope system. Silicon nitride probes with spring constant about 2 N/m and resonant frequencies about 70 kHz were used. The set point and all gains were adjusted to obtain minimal noise and a clear image of the examined surface. For each sample, topography images were acquired at several randomly chosen locations. The measurements were performed in air under ambient conditions (RT).

The vertical structure of surfaces examined with AFM is best described by the distribution of height in topographic images [19, 21] characterized in terms of its mean value and spread. Therefore, the average height $\langle h \rangle$ and its standard deviation, given by root mean square (RMS) roughness, are determined for each height distribution using the PicoImage software provided with the AFM equipment.

3.3.3.2 XPS

X-ray photoelectron spectroscopy (XPS) spectra were collected using a VSW Manchester spectrometer equipped with an Al Kα radiation source (1486.6 eV, 200 W). Angle-resolved XPS (ARXPS) measurements were performed for three different values (0°, 60° and 70°) of photoelectron take-off angle Θ (with respect to the surface normal). The operating pressure in the analytical chamber was less than 5×10^{-8} mbar. All XPS peaks were referenced to the neutral (C-C) carbon C1s peak, at a binding energy of 284.6 eV. Spectrum backgrounds were subtracted using the Shirley method. The bilayer model (see Section 2.2.3.3.2) used to determine the thickness of APTES film and the amount of immobilized proteins has been described in details in our earlier publications [4]. The procedure to estimate the thickness of GOPS film is presented below (Section 3.4.2.1).

3.3.3.3 ToF-SIMS

The surfaces with immobilized IgG were analysed using the TOF.SIMS 5 (ION-TOF GmbH) instrument, equipped with 30 keV bismuth liquid metal ion gun. Bi_3^+ clusters were used as the primary ions. The dose density deposited on the surface was identical for all samples and lower than 10^{12} ion/cm^2 to ensure static mode conditions. Positive ion static ToF-SIMS spectra, prior to and after immobilization of IgG, were acquired from three different non-overlapping spots (100 μm $\times$ 100 μm area). For all spectra the mass resolution m/Δm >7300 (at C_4H_5+ (m/z=53) peak) was maintained. Mass calibration was performed with H+, H_2+, CH+, C_2H_2+ and C_4H_5+ peaks. Principal Component Analysis (PCA) were performed on chosen ToF-SIMS signals characteristic for proteins and substrates using PLS_Toolbox (Eigenvector Research, Manson, WA) for MATLAB (MathWorks,Inc., Natick, MA) to enhance detection of subtle differences in surface chemistry between different samples. The peaks in each spectrum were normalized by total ion intensity and mean-centered before running PCA.

3.4 Results and discussion

3.4.1 Two surface types with immobilized proteins compared using AFM

AFM micrographs provide insight into local arrangement of biomolecules on organo-silanes modified silicon substrates. Representative topography micrographs of Si_3N_4 substrate modified with GOPS or APTES and incubated with a 0.66 μM IgG solution for 1 h, 4 h and 22 h are presented in Figure 3.1. These micrographs reveal surface features with the apparent protein size of $\sim$25 nm. Comparable values of 24 and 28 nm, respectively, are predicted for adsorbed IgG due to the broadening caused by the AFM tip (with 7 nm radius) for half-spherical [35] and spherical [21] molecular shapes (with the 'real' radius of 7 nm [20]). The AFM images indicate IgG molecules more loosely packed on the coated surfaces modified with epoxy- rather than amino-silanes. Moreover, the observed 3-D structure of protein overlayer seems to be not affected by the incubation time of APTES modified substrate with the IgG solution. On the other hand, the protein surface features on the GOPS modified substrates are becoming more densely packed as the incubation time increases.

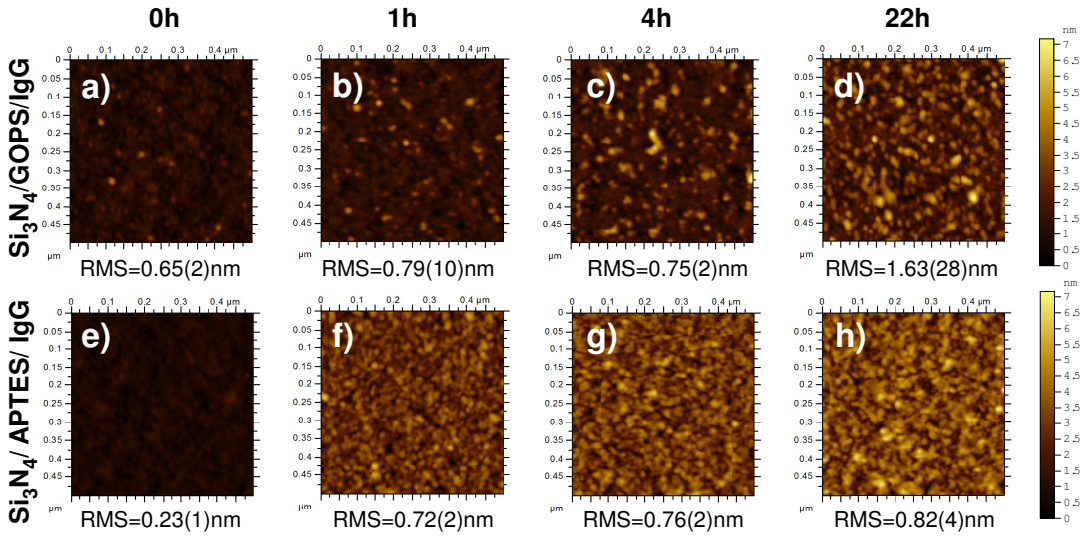

Figure 3.1: Representative AFM images of Si_3N_4 surfaces modified with GOPS (a-d) and APTES (e-h) prior to (a, e) and after incubation with a 0.66 μM rabbit gamma globulins solution for 1 h (b, f), 4 h (c, g) and 22 h (d, h), washing and drying. RMS error limits are Standard Error of the Mean each determined from 4-6 images of the same surface.

In addition, the analysis of AFM height histograms provides information about roughness and average height (Figure 3.2) of an organic layer. For the Si_3N_4 substrates prior to protein immobilization, the average height of organo-silane layer is 0.80($\pm$0.02) nm and 1.00($\pm$0.03) nm for the APTES and GOPS, respectively. These averages are in accordance with literature values, ranging from 0.8 to 1.3 nm for APTES layer deposited from aqueous solution [36] and from 0.75 to 1.1 nm for GOPS deposited from toluene solutions [37], and are expected for monomolecular layers. Roughness of silanized substrates is 0.23($\pm$0.01) nm for APTES and 0.65($\pm$0.02) nm for GOPS.

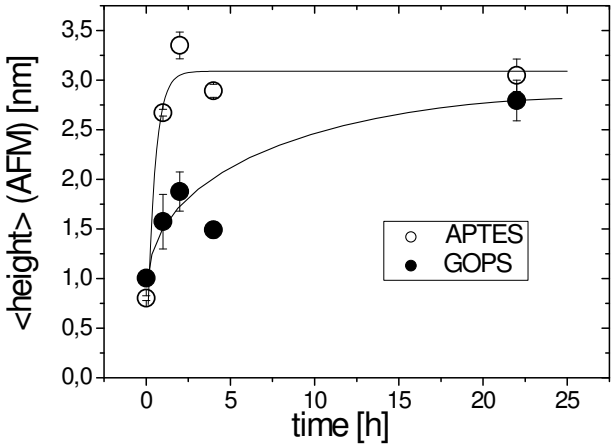

Figure 3.2: Mean AFM height of Si_3N_4 surfaces functionalized with APTES (open circles) and GOPS (solid circles) and its temporal evolution during immobilization of rabbit gamma globulins molecules. Error bars are Standard Error of the Mean each determined from 4-6 images of the same surface.

Analysis of AFM micrographs after IgG immobilization reveals that the average height of an organic

layer increases constantly with the incubation time for the substrates modified with GOPS. In particular, the thickness of the organic layer increases from 1.6($\pm$0.3) nm to 2.8($\pm$0.2) nm for 1 h and 22 h of incubation with IgG solution, respectively. For the APTES modified substrates no dependence between the incubation time and the average AFM height is observed, with a constant average AFM height of about 3 nm for incubation time larger than 1 hour. In addition, for the longest incubation time (22 h) the thickness of the organic layer is comparable for both silanes but the roughness is twice higher for IgG immobilized to GOPS (1.6$\pm$0.3 nm) than APTES (0.8$\pm$0.1 nm).

AFM data analysis suggests that the process of protein immobilization is faster for physical adsorption to a surface modified with amino-silane than covalent bonding to a surface modified with epoxy-silane. Moreover, the adsorbed proteins form a more densely packed structure compared to covalently bound one.

3.4.2 Surface coverage of adsorbed and covalently bound proteins

Spectroscopic methods (ARXPS and ToF-SIMS) have been implemented to quantify the amount of adsorbed proteins. Protein surface density is determined from ARXPS (Section 3.4.2.1), while subtle changes in protein coverage are detected with multivariate analysis ToF-SIMS (Section 3.4.2.2) and then both data sets are correlated with each other (Section 3.4.2.3). These data plotted together as a function of incubation time provide an insight into the yield and kinetics of immobilization processes to silicon surfaces modified either with amino- or epoxy-silane (Section 3.4.2.3).

3.4.2.1 Protein surface density determined with ARXPS

The ARXPS spectra depend on photoelectron take-off angle Θ, that modifies sampling vertical depth, and on XPS thickness of organic films, that justifies the effective attenuation of photoelectrons. To estimate the protein coverage of Si_3N_4 surfaces modified with organo-silanes the ARXPS data (Figures 3.3 and 3.4) were analysed using the bilayer model of protein overlayer on organo-silane film (see Section 2.2.3.3.2). This model allows to determine the XPS thickness d of protein layer, which yields surface density (coverage) when multiplied by the protein partial specific volume (0.73 cm^3/g). For proteins, the XPS thickness that justifies the effective attenuation of photoelectrons corresponds to an equivalent layer with the mass uniformly distributed rather than localized in molecular ellipsoids. For the bilayer analysis the photoelectrons from the amine groups (NH_2 and NH_3^+) (N1s core level) and silicon (Si2p core level) were taken into account as characteristic for protein overlayer or amino-silane/protein bilayer on the Si_3N_4 substrate modified with GOPS or APTES, respectively (see insets in Figure 3.4). To estimate the thickness D of organo-silane layers, relevant for the bilayer model, separate data were recorded for the silanized substrates (Figure 3.3) and analysed with respect to photoelectrons originating from silicon nitride (Si2p) and amine groups (N1s) or carbon (C1s) present in APTES or both APTES and GOPS, respectively.

The preliminary step was to estimate the stoichiometric molar fractions Z_i of the atoms emitting characteristic photoelectrons. Based on the ARXPS data for the bare Si_3N_4 substrate, the value Z_{Si} = 31.2($\pm$1.3)%, averaged for all take-off angles, was determined for silicon. This can be explained by the presence of silicone dioxide as indicated by additional XPS data and accords with our previous results [4]. Then, N (from amine groups) and C molar fractions for APTES were determined from atomic

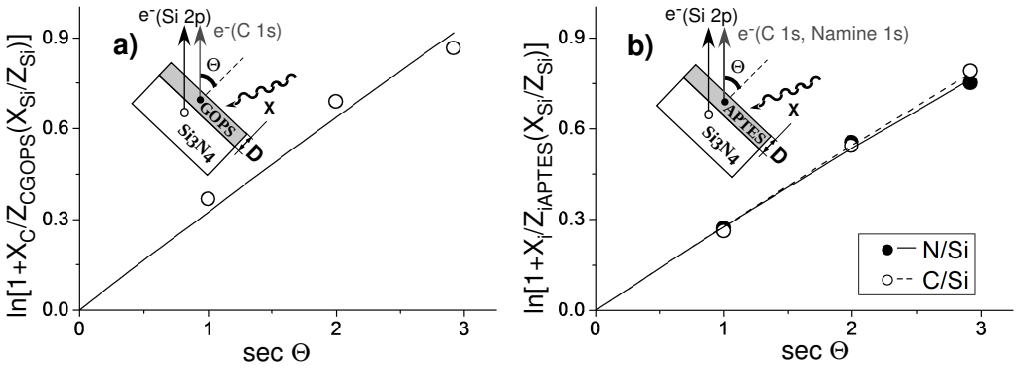

Figure 3.3: The ratio of normalized intensities of the photoelectrons characteristic for the organo-silanes (C1s (a, b) or N1s from amine groups (b)) and the Si_3N_4 substrate (Si2p) plotted (data points) versus the take-off angle function $\sec\Theta$ for GOPS (a) and APTES films (b) (see insets). Regression fitting (lines) provides the thickness D of the films.

concentrations of silanized substrate with no protein overlayers, averaged for Θ angles between 0° and 70°, (as it was described earlier [4]) yielding values of Z_{NAPTES} = 4.1($\pm$0.2)% and Z_{CAPTES}= 95.9($\pm$0.3)%, respectively. This approach was modified for GOPS contributing to oxygen concentration in excess of silicon dioxide, the latter evaluated assuming silicon stoichiometry equal to the one of bare Si_3N_4. As a result, the value of carbon molar fraction Z_{CGOPS} = 94.5($\pm$4.4)% was obtained. C molar fractions (Z_{CAPTES} and Z_{CGOPS}), higher than predicted from chemical structure of silanes, are ascribed to the presence of adventitious carbon incorporated into the silane brush layers [38, 39]. The nitrogen molar fraction for IgG of Z_{Namine} = 11% was determined in our previous publication [4].

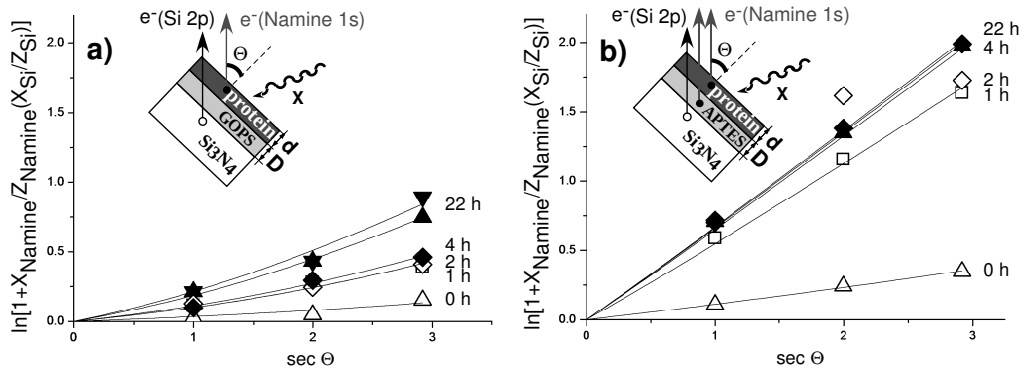

Figure 3.4: The ratio of normalized intensities of the photoelectrons characteristic for protein overlayer (a) or amino-silane/protein bilayer (b) (N1s from amine groups) formed on the Si_3N_4 substrate (Si2p) modified with GOPS (a) and APTES (b) (see insets). Regression fitting (lines) of individual data sets (different symbols for incubation time varied between 0 and 22 h) provide the XPS thickness of protein overlayer d, which multiplied by the protein density yields the surface coverage.

The structural features of the films were revealed by the ratio of intensities X_i of the characteristic photoelectrons plotted in a logarithmic form versus the take-off angle function $\sec\Theta$ (Figures 3.3 and 3.4).

The intensities X_i, calculated using tabulated sensitivity factors, were normalized with respect to molar fractions Z_i of the atoms emitting photoelectrons (see the axis of ordinates in Figures 3.3 and 3.4). The thicknesses D of the epoxy- (Figure 3.3a) and amino-silane layer (Figure 3.3b) obtained from the regression fitting procedure [4] were 0.97($\pm$0.05) nm for the GOPS layer, and 0.82($\pm$0.01) nm or 0.77($\pm$0.01) nm for APTES layer based on the analysis involving C1s or amine N1s XPS peak, respectively. These results accord with the values determined from AFM (see Section 3.4.1) and the ones reported earlier [36, 37]. In turn, the XPS thickness d of the protein overlayer was obtained from the regression fitting performed in the frame of the bilayer model [4] (see lines in Figure 3.4a, b) for the data sets (different symbols) corresponding to different incubation time. The resulting values of protein surface density are much higher for adsorbed proteins (from 1.55($\pm$0.05) mg/m^2 to 2.00($\pm$0.04) mg/m^2) than for covalently bound ones (from 0.20($\pm$0.02) mg/m^2 to 0.55($\pm$0.05) mg/m^2). These values are significantly lower than the value expected for the area covered by singular IgG molecule with side-on orientation (2.6 mg/m^2). Other orientations would result in even higher surface densities. So the determined values point to considerable surface coverage with physically adsorbed IgG in contrast to covalently bound proteins where more loose packing of molecules is concluded. Temporal dependence of protein surface density for both immobilization methods is analysed in Section 3.4.2.3.

3.4.2.2 Immobilized protein detection with multivariate ToF-SIMS analysis

Silicon nitride surface samples modified with epoxy- and amino-silane have been examined with ToF-SIMS prior to and after protein immobilization due to incubation with a IgG solution for 2 h, 4 h and 22 h. Three different ToF-SIMS spectra were recorded for each sample (5 for GOPS and 4 for APTES) of each series. Representative positive secondary ion ToF-SIMS spectra with marked signals characteristic for the substrates and IgG are presented in Figure 3.5. Even a brief inspection of these spectra reveals that intensities of NH_4+, CH_4N+, C_2H_6N+ and CH_2NO+ signals, characteristic for proteins, increase with incubation time. In turn, decreasing intensity for CH_3O+, which is characteristic for GOPS and APTES, and for C_3H_7+, characteristic for APTES can be noticed. This inspection reflects progressive protein immobilization.

To increase the ToF-SIMS reliability and to enhance detection of subtle changes in protein surface density, intensities of many ToF-SIMS signals were simultaneously inspected within Principal Component Analysis. For this purpose, 17 different signals unique for the protein and its individual amino-acids [40, 41] and 6 signals characteristic for the silanized substrates were chosen (see Table 3.1). For each series (GOPS or APTES modified substrates) the intensities of these 23 peaks from numerous ToF-SIMS spectra (12 and 15 for APTES and GOPS, respectively) form a large data set, visualized as the points in a 23-dimensional space. PCA analysis defines the directions of uncorrelated major variations within such a data set, so called principal components PCs. The first PC (PC1) captures already 91.2 % and 98.4% of the total variance in the data for the substrate silanized with GOPS and APTES, respectively. For both substrate types, the relation of the first PC with the original variables, i.e. 23 peaks, is presented as the loading plots (Figure 3.6a, b). In both cases, the PC1 is dominated by the positive loadings corresponding to the signals of the protein, while the negative or close to zero loadings are related with the silanized substrates. Such loading plots indicate that the PC1 is a suitable variable to reflect relative protein surface concentration.

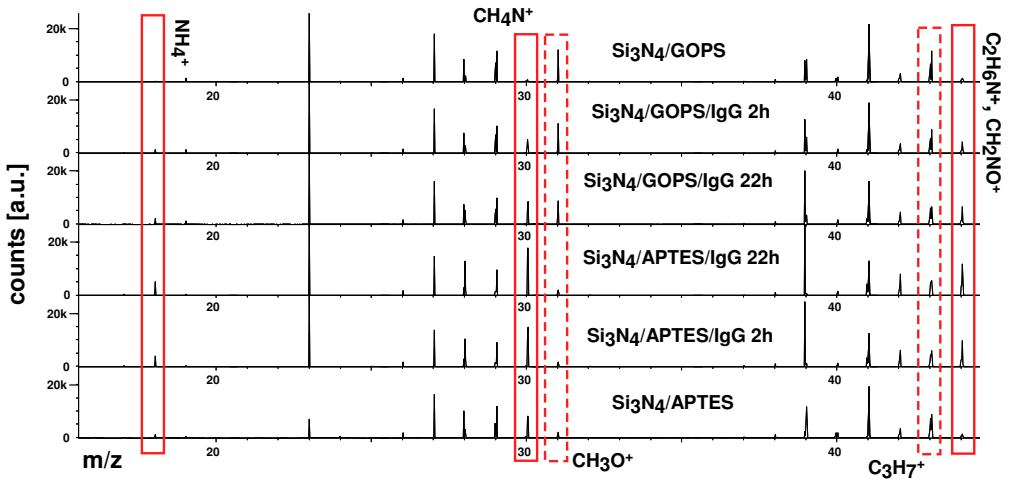

Figure 3.5: Representative positive ion ToF-SIMS spectra of the Si_3N_4 surfaces modified with GOPS and APTES prior to and after incubation with rabbit gamma globulins solution for 2 or 22 hours. Signals characteristic for the rabbit gamma globulins and the substrates are marked as solid and dashed rectangles, respectively.

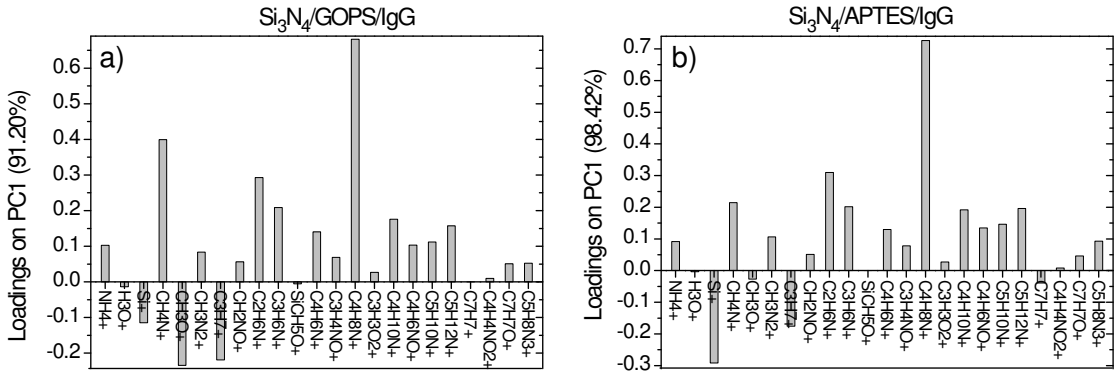

Figure 3.6: Principal component analysis (PCA) performed independently for two series of ToF-SIMS data sets recorded from Si_3N_4 surfaces functionalized with GOPS (a) or APTES (b), respectively, and coated with rabbit gamma globulins. Loading plots of the first principal component PC1 present ToF-SIMS peaks characteristic for the protein and the substrates.

3.4.2.3 ToF-SIMS data correlate with and confirm ARXPS results

To test whether quantitative results concerning protein surface coverage can be extracted from the analysis of ToF-SIMS data, the scores on the first Principal Component were compared to the protein surface density determined rigorously from ARXPS. As it is shown in Figure 3.7 a good linear relation, obtained from Principal Component Regression, is observed between the scores on PC1 and protein surface density for both data sets. Therefore, the scores can be rescaled to absolute units of protein surface concentration enabling quantification of immobilized proteins with ToF-SIMS.

Protein surface density data, rescaled from (the PC1 scores of) ToF-SIMS results (solid circles in Figure 3.8) and determined from ARXPS (open circles) are presented together versus incubation time in Figure

Table 3.1: Characteristic ToF-SIMS peaks selected for Principal Component Analysis.

Characteristic ion peak	centre mass	surface origin
NH_4+	18.04	IgG
CH_4N+	30.03	IgG (Gly)
CH_3N_2+	43.03	IgG (Arg)
CH_2NO+	44.01	IgG
C_2H_6N+	44.05	IgG (Ala)
C_3H_6N+	56.05	IgG (Lys)
C_4H_6N+	68.05	IgG (Pro)
C_3H_4NO+	70.03	IgG (Asn)
C_4H_8N+	70.07	IgG (Pro, Arg)
$C_3H_3O_2$+	71.01	IgG (Ser)
$C_4H_{10}N$+	72.09	IgG (Val)
C_4H_6NO+	84.04	IgG (Gln, Glu)
$C_5H_{10}N$+	84.09	IgG (Lys)
$C_5H_{12}N$+	86.10	IgG (Ile, Leu)
$C_4H_4NO_2$+	98.02	IgG (Asn)
C_7H_7O+	107.05	IgG (Tyr)
$C_5H_8N_3$+	110.06	IgG (His, Arg)
$SiCH_5O$+	61.01	GOPS
C_7H_7+	91.05	APTES
CH_3O+	31.02	APTES, GOPS
C_3H_7+	43.06	APTES, GOPS
H_3O+	19.02	substrate (Si_3N_4), APTES, GOPS
Si+	27.98	substrate (Si_3N_4)

3.8a and Figure 3.8b as separate plots for the Si_3N_4 surfaces modified with GOPS and APTES, respectively. These plots provide an insight into the yield and kinetics of immobilization processes performed through incubation in the same protein solution. Surface immobilization amount of IgG is higher and develops faster on the surfaces modified with amino-silane (average values of 1.8 and 2.1 mg/m^2 attained after 2 and 22 h, respectively) rather than with epoxy-silane (0.2 and 0.5 mg/ m^2 after 2 and 22 h, respectively).

Limited data sets preclude determination of precise parameters describing immobilization kinetics. However, they allow for some conclusions. First, temporal progress of immobilization (Figure 3.8a, b) is not governed by diffusion of proteins toward the silanized surfaces as observed immobilization rates are much lower than predicted values (for $D_0 = 3.9\times10^{-11}$ cm^2/s [33]) and square-root of time dependence does not fit the data. Second, the data sets in Figure 3.8a and Figure 3.8b show differences in the character of both immobilization processes reflected in different formulas best describing temporal evolution of surface coverage with proteins. The merged ARXPS and ToF-SIMS data recorded for protein immobilized on the

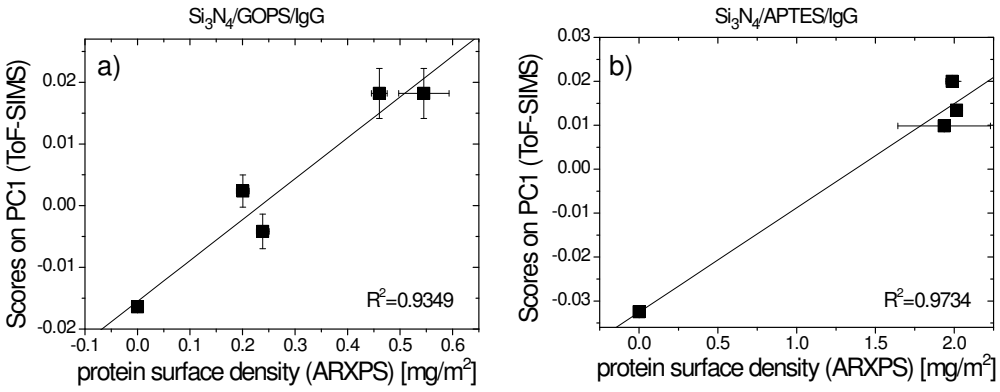

Figure 3.7: Correlation between scores on the first principal component PC1 and protein surface density from ARXPS determined for the Si_3N_4 surfaces functionalized with GOPS (a) or APTES (b) and coated with rabbit gamma globulins. This Principal Component Regression allows for protein coverage quantification by ToF-SIMS. Error bars for protein surface density determined from ARXPS measurements (the axis of abscissas) are given by the fitting procedure shown in Figure 3.4. Error bars for Scores on PC1 (the axis of ordinates) are Standard Error of the Mean for n=3.

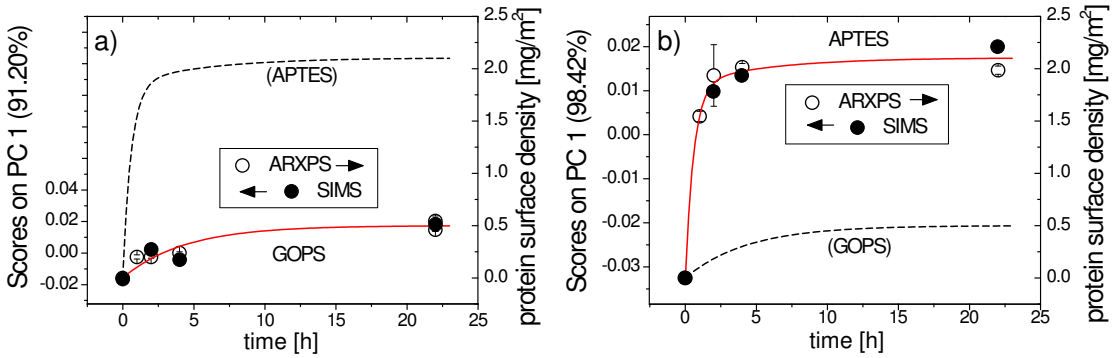

Figure 3.8: Effect of incubation time on immobilization of rabbit gamma globulins to Si_3N_4 surfaces modified either with GOPS (a) or APTES (b). Protein surface coverage determined from ARXPS data (open circles, right scales) and the scores on the first principal component PC1 (solid circles, left scales) corresponding to average of 3 ToF-SIMS measurements for each sample of two series (a, b) analysed separately within Principal Component Analysis. The lines result from regression fitting of different kinetics models.

substrate silanized with GOPS are well fitted (solid line in Figure 3.8a) with an exponential formula. While epoxy-modified surfaces are considered as hardly [42] and very slowly [43] reactive for direct (intermolecular) protein immobilization at neutral pH a more effective (intramolecular) covalent binding mechanism can be launched for previously adsorbed proteins [42, 43]. Therefore immobilization kinetics is most probably governed here by physical adsorption limiting subsequent covalent binding. In turn, in order to mimic the data for IgG proteins adsorbed to APTES modified surfaces a formula with two exponents is necessary (see solid lines fitted to the experimental points in Figure 3.8b). Rankl et al. showed that the IgG adsorption process could be characterized by a two step mechanism, where protein molecules firstly adsorb to the surface and then they can either desorb or undergo conformational reorientation to an irreversible state [7].

The analytical formula for the immobilization kinetics within this model, as determined by Krisdhasima et al. [44], is identical to that used to reproduce the data points in Figure 3.8b.

3.4.3 Vertical extent vs. surface coverage: distinct packing and conformation

An analysis of the AFM determined average height of protein overlayer as a function of surface coverage (Figure 3.9a, b) enables a new insight into surface nanostructure of adsorbed proteins. To analyse this issue a schematic model is presented in Figure 3.9c. Taking into account the weight M of a single molecule (2.49×10^{-16} mg) and its dimensions relevant for adsorption, such as thickness H and covered surface S, the ratio of molecular thickness to surface density is expressed as HS/M. This proportion, multiplied by surface density for the area covered with a single protein (with given orientation) would produce relevant thickness. It would also relate, when supplemented with the surface fraction η covered by proteins (0.92 and 0.55 from geometrical constraints [45] and random sequential adsorption theory [46], respectively), the average thickness of protein layer with actual surface density (Figure 3.9a, b). The complete formula HS/(Mη) is presented in Figure 3.9c.

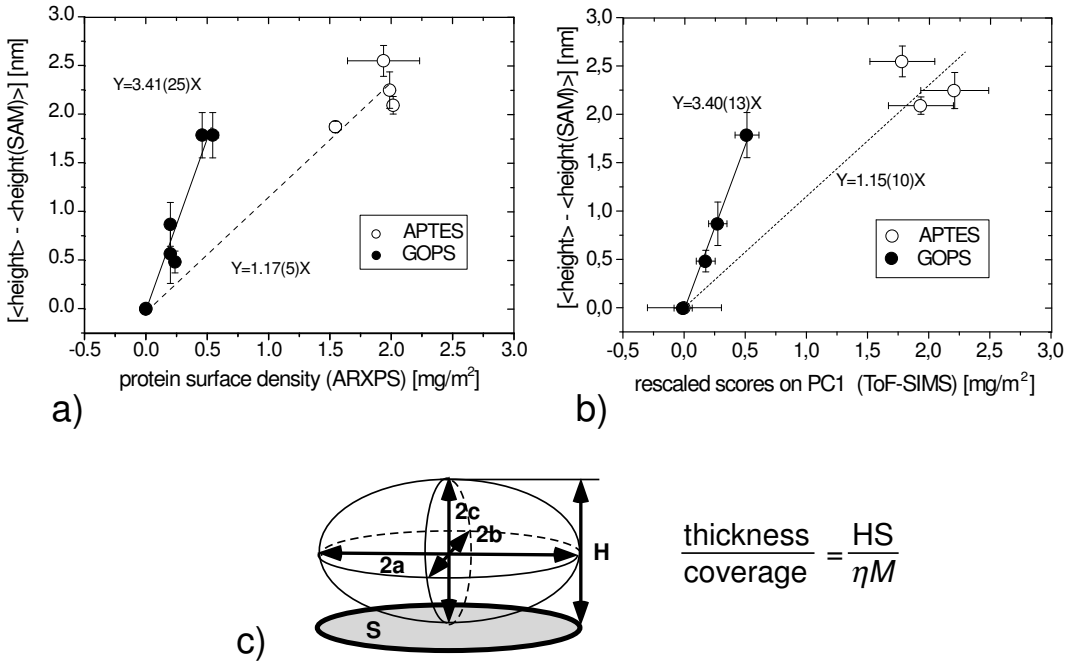

Figure 3.9: Average AFM height of protein overlayer plotted as a function of protein coverage determined by ARXPS (a) and ToF-SIMS (through principal component regression) (b). The difference in the slopes of the linear regression lines (a, b) for the Si_3N_4 surfaces functionalized with GOPS (solid circles) or APTES (open circles), respectively, point to different surface protein packing density η and conformation (molecular dimensions, H and S) of proteins (c) immobilized by covalent binding (GOPS) or physical adsorption (APTES). Error bars are specified in Figure 3.2 and Figure 3.7.

Detailed Y- or T-shaped IgG structure, with one F_c ($7.0 \times 6.3 \times 3.1$ nm^3) and two F_{ab} fragments ($8.2 \times 5.0 \times 3.8$ nm^3), is used [9, 16] to analyse a single molecule with different side-on and end-on configurations (with HS/M = 2.3 and 2.8 - 4.4 nm.m^2/mg, respectively) in order to interpret surface density

data. A simpler model of globular molecule with the dimensions 2a $\times$ 2b $\times$ 2c (14.5 $\times$ 8.5 $\times$ 4 nm^3) [20, 21, 26, 47, 48] is commonly applied [20, 21, 26, 48–50], especially when vertical structure of IgG overlayers is analysed from topographic AFM images (convoluted with tip shape) [20, 21, 26, 48]. This model yields the molecular ratio 2c (πab/M) of thickness to surface density (HS/M = 1.6 nm.m^2/mg) that is independent on protein orientations as all ellipsoid dimensions are in its numerator. The HS/M values given above could be used to interpret the results shown in Figure 3.9 keeping in mind that the other results suggest preferential side-on or coexisting side-on and end-on orientations for IgG molecules adsorbed to surfaces modified with APTES (see Chapter 4 and Chapter 5) or NH_2-terminated thiols [13, 15], respectively.

The average AFM height of protein overlayer (i.e. the sample height with the value for pure organosilane subtracted) is plotted in Figure 3.9 versus the protein surface density determined from ARXPS (Figure 3.9a) and ToF-SIMS (through PCR, Figure 3.9b) for the Si_3N_4 surface modified with GOPS (solid circles in Figure 3.9) and APTES (open circles). On both graphs linear relations are observed for both GOPS and APTES data sets. However, linear regression coefficients are different for the two substrates. The coefficient values for the physically adsorbed proteins, equal to 1.14($\pm$0.11) nm.m^2/mg (AFM vs. ToF-SIMS) and 1.17($\pm$0.05) nm.m^2/mg (AFM vs. ARXPS), are both lower than the HS/(Mη) predictions for the idealized case (> 1.6 nm.m^2/mg for η < 1). This finding can be attributed to conformation changes of IgG molecules during the adsorption process (reducing vertical extent H of a molecule). Such changes are expected and, in fact, included in the two step mechanism that best describes the immobilization kinetics data (solid line in Figure 3.8b). In turn, the linear regression coefficients determined for the covalently bound proteins are equal to 3.40($\pm$0.13) nm.m^2/mg and 3.41($\pm$0.25) nm.m^2/mg for the analysis using ToF-SIMS and ARXPS results, respectively. They reflect a loosely packed surface structure (packing density $\eta << 1$) that is recorded in the AFM topography micrographs (Figure 3.1b-d).

3.5 Conclusions

To conclude, this study demonstrates the complementarity of AFM, ARXPS and ToF-SIMS methods when biomolecules immobilization onto surfaces is investigated and differences between physical adsorption and covalent binding of proteins are analysed.

Correlation between the scores on PC1, obtained from PCA analysis of ToF-SIMS data, with protein surface density estimated rigorously from ARXPS allowed for quantification of protein amount immobilized to the surface with ToF-SIMS measurements. Moreover, the merged ToF-SIMS and ARXPS data show different immobilization kinetics of the protein immobilization onto the surface by physical adsorption and covalent binding. Kinetics of physical adsorption of IgG molecules is better described by a formula with two exponents, as for two-step adsorption model [7, 44], while kinetics of covalent binding by exponential formula, as for adsorption that limits subsequent covalent binding [42, 43]. Protein surface coverage plotted as a function of incubation time revealed that surface coverage is higher and develops faster for adsorption rather than for covalent binding, in accord with literature [42, 43].

The nanostructure of immobilized proteins observed in AFM micrographs confirms the results obtained from the spectroscopic methods. Furthermore, the correlation between average AFM height and protein surface density obtained from ARXPS or ToF-SIMS data reflect distinct packing and conforma-

tion of IgG molecules depending on the immobilization method, physical adsorption or covalent binding. The adsorbed IgG molecules are more densely packed than the covalently bound ones (what was revealed by AFM micrographs) but their conformation has changed to a more flattened one than that of covalently bound molecules. The presented approach (Figure 3.9) combining AFM, ARXPS and ToF-SIMS yields no readily available information about protein orientation as some ToF-SIMS studies do [15, 51–53]. Instead, it provides an insight into vertical structure in relation to surface coverage of protein overlayer.

Bibliography

[1] Goddard, J. M. and Erickson, D. *Analytical and Bioanalytical Chemistry* **394**(2), 469–479 (2009).

[2] Psarouli, A., Bourkoula, A., Petrou, P., Misiakos, K., Chaniotakis, N., and Kakabakos, S. *Procedia Engineering* **25**, 350–353 (2011).

[3] Williams, E. H., Davydov, A. V., Motayed, A., Sundaresan, S. G., Bocchini, P., Richter, L. J., Stan, G., Steffens, K., Zangmeister, R., Schreifels, J. A., and Rao, M. V. *Applied Surface Science* **258**(16), 6056–6063 (2012).

[4] Awsiuk, K., Bernasik, A., Kitsara, M., Budkowski, A., Rysz, J., Haberko, J., Petrou, P., Beltsios, K., and Raczkowska, J. *Colloids and Surfaces B: Biointerfaces* **80**(1), 63–71 (2010).

[5] Kim, J., Cho, J., Seidler, P. M., Kurland, N. E., and Yadavalli, V. K. *Langmuir* **26**(4), 2599–2608 (2010).

[6] Rabe, M., Verdes, D., Rankl, M., Artus, G. R. J., and Seeger, S. *ChemPhysChem* **8**(6), 862–872 (2007).

[7] Rankl, M., Ruckstuhl, T., Rabe, M., Artus, G. R. J., Walser, A., and Seeger, S. *ChemPhysChem* **7**(4), 837–846 (2006).

[8] Adamczyk, Z., Bratek-Skicki, A., Dąbrowska, P., and Nattich-Rak, M. *Langmuir* **28**(1), 474–485 (2012).

[9] Bagchi, P. and Birnbaum, S. M. *Journal of colloid and interface science* **83**(2), 460–478 (1981).

[10] Serra, J., Puig, J., Martín, A., Galisteo, F., Gálvez, M., and Hidalgo-Alvarez, R. *Colloid & Polymer Science* **270**(6), 574–583 (1992).

[11] Buijs, J., Van Den Berg, P. A. W., Lichtenbelt, J. W. T., Norde, W., and Lyklema, J. *Journal of colloid and interface science* **178**(2), 594–605 (1996).

[12] Buijs, J., White, D. D., and Norde, W. *Colloids and Surfaces B: Biointerfaces* **8**(4-5), 239–249 (1997).

[13] Chen, S., Liu, L., Zhou, J., and Jiang, S. *Langmuir* **19**(7), 2859–2864 (2003).

[14] Lu, B., Smyth, M. R., and O'Kennedy, R. *Analyst* **121**(3), 29R–32R (1996).

[15] Wang, H., Castner, D. G., Ratner, B. D., and Jiang, S. *Langmuir* **20**(5), 1877–1887 (2004).

[16] Buijs, J., Lichtenbelt Th., J. W., Norde, W., and Lyklema, J. *Colloids and Surfaces B: Biointerfaces* **5**(1-2), 11–23 (1995).

[17] Agheli, H., Malmström, J., Larsson, E. M., Textor, M., and Sutherland, D. S. *Nano Letters* **6**(6), 1165–1171 (2006).

[18] Bergkvist, M., Carlsson, J., and Oscarsson, S. *Journal of Biomedical Materials Research - Part A* **64**(2), 349–356 (2003).

[19] Bergkvist, M., Carlsson, J., and Oscarsso, S. *Journal of Physical Chemistry B* **105**(10), 2062–2069 (2001).

[20] Lee, K. ., Park, S. ., Mirkin, C. A., Smith, J. C., and Mrksich, M. *Science* **295**(5560), 1702–1705 (2002).

[21] Ouerghi, O., Touhami, A., Othmane, A., Ben Ouada, H., Martelet, C., Fretigny, C., and Jaffrezic-Renault, N. *Sensors and Actuators, B: Chemical* **84**(2-3), 167–175 (2002).

[22] Young, M. B., Oh, B. ., Lee, W., Won, H. L., and Choi, J. . *Biosensors and Bioelectronics* **21**(1), 103–110 (2005).

[23] Makky, A., Berthelot, T., Feraudet-Tarisse, C., Volland, H., Viel, P., and Polesel-Maris, J. *Sensors and Actuators, B: Chemical* **162**(1), 269–277 (2012).

[24] Coen, M. C., Lehmann, R., Gröning, P., Bielmann, M., Galli, C., and Schlapbach, L. *Journal of colloid and interface science* **233**(2), 180–189 (2001).

[25] Kitsara, M., Petrou, P., Kontziampasis, D., Misiakos, K., Makarona, E., Raptis, I., and Beltsios, K. *Microelectronic Engineering* **87**(5-8), 802–805 (2010).

[26] Ouerghi, O., Touhami, A., Othmane, A., Ben Ouada, H., Martelet, C., Fretigny, C., and Jaffrezic-Renault, N. *Biomolecular engineering* **19**(2-6), 183–188 (2002).

[27] Park, J. W., Min, H., Kim, Y. P., Shon, H. K., Kim, J., Moon, D. W., and Lee, T. G. *Surface and Interface Analysis* **41**(8), 694–703 (2009).

[28] Kim, Y. P., Hong, M. Y., Shon, H. K., Moon, D. W., Kim, H. S., and Lee, T. G. *Applied Surface Science* **252**(19), 6801–6804 (2006).

[29] Ferrari, S. and Ratner, B. D. *Surface and Interface Analysis* **29**(12), 837–844 (2000).

[30] Kim, Y. P., Hong, M. Y., Shon, H. K., Chegal, W., Cho, H. M., Moon, D. W., Kim, H. S., and Lee, T. G. *Applied Surface Science* **255**(4), 1110–1112 (2008).

[31] Wagner, M. S., McArthur, S. L., Shen, M., Horbett, T. A., and Castner, D. G. *Journal of Biomaterials Science, Polymer Edition* **13**(4), 407–428 (2002).

[32] Altankov, G., Richau, K., and Groth, T. *Materialwissenschaft und Werkstofftechnik* **34**(12), 1120–1128 (2003).

[33] Williams, A. R., Douglas, A. D., Miura, K., Illingworth, J. J., Choudhary, P., Murungi, L. M., Furze, J. M., Diouf, A., Miotto, O., Crosnier, C., Wright, G. J., Kwiatkowski, D. P., Fairhurst, R. M., Long, C. A., and Draper, S. J. *PLoS Pathogens* **8**(11) (2012).

[34] Clauss, M. A. and Jain, R. K. *Cancer research* **50**(12), 3487–3492 (1990).

[35] Lv, Z., Wang, J., Chen, G., and Deng, L. *International journal of biological macromolecules* **47**(5), 661–667 (2010).

[36] Kim, J., Seidler, P., Wan, L. S., and Fill, C. *Journal of colloid and interface science* **329**(1), 114–119 (2009).

[37] Luzinov, I., Julthongpiput, D., Liebmann-Vinson, A., Cregger, T., Foster, M. D., and Tsukruk, V. V. *Langmuir* **16**(2), 504–516 (2000).

[38] Howarter, J. A. and Youngblood, J. P. *Langmuir* **22**(26), 11142–11147 (2006).

[39] Strein, E. and Allred, D. *Thin Solid Films* **517**(3), 1011–1015 (2008).

[40] Wagner, M. S. and Castner, D. G. *Langmuir* **17**(15), 4649–4660 (2001).

[41] Wald, J., Müller, C., Wahl, M., Hoth-Hannig, W., Hannig, M., Kopnarski, M., and Ziegler, C. *Physica Status Solidi (A) Applications and Materials Science* **207**(4), 831–836 (2010).

[42] Mateo, C., Torres, R., Fernández-Lorente, G., Ortiz, C., Fuentes, M., Hidalgo, A., López-Gallego, F., Abian, O., Palomo, J. M., Betancor, L., Pessela, B. C. C., Guisan, J. M., and Fernández-Lafuente, R. *Biomacromolecules* **4**(3), 772–777 (2003).

[43] Mateo, C., Fernández-Lorente, G., Abian, O., Fernández-Lafuente, R., and Guisán, J. M. *Biomacromolecules* **1**(4), 739–745 (2000).

[44] Krisdhasima, V., McGuire, J., and Sproull, R. *Journal of colloid and interface science* **154**(2), 337–350 (1992).

[45] Vasina, E. N., Paszek, E., Nicolau Jr., D. V., and Nicolau, D. V. *Lab on a Chip - Miniaturisation for Chemistry and Biology* **9**(7), 891–900 (2009).

[46] Rabe, M., Verdes, D., and Seeger, S. *Advances in Colloid and Interface Science* **162**(1-2), 87–106 (2011).

[47] Silverton, E. W., Navia, M. A., and Davies, D. R. *Proceedings of the National Academy of Sciences of the United States of America* **74**(11), 5140–5144 (1977).

[48] Bano, F., Fruk, L., Sanavio, B., Glettenberg, M., Casalis, L., Niemeyer, C. M., and Scoles, G. *Nano Letters* **9**(7), 2614–2618 (2009).

[49] Chen, A., Kozak, D., Battersby, B. J., Forrest, R. M., Scholler, N., Urban, N., and Trau, M. *Langmuir* **25**(23), 13510–13515 (2009).

[50] Snopok, B., Yurchenko, M., Szekely, L., Klein, G., and Kashuba, E. *Analytical and Bioanalytical Chemistry* **386**(7-8), 2063–2073 (2006).

[51] Lhoest, J. B., Detrait, E., Van Den Bosch De Aguilar, P., and Bertrand, P. *Journal of Biomedical Materials Research* **41**(1), 95–103 (1998).

[52] Tidwell, C. D., Castner, D. G., Golledge, S. L., Ratner, B. D., Meyer, K., Hagenhoff, B., and Benninghoven, A. *Surface and Interface Analysis* **31**(8), 724–733 (2001).

[53] Cho, I. H., Park, J. W., Lee, T. G., Lee, H., and Paek, S. H. *Analyst* **136**(7), 1412–1419 (2011).

Chapter 4

Characterization of biosensor surfaces with protein/amino-organosilane/silicon structure

4.1 Abstract

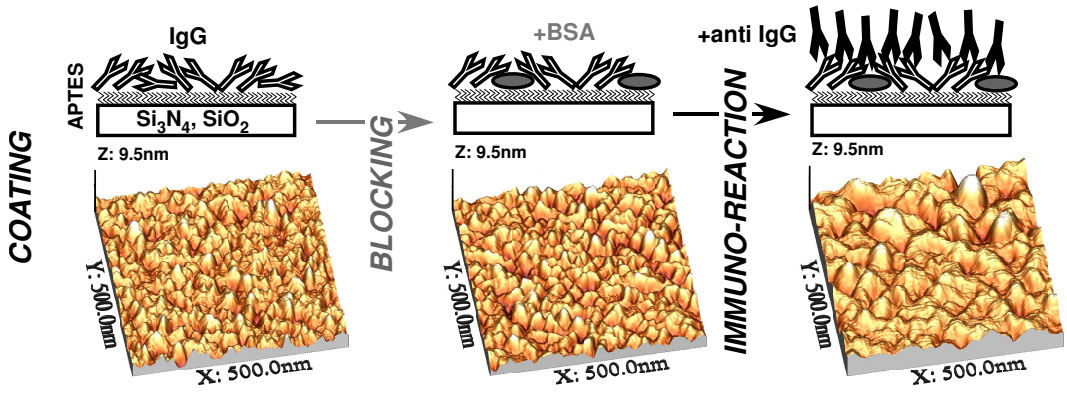

Composition and structure of biorecognition protein layers created on silicon substrates modified with amino-organosilanes determine the sensitivity and specificity of silicon based biosensing devices. In the present work, diverse spectroscopic and microscopic methods were applied to characterize model biosensor surfaces, formed on Si_3N_4 or SiO_2 by modification with (3-aminopropyl)triethoxysilane, coating with rabbit gamma-globulins (IgGs) through physical adsorption, blocking with bovine serum albumin (BSA) and specific binding of an anti-rabbit IgG antibody. In addition, silanized substrates with directly adsorbed BSA or anti-rabbit IgG antibody were examined as reference surfaces. The protein/amino-organosilane/silicon structure of all surfaces was confirmed by X-ray photoelectron spectroscopy. Homogeneity of protein coverage was verified with near-field scanning optical microscope, working in reflection and fluorescence mode. Surface coverage with proteins was determined with angle-resolved XPS using a previously established bilayer approach. Inner structure of protein layers was examined with atomic force microscopy. Vertical arrangement of carbon functional groups was revealed by high resolution ARXPS. Combined spectroscopic and microscopic data reveal the complex character of interactions with the immobilized IgG molecules dur-

ing blocking with BSA and immunoreaction with anti-IgG antibody. Within experimental error, neither surface coverage nor lateral structural scales of protein layer (provided by Fourier and auto-correlation analysis of topographic and phase images) increase during blocking procedure. On the other hand, coverage and all structural measures rise considerably after immunoreaction. In addition, it was found that polar functional groups orient towards substrate for all protein layers, independently of coverage, prior to and after both blocking and specific binding.

Highlights

• Biorecognition protein layers created on silicon modified with amino-organosilanes. • Complex impact of blocking of non-specific binding and immunoreaction with antibody. • Lateral nanostructures not affected by blocking but coarsen due to specific binding. • Protein surface coverage, not increased due to blocking, rises after immunoreaction. • Polar functional groups orient towards substrate for all protein layers.

Keywords

Immunoglobulins; Amino-organosilane films; Specific binding; Angle-resolved X-ray photoelectron spectroscopy; Atomic force microscopy; Near-field scanning optical microscopy

4.2 Introduction

In recent years, silicon-based micro- and nano-fabrication technology has been successfully combined with biochemistry, enabling fabrication of novel biosensing devices with high sensitivity and selectivity. Different sensing principles have resulted in sensors based on different silicon surface geometries, e.g. nanowires [1], nanoparticles [2], ring cavities [3], cantilevers [4], waveguides [5] and porous films [6]. Such surfaces are usually modified with organosilanes carrying chemically active groups [1–6], such as (3-aminopropyl)triethoxysilane (APTES), to provide a suitable interface between silicon-based transducer and immobilized biomolecules. For sensors where the biorecognition molecule is a protein, silicon surfaces with amino-organosilane films should accommodate these molecules in such a way that their functionality is essentially retained since the sensitivity and specificity of biosensor surfaces depends mainly on that. The immobilization of proteins onto these surfaces can be performed either direct by physical adsorption or after some additional functionalization step via covalent bonding. The first approach remains one of the most popular and efficient ways to immobilize proteins onto solid surfaces despite the increasing number of available covalent bonding methods. Therefore, the characterization of silicon surfaces modified with organosilanes prior to and after immobilization of proteins, blocking of free surface sites with a non-functional protein and specific antibody binding is of considerable interest.

The advent and extensions of microscopic and spectroscopic techniques have enabled precise but so far rather selective characterization of protein nanolayers, such as commonly studied immunoglobulins (IgGs), positioned on amino-organosilane films [7–12]. Atomic force microscopy (AFM) has revealed with molecular resolution, that lateral IgG nanostructures are changing due to specific antigen-antibody binding [7]. Several AFM studies have shown that such immunoreaction increases also the vertical extent of the protein/organosilane/silicon structure [8, 9] but the IgG thickness has not been determined since the

tip-scratch method could not be applied to soft substrates [13]. In a previous report, we employed angle-resolved X-ray photoelectron spectroscopy (ARXPS) to determine the amount and thereof the thickness of IgG proteins adsorbed on APTES modified silicon oxide surfaces [11]. As other spectroscopic techniques, ARXPS requires a pre-specified lateral uniformity. The homogeneity of IgG on amino-organosilane spots could be examined with near-field scanning optical microscopy (NSOM) [12], through recording with mesoscopic resolution pairs of topographic and optical (e.g. fluorescence) images at every single surface area. In addition, high resolution ARXPS spectra can reveal preferential orientation of functional groups existing to adsorbed protein molecules towards the substrate [11].

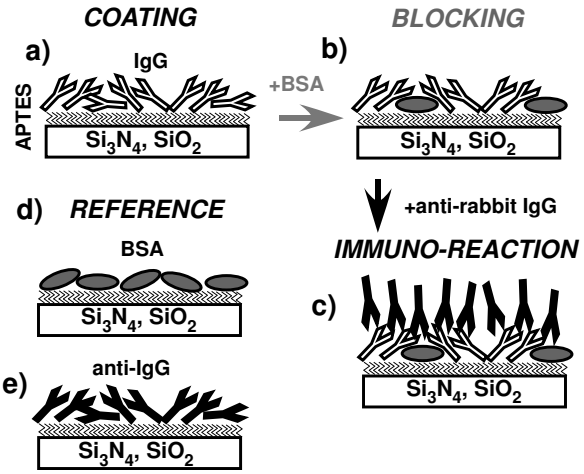

Figure 4.1: Schematic representation of model immunosensor Si_3N_4 or SiO_2 surfaces modified with 3-aminopropyltriethoxysilane (APTES) and additional protein layer films formed by successive steps of coating with rabbit IgG (a), blocking with BSA (b) and specific binding of anti-rabbit IgG antibody (c). Silanized substrates coated with BSA (d) and anti-rabbit IgG antibody (e) are used as reference.

In this Chapter, a complete characterization of model immunobiosensor surfaces with protein/amino-organosilane/silicon structure by implementing several spectroscopic and microscopic techniques is presented. More specifically, the surfaces are characterized with spectroscopic (XPS, ARXPS) and microscopic (NSOM, AFM) techniques to determine mesoscopic homogeneity, total protein coverage (thickness), lateral nanostructures, and vertical arrangement of functional groups. In addition, lateral structural scales are determined with auto-correlation and Fourier analysis from AFM data independently from topographic and phase images. All these different features were determined for two types of silicon substrates (SiO_2, Si_3N_4) modified with APTES, prior to and after the successive steps of immobilization of rabbit gamma globulins (IgGs), blocking and reaction with an anti-species specific antibody (Figure 4.1), in order to mimic the creation of protein layers on a silicon transducer surface during immunoreaction. The impact of blocking and specific antibody binding on the molecular arrangement and makeup of adsorbed protein layers is explicitly discussed.

4.3 Materials and methods

4.3.1 Preparation of biosensor surfaces

The substrates used are silicon wafers purchased from Montco Silicon Technologies, Inc. (Spring City, PA, USA). Silicon oxide surfaces were obtained by low pressure chemical vapour deposition of a 1000 nm thermally grown silicon dioxide layer, whereas through an additional deposition of a 150 nm thick silicon nitride layer the Si_3N_4 surfaces were obtained. The amino-organosilane and proteins used to modify both silicon oxide and silicon nitride surfaces were purchased from Sigma Chemical Co., St. Louis, MO, USA. Cleaning and hydrophilization of the substrates were performed with oxygen plasma (using a reactive ion etcher) applied for 30 s under pressure of 10 mTorr and power of 400 W. The hydrophilized surfaces were then immersed in an 0.5% (v/v) 3-aminopropyl(triethoxysilane) (APTES) solution in distilled water for a 2 min, gently washed with distilled water and cured at 120 °C for 20 min.

Model immunosensor surfaces were prepared in successive steps as follows: (a) coating with IgG through incubation with a 0.66 μM rabbit gamma-globulins solution in 0.05 M phosphate buffer, pH 7.4, for 1 h at room temperature (RT), followed by washing with 0.05 M phosphate buffer, pH 7.4, and distilled water, and drying under nitrogen stream; (b) blocking of free-protein binding sites of the surface via immersion in a 10 mg/ml bovine serum albumin (BSA) solution in 0.05 M phosphate buffer, pH 7.4 (blocking solution), for 1 h at RT, followed by washing and drying as described above; (c) immunoreaction through incubation for 1 h with a 0.33 μM solution of anti-rabbit IgG antibody in 0.05 M phosphate buffer, pH 7.4, containing 10 mg/ml BSA, followed by washing with 0.05 M phosphate buffer, pH 7.4, containing 0.05% (v/v) Tween 20, distilled water and drying under nitrogen stream. In addition, reference immunosensor surfaces were obtained by incubating the silanized with APTES substrates with the blocking or anti-rabbit IgG antibody solution following the procedures and conditions described above.

4.3.2 Microscopic surface characterization

The optical properties of the model immunosensor surfaces at mesoscopic scale were analysed in air at room temperature using a MultiView 1000 (Nanonics Imaging Ltd., Jerusalem, Israel) microscope with a reflection NSOM set up. The surfaces were illuminated with a laser light (473 nm) using a commercial (Nanonics) metal-coated fiber probe (nominal apical aperture of 100 nm) attached to a quartz tuning fork, which controlled the probe-surface distance. NSOM topographic images were recorded simultaneously with the maps of optical signal. Reflected light was collected by standard objective lens (in far-field region) and then was driven to a photodetector. In addition, when the anti-rabbit IgG antibody used to detect the adsorbed IgGs was labelled with the fluorescent dye AlexaFluor488, the light collected was filtered with the Olympus barrier filter BA515 placed in front to the photodetector. The maps of optical signal were considered meaningful only when the average intensities were higher than 100 Hz (counts per second).

AFM imaging of the model immunosensor surfaces was performed at ambient conditions (air, room temperature) with MultiView 1000 (Nanonics) and Agilent 5500 microscopes working in non-contact mode. The set point and gains were adjusted to obtain minimal noise and clear image of the analysed surface. For each sample, topography and phase images were acquired simultaneously at several different randomly

chosen locations.

Root-mean-square (RMS) roughness was determined from AFM images using the software provided along with the AFM instruments, but also using the WSxM free software [14] (downloadable at http://www.nanotec.es). For each sample its deviations from flat surface were characterized by the mean RMS value, averaged from 4 to 7 topographic micrographs. When the average RMS roughness was larger than 0.4 nm, then meaningful radially averaged autocorrelation function could be computed for the analysed surface. This function was expressed by the double value of its width-at-half-maximum (2whm), which can be considered as a measure for the lateral extent of surface features. In addition, their 2-dimensional fast Fourier transforms (FFTs) were calculated from both topographic and phase images. The reversal of wave vector at the maximum of radially averaged FFT spectra (1/k) was taken as a characteristic lateral scale of surface structures visible in topographic or phase images.

4.3.3 Spectroscopic surface characterization

XPS measurements were performed using a VSW Manchester spectrometer with Al Kα radiation (1486.6 eV, 200 W). Angle-resolved XPS spectra were collected for three values of photoelectron take-off angle Θ equal to 0°, 60° and 70°. The operating pressure in the analytical chamber was less than 5×10^{-8} mbar. All XPS peaks were charge referenced to the neutral (C-C) carbon C1s peak at 284.6 eV. Spectrum backgrounds were subtracted using the Shirley method.

The bilayer model used to determine the thickness of APTES film and the amount (thickness) of immobilized proteins has been described in details in Section 2.2.3.3.2 and a previous publication [11].

4.4 Results and discussion

Spectroscopic and microscopic characterization of model immunosensor surfaces (Figure 4.1) is performed from different viewpoints. First, the protein/amino-organosilane/silicon structure is verified with XPS (Section 4.4.1). Second, the uniformity of immobilized protein overlayers is examined with NSOM (Section 4.4.2). Third, a multilayer extension of ARXPS data analysis is applied to quantify the amount of proteins immobilized after the different steps providing insight about the surface coverage in Section 4.4.3. Forth, lateral nanostructures in protein overlayers are examined with AFM (Section 4.4.4). And finally, vertical arrangement of functional carbon groups is determined for all protein layers through analysis with high resolution ARXPS in Section 4.4.5.

4.4.1 Protein/amino-organosilane/silicon structure confirmed by XPS

General analysis of photoelectron spectra is a preliminary step to characterize the model immunosensor surfaces after the successive steps, i.e., modification with APTES, coating with rabbit IgG, blocking with BSA and immunoreaction with anti-rabbit IgG antibody. A particularly distinct analysis of these model surfaces is provided by high resolution XPS for the silicon nitride substrates in Figure 4.2. In this case, the high resolution XPS spectra of N 1s core-level consist of the signals characteristic for the Si_3N_4 substrate (binding energy of 397.5 eV) but also for amine (NH_2, 399.8 eV) and protonated amino groups (NH_3^+, 401.4 eV).

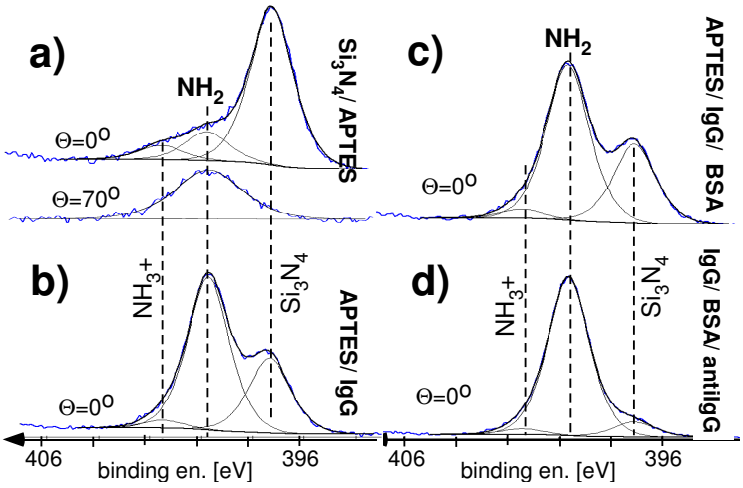

Figure 4.2: Vertical composition of model immunosensor Si_3N_4 surfaces analysed with X-ray photoelectron spectroscopy. N1s core-level XPS spectra recorded with photoelectrons sampling 8 nm thick regions of analysed surfaces (sampling vertical depth is reduced to 2.7 nm for take-off angle $\Theta = 70°$ rather than 0°). Distinct contributions from Si_3N_4 substrates and from amine (NH_2 and protonated NH_3^+) groups are visible, characteristic for APTES films (a) and for protein overlayers formed due to successive steps of coating with rabbit IgG (b), blocking with BSA (c), and specific binding of anti-rabbit IgG antibody (d).

Silicon surface modification with APTES is performed mainly via APTES hydrolysis followed by surface condensation reaction with the hydroxyl groups of the hydrophilized silicon surfaces, resulting in a film with short APTES hydrocarbon chains terminated with NH_2 groups which point away from the surface siloxane network [15, 16]. Attached APTES brushes with such an orientation are characterized by the NH_2 signal in XPS spectra [17, 18]. An alternative although less effective coupling mechanism is driven by protonated amino groups pointing towards (charged) silicon [15]. This leads to APTES attachment with reversed orientation (amino groups directed to the surface), manifested in XPS spectra as NH_3^+ signal [17, 18]. The contributions from NH_2 and NH_3^+, although less pronounced, are visible in the XPS spectrum in addition to the dominant Si_3N_4 line taken for photoelectron take-off angle $\Theta = 0°$ (upper envelope in Figure 4.2a). However, for $\Theta = 70°$ the sampling vertical depth 3 λ cosΘ of N 1s photoelectrons is reduced from 8 to 2.7 nm. In this case, the resulting spectrum (lower envelope in Figure 4.2a) shows dominant APTES line with amine groups oriented away from the substrate, and negligible contributions from both the silicon nitride substrate and APTES from reversed orientation (NH_3^+).

The subsequent protein adsorption and detection steps applied to silanized substrate which lead to the creation of protein overlayer, are reflected in the increased contribution of amine groups in the N1s core-level XPS spectra at expense of reduced Si_3N_4 and NH_3^+ lines, corresponding exclusively to the substrate and the APTES film (compare Figure 4.2a and Figure 4.2b-d). Therefore, the creation of protein/APTES/silicon structure on the examined silicon surfaces is confirmed.

Moreover, the high resolution N1s core-level XPS spectra allow for a preliminary comparison of the coated surfaces prior to and after blocking and specific antibody binding. The relative contribution of the NH_2 line attributed mainly to protein attachment to the surface is slightly reduced due to blocking with

BSA, whereas the Si_3N_4 signal is somewhat more pronounced in Figure 4.2c than in Figure 4.2b. This suggests the blocking procedure can have a more complex effect on the surface and the already immobilized proteins than the anticipated coverage of the free binding sites of the surface. In contrast, the line from amine groups is considerably increased and the nitride substrate signal diminished in Figure 4.2d as compared to Figure 4.2c, indicating that the immunoreaction had a great impact onto the surface composition as it was expected from the fact that it leads to the creation of a second protein layer.

4.4.2 Uniformity of protein overlayers examined with NSOM

Simultaneous collection of topography and optical signal maps, both with high spatial resolution, is the main advantage of surface analysis by NSOM providing a new insight into local arrangement of biomolecules on soft organic substrates [12, 19, 20]. In the used NSOM set up (see Figure 2.5), the intensity of light reflected from the analysed surface was recorded along with topography as a function of tip position. The surface was 'illuminated' locally with laser light through the scanning NSOM probe with 100 nm aperture, which was kept within a small, sub-wavelength distance from the sample (near field zone), with the distance controlled by a tuning fork. The scanned intensity of light corresponds to the complete spectrum emitted from the analysed surface ('reflection' mode, Figure 2.5a) or to the fluorescence signal of AlexaFluor488 labels attached onto the immobilized anti-rabbit IgG antibody ('fluorescence' mode, Figure 2.5b).

Two representative pairs of topography micrographs and scanned intensity maps of 'reflection' spectrum are shown in Figure 4.3 for the Si_3N_4 surfaces after coating with IgG (Figure 4.3a and b) and blocking and specific antibody binding (Figure 4.3c and d). A uniform spatial distributions of light intensity recorded with mesoscopic NSOM resolution, with image-averaged values (and standard deviations) of 172($\pm$81) kHz (Figure 4.3b) and 228($\pm$50) kHz (Figure 4.3d) were determined, which corresponds to relatively small surface height fluctuations with RMS roughness of 0.3 nm (Figure 4.3a) and 0.7 nm (Figure 4.3c), respectively. Since APTES layers on silicon surfaces are homogeneous and their surfaces are featureless [9, 11], the results of Figure 4.3a-d indicate the uniformity of protein overlayers. Such a conclusion is confirmed also by the NSOM results obtained in the 'fluorescence' mode. A pair of topography and scanned intensity map of 'fluorescence' spectrum is presented in Figure 4.3e-f for the silanized silicon surface after subsequent exposure to the solutions of rabbit IgG, BSA and anti-rabbit IgG antibody, the later labelled with the fluorescent dye AlexaFluor488. The pair of images shows a uniform film with a singular protein cluster [11] (the left-lower corner in Figure 4.3e-f), used as a focal point. Except for this region, the fluorescent light intensity is homogeneous with an image-averaged value equal to 612($\pm$178) Hz. This verifies uniformity of (fluorescently labelled) anti-IgG molecules after immunoreaction.

To conclude, NSOM data confirm the uniformity of protein layers, a prerequisite in order to apply the bilayer extension of ARXPS data analysis to determine the surface coverage with proteins.

4.4.3 Surface coverage with proteins determined with ARXPS

Protein coverage of silicon surfaces modified with APTES can be determined by analysis of ARXPS data using the aminosilane-organic bilayer model. Protein coverage or protein surface density can be ex-

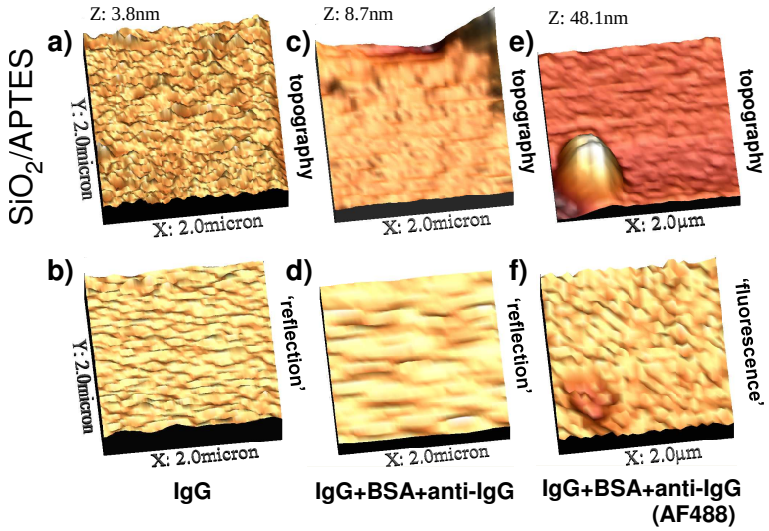

Figure 4.3: Uniformity of surface coverage with proteins determined by NSOM. Pairs of topography and light intensity maps (the latter corresponding to reflection or fluorescence spectrum) acquired for SiO_2 substrates modified with APTES and coated with rabbit IgG prior to (a and b) and after blocking and specific binding of anti-rabbit IgG antibody unlabelled (c and d) or labelled with AlexaFluor488 (e and f).

pressed, after being multiplied by the protein partial specific volume (0.73 cm^3/g), by the thickness d of equivalent protein layer, assuming that the protein is uniformly distributed rather than localized in close packed molecular spheres or ellipsoids [21]. It is this equivalent protein layer that justifies effective attenuation of photoelectrons, and therefore d can be considered as XPS thickness of protein layer.

4.4.3.1 ARXPS data analysis with bilayer model

The protein/APTES/silicon structure is described by the aminosilane-organic bilayer model, depicted in the inset to Figure 4.4. The photoelectrons from amine (NH_2, 399.8 eV) and protonated amino groups (NH_3^+, 401.4 eV) of the N1s core-level are taken as characteristic for both the APTES film and protein layer, with thickness D and d, respectively, and stoichiometric molar fraction of the atoms emitting characteristic XPS lines Z_{APTES} and Z_{Nami}, respectively. In turn, the photoelectrons from the Si2p core-level (101.3-102.7 eV) characterize the silicon substrate with stoichiometric Si molar fraction Z_{Si}.

As value for the molar fraction Z_{Nami} for all proteins, the atomic concentration (11.0%) determined from XPS analysis of the bulk rabbit IgG material is taken [11]. This assumption seems reasonable for several reasons. First, the anti-rabbit IgG antibody should have similar composition as IgG. Second, the rabbit IgG (and anti-rabbit IgG antibody) molecules constitute the main component of analysed protein layers. Third, the thickness of directly adsorbed BSA layer (reference) is statistically the same, when the bulk atomic concentration of BSA rather than of IgG is taken for the calculation of Z_{Nami} stoichiometry. The respective molar fractions for APTES and silicon substrate were determined from concentrations of constituent atoms using ARXPS data for the silanized substrates with no protein overlayers, averaged for Θ angles between 0° and 70° [11]. This approach yields values of Z_{APTES} =5.4($\pm$1.2)% and Z_{Si} =31.2($\pm$0.6)% for silanized Si_3N_4, and of Z_{APTES} =2.6($\pm$0.4)% and Z_{Si} =32.5($\pm$1.4)% for silanized SiO_2. Low Z_{APTES}

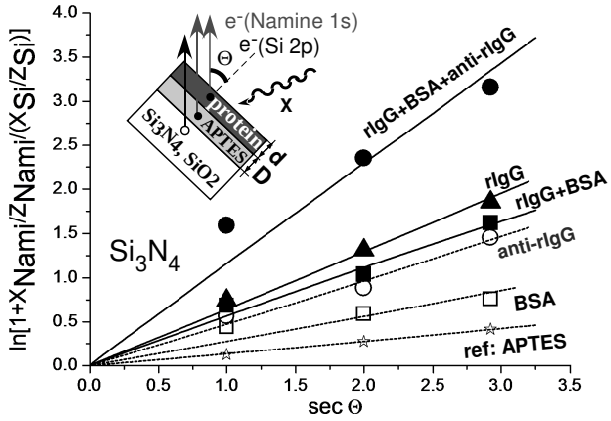

Figure 4.4: Multilayer structure (see inset) of model immunosensor surfaces characterized with angle-resolved XPS. The ratio of normalized intensities of the photoelectrons characteristic for APTES film with protein overlayer (N1s from NH_2 and NH_3^+, see Figure 4.2) created on a Si_3N_4 substrate (Si2p) is plotted versus the take-off angle function $\sec\Theta$. The slopes of lines result from regression fitting of individual points and provide the XPS thickness of APTES film and protein overlayer (D and d, respectively, marked in the inset). The inset presents the model used to evaluate the ARXPS data for both Si_3N_4 and SiO_2.

values, different for the silicon substrate surfaces, are ascribed to the presence at various amounts of adventitious carbon incorporated in the APTES films [16, 22]. The Z_{Si} estimations are reasonable since the values accord with, for the SiO_2 substrate, or are close to, for the Si_3N_4 substrate, the nominal stoichiometry of SiO_2 surface (33.3%). In the case of Si_3N_4 it is expected that oxygen plasma treatment [23] and subsequent silanization in aqueous solution [24] result in simultaneous disappearance of Si-N and increase of Si-O functionality in a nanolayer adjacent to the surface. Formation of such a layer is confirmed by vanishing contribution of Si_3N_4 to the N1s core-level spectrum for photoelectron sampling depth reduced below 4 nm (i.e., for take-off angle $\Theta \geq 60°$, see Figure 4.2a). This is why the stoichiometry of the Si_3N_4 substrate determined with ARXPS resembles that of SiO_2 surface.

The normalized photoelectron intensities X_i are calculated using the equation (2.5) specified by photoionization cross-sections σ_i [25] and attenuation lengths λ_i [26]. The structural features of the protein/APTES/silicon multilayers are revealed by the ratio of X_i of the photoelectrons (see Figure 2.7 and inset to Figure 4.4) characteristic for APTES film with protein overlayer (N1s from NH_2 and NH_3^+, element A) and for silicon substrate (Si2p, element B), calculated by the formula:

$$\frac{X_{Nami}(\Theta)/Z_{Nami}}{X_{Si}(\Theta)/Z_{Si}} = \frac{\left[1 - exp\left(\frac{-d\sec\theta}{\lambda_{Nami}}\right)\right] + \left(\frac{Z_{APTES}}{Z_{Nami}}\right)\left[1 - exp\left(\frac{-D\sec\theta}{\lambda_{Nami}}\right)\right]\left[exp\left(\frac{-d\sec\theta}{\lambda_{Nami}}\right)\right]}{exp\left(\frac{-D\sec\theta}{\lambda_{Si}}\right) exp\left(\frac{-d\sec\theta}{\lambda_{Si}}\right)} \quad (4.1)$$

for bilayer model (see also Section 2.2.3.3.2) .

The ratio of photoelectron intensities is usually plotted in a rearranged logarithmic form versus the take-off angle function $\sec\Theta$, as it is shown in Figure 4.4. There are two reasons for this. First, the slope of the rearranged formula depends on the total bilayer thickness (D with d). Second, the theoretical (nearly linear) regression fitting of the data in such plots must always start at the origin of coordinate axes, therefore limiting the number of independent data point required. The thickness D of the APTES film was determined

in separate ARXPS measurements performed for the two types of silanized silicon surfaces, for SiO_2 was D=0.8 nm and for Si_3N_4 D=0.7 nm. These D values are typical for monomolecular APTES film [15]. With the D values known, the XPS thickness d of protein overlayer remains the only structural fitting parameter of Equation (2.9).

4.4.3.2 Determination of protein coverage

The ARXPS data, shown in Figure 4.4 for the Si_3N_4 surfaces, were fitted with Equation (2.9) to yield the values of the XPS protein thickness d. The resulting d values are represented as surface coverage of protein layer for silanized Si_3N_4 and SiO_2 in Figure 4.5a and b, respectively.

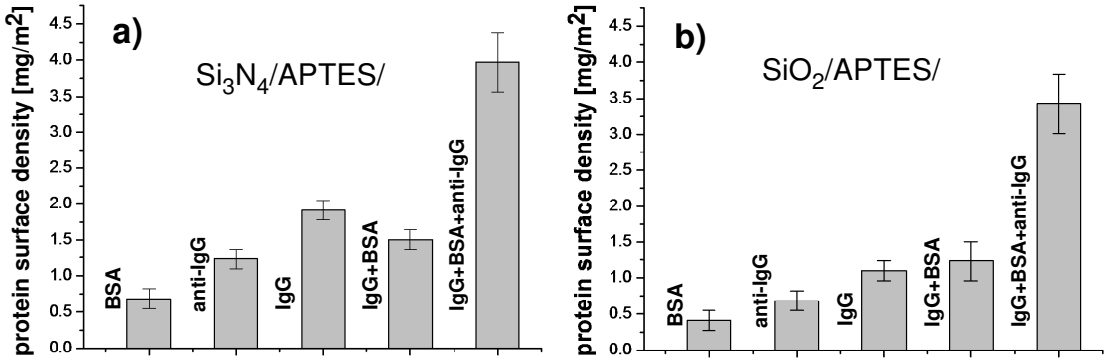

Figure 4.5: Protein surface coverage determined from ARXPS data, obtained from silanized Si_3N_4 (a) and SiO_2 (b) substrates coated with BSA or anti-rabbit IgG antibody (reference surfaces) or rabbit IgG. The latter surfaces were blocked with BSA, and reacted with anti-rabbit IgG antibody (model immunosensor surfaces). Error bars are given by the fitting procedure described in Figure 4.4.

The exposure of the silanized and IgG coated Si_3N_4 surface to the BSA solution results in a slight decrease of protein surface coverage from 1.9($\pm$0.1) mg/m^2 to 1.5($\pm$0.1) mg/m^2 (Figure 4.5a). This suggests not only adsorption of BSA molecules to the surface sites remaining free after IgG adsorption, but also partial exchange of some loosely bound IgG globulins with BSA molecules, which are smaller (with dimensions 14 nm $\times$ 4 nm $\times$ 4 nm [27] compared with 14.5 nm $\times$ 8.5 nm $\times$ 4 nm [8] for IgG). Thus after blocking the protein thickness (coverage) of silanized Si_3N_4 surfaces decreases compared to that prior to blocking (see Figure 4.5a). Such conclusion is in accord with the results for the SiO_2 series (see Figure 4.5b), with surface coverage of 1.1($\pm$0.1) mg/m^2 and 1.2($\pm$0.3) mg/m^2 prior to and after, respectively, the blocking procedure. In this case, the combined result of covering the free surface sites with BSA and remove of loosely adsorbed IgG molecules leads to statistically indistinguishable protein layer thickness prior to and after blocking.

In contrast to marginal increase or decrease in protein coverage of the IgG coated silicon surfaces, resulting from blocking procedure, their subsequent exposure to the anti-rabbit IgG antibody solution induces a dramatic ($\sim$270% in average) increase in protein coverage reaching the value of 4.0($\pm$0.4) mg/m^2 for the Si_3N_4 surface (Figure 4.5a) and of 3.4($\pm$0.4) mg/m^2 for the SiO_2 surface (Figure 4.5b). This implies

an increase in surface coverage of 2.5($\pm$0.5) mg/m^2 and 2.2($\pm$0.7) mg/m^2 for the Si_3N_4 and SiO_2 surfaces, respectively, when the anti-rabbit IgG antibodies bind to already adsorbed rabbit IgG. On the other hand, the direct adsorption of the anti-rabbit IgG antibody resulted in an average coverage of 1.2($\pm$0.1) mg/m^2 and 0.7($\pm$0.1) mg/m^2 for the Si_3N_4 and SiO_2 surfaces, respectively, that are comparable with the values determined for the adsorbed rabbit IgG. This difference can be ascribed to the fact that the directly adsorbed molecules undergo structural deformation during the adsorption process leading to "flattening" of the molecules as compared to their shape in solution. The anti-rabbit IgG molecules, however, retain their natural size to a greater extent since they do not interact directly with the solid surface.

To evaluate additionally how the blocking procedure modifies the exposure of IgG-covered surfaces to anti-IgG antibody solution we have performed test experiments for silanized SiO_2 substrates: They showed an increase in protein surface coverage of $\sim$3.4 mg/m^2 for the non-blocked IgG layers exposed to anti-IgG antibody, as compared to the increase of 2.2 mg/m^2 observed for the IgG-covered surface blocked with BSA. This shows that blocking is inevitable to separate immunoreaction from adsorption.

The Si_3N_4 and SiO_2 substrates have similar final surface composition, as revealed by ARXPS (Section 4.4.3.1). However, their silanization, although performed at identical conditions, resulted in APTES films with different composition. Results suggest that the protein coverages of the silanized Si_3N_4 surfaces are slightly but systematically larger that those of the silanized SiO_2 substrates (cf. relevant columns in Figure 4.5a and b). This is induced by somewhat different composition of APTES film created on these surfaces, as suggested by the higher Z_{APTES} fraction value for the Si_3N_4 surfaces rather than for the SiO_2 ones. The composition impact of APTES film on protein surface density has been confirmed in additional experiments. The silanized Si_3N_4 substrates with reduced Z_{APTES} value ($\sim$1.7%) exhibited protein coverage comparable to that observed for SiO_2.

4.4.4 Lateral structure of protein overlayers examined with AFM

While the overall uniformity of protein layers was indicated by NSOM microscopy (Section 4.4.2), their inner structure is revealed by AFM. Representative topography micrographs of the model immunosensor surfaces created on silanized SiO_2 and Si_3N_4 substrates after coating with IgG, blocking with BSA and binding of anti-rabbit IgG antibody are presented in Figure 4.6. The structure of protein overlayer can be described as a random set of surface features, with specified average feature size and average distance between the features. Apparent IgG molecule radius of 23.5 nm [28] or 18 nm [7] is predicted due to broadening caused by AFM tip (with 20 nm radius) for assumed spherical or half-spherical, respectively, shape of adsorbed IgG globulin with 'real' radius of 7 nm. In turn, intermolecular spacing of about 17 nm or 23 nm is suggested by surface coverage data for the SiO_2 or Si_3N_4 surfaces, respectively, assuming a value of 2.5×10^{-16} mg for the weight of single IgG molecule and an idealized hexagonal molecular arrangement.

The inner structure, visible in AFM images, can be also expressed by the mean value of root mean square (RMS) roughness of the surfaces. Even such a simple measure can reveal interesting features. In particular, for both substrate types, the RMS roughness is statistically not affected by blocking procedure but only by immunoreaction as it is shown in Figure 4.6. A closer look at Figure 4.6a-c and Figure 4.6d-f confirms this observation with respect to both the average size of surface feature as well as to the typical

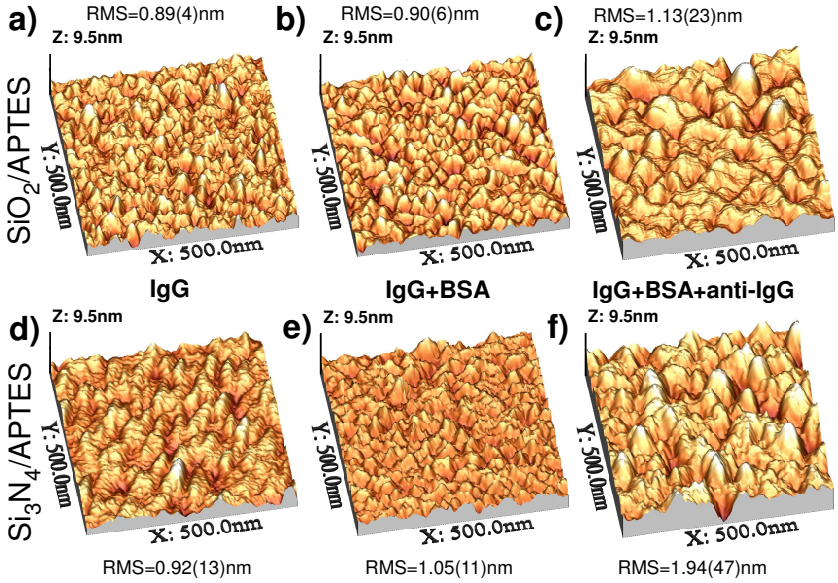

Figure 4.6: Lateral topographic structure of protein layers determined with AFM for silanized SiO_2 (a-c) and Si_3N_4 (d-f) substrates after coating with rabbit IgG (a and d), blocking with BSA (b and e), and specific binding of anti-rabbit IgG antibody (c and f). RMS roughness error limits are standard deviations, each determined from 5 images of the same surface.

distance between the features.

To determine quantitatively the impact of blocking and specific binding on the inner structure of protein overlayer we have applied autocorrelation and Fourier analysis to the AFM data obtained from the SiO_2 surfaces (see Section 2.2.1.1 for details). The double-value of the width at half-maximum, 2whm, of radial averaged autocorrelation provides a measure of the size (extent) of topographic surface feature (Figure 4.7a). In turn, reversal of wave vector at maximum, (1/k), of radial averaged power spectrum provides a measure of the distance between the features observed in the topography (Figure 4.7a) and phase (Figure 4.7b) AFM images. The determined values of lateral scales of protein overlayer inner structure are presented in Figure 4.7c. All three structural measures show the same effect of blocking and immunoreaction steps on the inner structure of the adsorbed IgG layer. Within error bars, they are hardly affected by the blocking procedure but are considerably increased by the specific antibody binding.

Let analyse in details the lateral scales presented in Figure 4.7. The 2whm extent of topographic features of immobilized IgG (16-19 nm) accords with apparent radius of IgG molecule (18-23.5 nm). However, the characteristic scales (1/k) of phase (28-25 nm) and topographic (55-65 nm) structures of immobilized IgG are somewhat larger than the spacing (17 nm) suggested by surface coverage data. In addition, the Fourier lengths from topography are twice larger than those from phase micrographs. This suggests that topography AFM images show modulated height of random surface arrangements of immobilized IgG molecules.

Hardly any effect on the three lateral structural scales due to blocking was observed. This can be ascribed to the fact that during this step apart from adsorption of BSA molecules to the free surface sites partial exchange of BSA and IgG molecules also occurs (comparable in size except for one dimension [8,

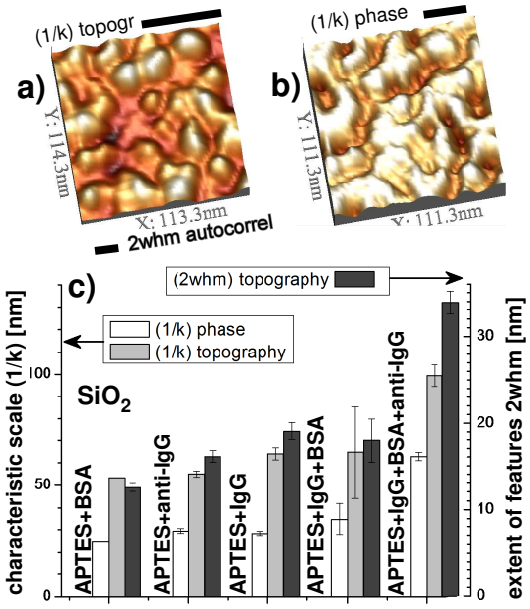

Figure 4.7: Topography (a) and phase (b) AFM micrographs of protein overlayers on silanized SiO_2 (illustrated after coating with anti-rabbit IgG antibody) and (c) characteristic scale of surface structures, (1/k) (left axis, open and gray columns), determined by Fourier analysis (reversal of wave vector at maximum of radial averaged power spectrum), and spatial extent of topographic surface features, 2whm (right axis, dark grey columns), calculated by autocorrelation analysis (double-value of width at half-maximum of radial averaged autocorrelation). Error bars are standard deviations, each determined from 5 images.

27]), as it was concluded in the discussion of surface coverage data (Section 4.4.3.2). In contrast, the specific binding of anti-rabbit IgG antibodies to the immobilized rabbit IgG molecules induces a dramatic rise in all structural scales: the size, expressed by 2whm, was increased by ∼190% and the distance (1/k) between the surface features by ∼165%. These values can be considered along with the even larger increase in surface coverage by proteins by ∼280%. A distinct increase upon immunoreaction of the size of the surface features has been reported recently for a human IgG/anti-human IgG antibody interaction [7]. In our case, comparison of the changes in both vertical (surface coverage) and lateral (2whm, 1/k) features magnitude allows an additional insight. The rise in the surface coverage and in the size 2whm of surface features reflects formation of antigen-antibody complexes, but these complexes are not formed homogeneously across the surface since the distance (1/k) between the surface features also increases. This might be due to the fact that some surface features correspond to BSA rather than IgG molecules. Thus, the anti-rabbit IgG binding to the immobilized IgG molecules occurs in a cluster like way rather than as a homogeneous layer across the surface. This finding is in accordance with the observations of other investigators concerning the creation of “protein islands” during adsorption of IgG molecules onto solid surfaces [29]. In addition, IgG can receive a variety of orientations during their adsorption onto a surface leading to variations in protein layer thickness across the surface [30, 31]. Thus, the calculated coverage of SiO_2 (1.1($\pm$0.1) mg/m^2) and Si_3N_4 (1.9($\pm$0.1) mg/m^2) with immobilized IgG can be compared with the values of 10.1, 5.6 and 2.8 mg/m^2 for the areas covered by singular IgG globulins with head-on, end-on and side-on orientation, respectively.

This suggests an immobilized IgG side-on orientation without, however, excluding head-on and end-on orientation at least to some extent.

4.4.5 Vertical arrangement of polar functional groups revealed by ARXPS

Previously preferential orientation of specific (polar carbon) functional groups towards silicon (SiO_2, Si_3N_4) substrates modified with APTES, observed with XPS and ARXPS for the adsorbed layers of rabbit IgG has been reported [11]. Here this aspect is examined for all model immunosensor surfaces (Figure 4.1). Especially helpful is the analysis of high-resolution ARXPS spectra of the same core-level, where different peaks that correspond to the same element in various functional groups might contribute to a different extent when analysed as a function of photoelectron take-off angle Θ. Such an analysis is performed for the C1s core-level spectra, and illustrated in Figure 4.8 for the model immunosensor surfaces formed by adsorbing rabbit IgG on silanized Si_3N_4, after blocking with BSA (Figure 4.8a and b) and subsequent specific binding of anti-rabbit IgG antibody (Figure 4.8c and d). The C1s envelope can be resolved into four contributions referred to neutral carbon (C-C) at 284.6 eV and three peaks with modified electron environment positioned at 282.1 eV (C-Si), 286.0 eV (C-O, C-N) and 287.9 eV (C=O, NC=O). When the take-off angle Θ is increased from 0° to 70°, then the contribution of polar O- and N-containing carbon groups to the C1s envelope is visibly reduced in both cases (Figure 4.8a, b and c, d).

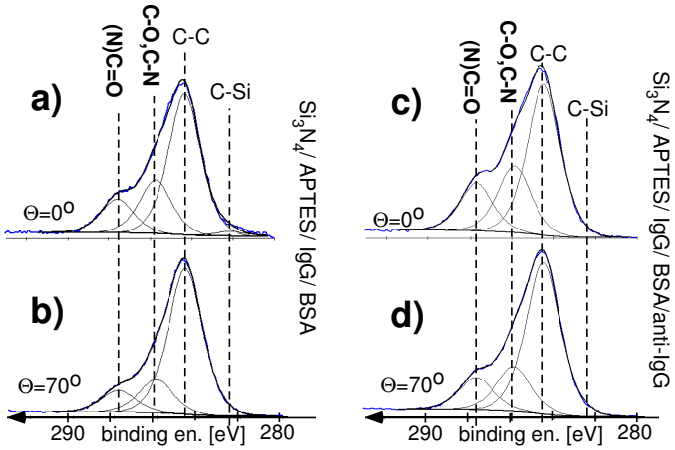

Figure 4.8: Vertical arrangement of functional groups analysed with angle-resolved XPS. C1s core-level spectra recorded from model immunosensor surfaces with photoelectrons with sampling vertical depths of 8.7 nm and 3.0 nm for take-off angle $\Theta = 0°$ and 70°, respectively. Distinct contributions of polar, NC=O and C-O or C-N, and non-polar, C-C and C-Si, carbon groups are visible. Representative data (a and b) and (c and d) correspond to situations in Figure 4.2c and d, respectively. XPS intensities were rescaled to their maximal values to enable easier comparison between different contributions.

The effect manifested in Figure 4.8 is expressed quantitatively in the form of fractional contribution of polar (O- and N-containing) carbon groups to total carbon concentration determined for two take-off angles $\Theta = 0°$ and 70°, and plotted in Figure 4.9 for all model immunosensor Si_3N_4 surfaces as a function of their protein layer XPS thickness d. Consistent decrease in the abundance of polar carbon groups, observed for each d value when the vertical sampling depth is reduced (higher Θ), indicates that the polar groups are

always located preferentially closer to the silanized silicon substrate (see inset to Figure 4.9). The solid lines sketched in Figure 4.9 are a guide to eye and reflect merely photoelectron attenuation modified by XPS thickness of protein layer.

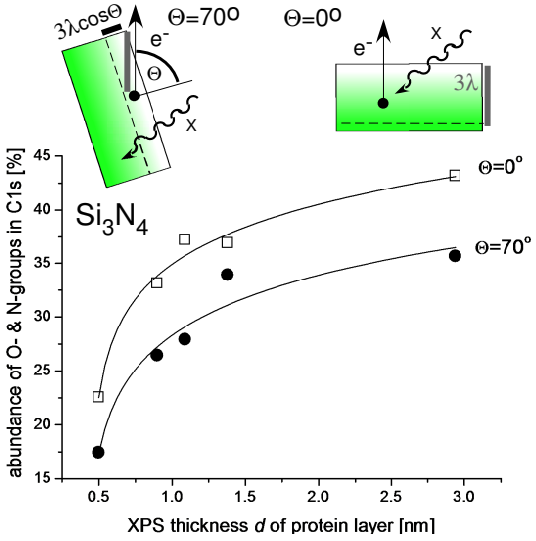

Figure 4.9: Fractional contribution of O- and N-containing carbon polar groups to total carbon concentration determined for silanized Si_3N_4 substrate as a function of XPS thickness d of protein overlayer. Comparison of the data obtained for photoelectron take-off angle $\Theta = 0^\circ$ (open square, higher sampling depth) and 70° (solid circle) indicates that the polar groups (shaded areas in the inset) are located preferentially closer to the substrate. The solid lines are a guide to eye.

The results presented in Figure 4.9 accord with previous observations of substrate-directed orientation of specific functional groups, which is preserved for the same protein independently of the surface coverage [32,33]. As a completely novel observation, the data in Figure 4.9 show that the orientation effect is not only independent of surface coverage, but it is also visible prior to and after both blocking and specific antibody binding. These observations are not unexpected, since the preferential orientation of polar functional groups towards polar substrate is observed for adsorbed rabbit IgG and BSA, then it should be also preserved during adsorption phenomena taking place during blocking of the IgG coated surfaces with BSA [34,35]. Similarly, the preferential orientation, observed for adsorbed rabbit IgG and anti-rabbit IgG antibody, should prevail in the immunocomplexes of rabbit IgG with anti-rabbit IgG antibodies.

4.5 Conclusions

To conclude, combined spectroscopic (XPS, ARXPS, high-resolution ARXPS) and microscopic (AFM, NSOM) analysis has enabled complete characterization of the model immunosensor surfaces (Figure 4.1), created by adsorption of a protein/antigen (rabbit IgG) on silicon surfaces (SiO_2, Si_3N_4) previously modified with an amino-organosilane (APTES), prior to and after blocking (with BSA) and immunoreaction (with anti-rabbit IgG antibody). The multilayer protein/amino-organosilane/silicon structure of the surfaces is confirmed with high resolution XPS.

Mesoscopic uniformity is concluded, based on micrograph pairs of topography and light signal provided by NSOM, the latter with image-averaged intensity values larger than 170 kHz, for whole spectrum, or 600 Hz, for fluorescence spectrum of the labelled antibody.

Lateral nanostructures, recorded with AFM are characterized by RMS roughness, the size 2whm of surface features (from auto-correlation) and the distance between them (1/k) (from the Fourier analysis) in topography and phase images, independently. It was found that all four measures do not, within experimental error, increase due to blocking procedure but rise considerably after specific antibody binding.

Exactly the same conclusion stems from the analysis of protein surface coverage (thickness) data, provided by ARXPS analysis of SiO_2 surfaces. This finding indicates that during the blocking procedure apart from adsorption of BSA molecules to the free surface sites significant role plays the partial exchange of immobilized IgG for smaller BSA molecules. This is further supported by the surface coverage data obtained from the Si_3N_4substrates.

In turn, the study of immunoreaction effect for the SiO_2 model immunosensor surface, shows rises in the size of surface features 2whm by $\sim$190% and the distance between them (1/k) by $\sim$165%, accompanied by even larger increase in protein surface coverage ($\sim$280%). Apparently antigen-antibody complexes are not formed at each feature existing in the blocked surface since some of these surface features correspond to BSA rather than IgG molecules.

The surface features visible in topography AFM images reflect modulated height of random surface arrangements of protein molecules. This is suggested by the fact that the Fourier lengths of topography are twice larger than those of phase images. This shows also that phase images obtained in this study are not merely clearer topographical images.

Preferential vertical arrangement of polar functional groups towards polar (silanized silicon) substrate is observed with high-resolution ARXPS for all protein nanolayers, independently on surface coverage, prior to and after blocking and specific antibody binding. This orientation effect is preserved not only for nanolayers of different proteins (BSA, IgG, anti-IgG antibody), but also for their mixtures (IgG with BSA) and immunocomplexes (IgG with anti-IgG antibody).

These findings demonstrate the potential of the combined use of different spectroscopic and microscopic methods to throw light on protein layer arrangements on silicon surfaces and thus help to improve the performance of silicon based biosensors.

Bibliography

[1] Cui, Y., Wei, Q., Park, H., and Lieber, C. M. *Science* **293**(5533), 1289–1292 (2001).

[2] Tan, W., Wang, K., He, X., Zhao, X. J., Drake, T., Wang, L., and Bagwe, R. P. *Medicinal Research Reviews* **24**(5), 621–638 (2004).

[3] De Vos, K., Bartolozzi, I., Schacht, E., Bienstman, P., and Baets, R. *Optics Express* **15**(12), 7610–7615 (2007).

[4] Raiteri, R., Grattarola, M., Butt, H.-J., and Skládal, P. *Sensors and Actuators, B: Chemical* **79**(2-3), 115–126 (2001).

[5] Kitsara, M., Misiakos, K., Raptis, I., and Makarona, E. *Optics Express* **18**(8), 8193–8206 (2010).

[6] Dancil, K. S., Greiner, D. P., and Sailor, M. J. *Journal of the American Chemical Society* **121**(34), 7925–7930 (1999).

[7] Lv, Z., Wang, J., Chen, G., and Deng, L. *International Journal of Biological Macromolecules* **47**(5), 661–667 (2010).

[8] Lee, K.-B., Park, S.-J., Mirkin, C. A., Smith, J. C., and Mrksich, M. *Science* **295**(5560), 1702–1705 (2002).

[9] Kitsara, M., Petrou, P., Kontziampasis, D., Misiakos, K., Makarona, E., Raptis, I., and Beltsios, K. *Microelectronic Engineering* **87**(5-8), 802–805 (2010).

[10] Bae, Y. M., Oh, B. K., Lee, W., Lee, W. H., and Choi, J. W. *Biosens. Bioelectron.* **21**(1), 103–110 (2005).

[11] Awsiuk, K., Bernasik, A., Kitsara, M., Budkowski, A., Rysz, J., Haberko, J., Petrou, P., Beltsios, K., and Raczkowska, J. *Colloids and Surfaces B: Biointerfaces* **80**(1), 63–71 (2010).

[12] Gokarna, A., Kim, Y. H., Cho, Y.-H., Lee, M. S., Kang, I. C., Park, H. K., Kim, M. G., and Chung, B. H. *Optical Review* **13**(4), 288–291 (2006).

[13] Tencer, M., Charbonneau, R., Lahoud, N., and Berini, P. *Applied Surface Science* **253**(23), 9209–9214 (2007).

[14] Horcas, I., Fernández, R., Gómez-Rodríguez, J. M., Colchero, J., Gómez-Herrero, J., and Baro, A. M. *Review of Scientific Instruments* **78**(1) (2007).

[15] Kim, J., Seidler, P., Wan, L. S., and Fill, C. *Journal of Colloid and Interface Science* **329**(1), 114–119 (2009).

[16] Howarter, J. A. and Youngblood, J. P. *Langmuir* **22**(26), 11142–11147 (2006).

[17] Kowalczyk, D., Slomkowski, S., Chehimi, M. M., and Delamar, M. *International Journal of Adhesion and Adhesives* **16**(4), 227–232 (1996).

[18] Horner, M. R., Boerio, F. J., and Clearfield, H. M. *J. Adhes. Sci. Technol.* **6**(1), 1–22 (1992).

[19] Anastasi, G., Cutroneo, G., Pisani, A., Bruschetta, D., Milardi, D., Princi, P., Gucciardi, P. G., Bramanti, P., Soscia, L., and Favaloro, A. *Journal of Microscopy* **228**(3), 322–329 (2007).

[20] Dickenson, N. E., Armendariz, K. P., Huckabay, H. A., Livanec, P. W., and Dunn, R. C. *Analytical and Bioanalytical Chemistry* **396**(1), 31–43 (2010).

[21] Vasina, E. N., Paszek, E., Nicolau Jr., D. V., and Nicolau, D. V. *Lab on a Chip - Miniaturisation for Chemistry and Biology* **9**(7), 891–900 (2009).

[22] Strein, E. and Allred, D. *Thin Solid Films* **517**(3), 1011–1015 (2008).

[23] Jiménez, C., Perriére, J., Vickridge, I., Enard, J., and Albella, J. *Surface and Coatings Technology* **45**(1-3), 147–154 (1991).

[24] Senden, T. J. and Drummond, C. J. *Colloids and Surfaces A: Physicochemical and Engineering Aspects* **94**(1), 29–51 (1995).

[25] Scofield, J. H. *Journal of Electron Spectroscopy and Related Phenomena* **8**(2), 129–137 (1976).

[26] Briggs, D. *Surface analysis of polymers by XPS and static SIMS*. Cambridge University Press, (1998).

[27] Jeyachandran, Y. L., Mielczarski, J., Mielczarski, E., and Rai, B. *Journal of Colloid and Interface Science* **341**(1), 136–142 (2010).

[28] Ouerghi, O., Touhami, A., Othmane, A., Ben Ouada, H., Martelet, C., Fretigny, C., and Jaffrezic-Renault, N. *Biomolecular Engineering* **19**(2-6), 183–188 (2002).

[29] Zhou, C., Friedt, J.-M., Angelova, A., Choi, K.-H., Laureyn, W., Frederix, F., Francis, L. A., Campitelli, A., Engelborghs, Y., and Burghs, G. *Langmuir* **20**(14), 5870–5878 (2004).

[30] Chen, S., Liu, L., Zhou, J., and Jiang, S. *Langmuir* **19**(7), 2859–2864 (2003).

[31] Lu, B., Smyth, M. R., and O'Kennedy, R. *Analyst* **121**(3), 29R–32R (1996).

[32] Mielczarski, J. A., Dong, J., and Mielczarski, E. *Journal of Physical Chemistry B* **112**(16), 5228–5237 (2008).

[33] Browne, M. M., Lubarsky, G. V., Davidson, M. R., and Bradley, R. H. *Surface Science* **553**(1-3), 155–167 (2004).

[34] Mrksich, M. and Whitesides, G. M. *Annual Review of Biophysics and Biomolecular Structure* **25**, 55–78 (1996).

[35] Rabe, M., Verdes, D., and Seeger, S. *Advances in Colloid and Interface Science* **162**(1-2), 87–106 (2011).

Chapter 5

Model immunoassay on silicon surfaces: vertical and lateral nanostructure vs. protein coverage

5.1 Abstract

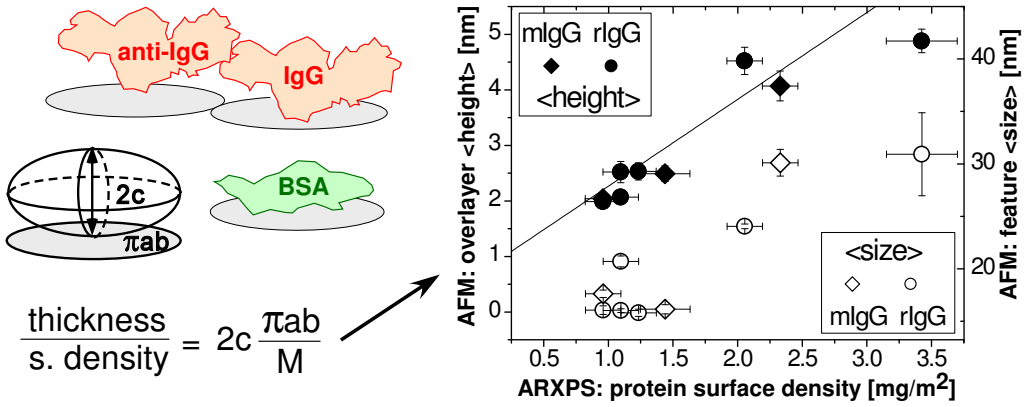

To provide complete characterization of immunoassay on silicon biosensor surfaces, atomic force microscopy, (angle-resolved) X-ray photoelectron spectroscopy and time-of-flight secondary ion mass spectrometry were applied to examine Si_3N_4 surfaces modified with (3-aminopropyl)triethoxysilane, coated with gamma globulins (IgG), blocked with bovine serum albumin and then reacted with anti-IgG antibody for two complementary pairs (rabbit and mouse IgG) at various concentrations (from 0.3 nM to 330 nM). Protein coverage, as reflected in (amine to total N1s) XPS signal ratio and determined from ARXPS, decreases slightly due to blocking and then increases monotonically for anti-IgG antibody concentrations higher than 1 nM. AFM images reveal hardly any change of lateral nanostructure due to blocking but response to antibody solutions, based on both the mean size (from autocorrelation) and dominant spacing (from Fourier analysis) of surface features, similar to that given by ARXPS. AFM height histograms provided information about the vertical nanostructure and the parameters of height distribution (average height, spread - rough-

ness and skewness) were distinctly influenced by coating, blocking and immunoreaction. Average protein layer thickness values determined based on protein structure (molecular weight, dimensions) and surface coverage provided from ARXPS were in accord with average height of protein layer determined from AFM. ToF-SIMS analysis indicated that BSA blocks free surface sites and in addition replaces some already adsorbed IgGs.

Highlights

• Immunoassay performed for 2 antigen-antibody pairs and varied amount of antibody. • ARXPS and AFM reveal protein coverage and its vertical and lateral nanostructure. • Measures of AFM height distribution substantiate coating, blocking and immunoassay. • Protein structure and coverage yield average thickness in accord with AFM height. • ToF-SIMS indicates BSA blocking free sites and replacing part of adsorbed IgGs.

Keywords

Immunoglobulins; Amino-organosilane films; Specific binding; Angle-resolved X-ray photoelectron spectroscopy; Atomic force microscopy;Time-of-flight secondary ion mass spectrometry

5.2 Introduction

Due to the specificity and selectivity of recognition between antigen and antibody, immunoassays are exploited routinely in diagnostic laboratories. Recently, silicon-based micro- and nanofabrication technology has enabled construction of immunosensors,where the antigen-antibody binding takes place at the surface of silicon transducers [1–4]. To provide a suitable interface for the biomolecules, the silicon surface is frequently modified with amino-organosilanes [1, 3]. After the immobilization of the specific recognition biomolecules, free surface sites are blocked, usually with non-functional proteins, to limit non-specific binding of targeted analytes [3, 5–7].

Model antigen-antibody binding reactions between immobilized gamma globulins (IgG) and secondary anti-species specific antibody (anti-IgG) have been examined with atomic force microscopy [6, 8–11]. Even a single specific recognition event has been discriminated from non-specific binding in situ by acquiring AFM images at the same spot before and after analyte injection [8]. In most of the AFM studies, however, the examined surfaces are covered with a large number of biomolecules, a situation more elevant to operative biosensors. Nevertheless, in all cases, the antigen-antibody complexes were characterized only fragmentally by the determined changes in either the average size [9] or the average height [6, 10] of surface features manifested in AFM images (recorded in liquid [8, 9] or air [6, 10, 11]).

In previous Chapter, in order to provide a more direct insight about biomolecular layers created onto biochips within multistep procedures, silicon surfaces have been examined with AFM in air after silanization, immobilization of IgG, blocking and specific binding reaction (see Section 4.4.4). In addition, to allow for a more complete characterization, the local AFM analysis has been augmented with spectroscopic inspection (see Sections 4.4.1 and 4.4.3). For instance, lateral nanostructural features determined from AFM images (such as the mean size and dominant spacing of surface features) were supplemented with pro-

tein surface coverage, determined rigorously from analysis of the same surfaces with angle-resolved X-ray photoelectron spectroscopy (ARXPS).

In this Chapter, the above approach (Chapter 4) is extended to study two model immunoassays, based on recognition between anti-IgG antibody and the respective IgG, as a function of anti-IgG antibody concentration. In particular, rabbit or mouse IgGs have been immobilized onto aminosilane-modified silicon nitride surfaces and after blocking probed with the respective anti-species specific antibodies. AFM inspection revealed not only the lateral but also the vertical nanostructure of the biomolecule modified silicon surfaces. The AFM histograms of height distribution provided three measures of imaged surfaces, namely the distribution's mean value (average height), spread (roughness) and asymmetry (skewness). As it was expected, these measures were greatly influenced by the contributions of biomolecules attached to substrate after the successive immobilization, blocking and immunoreaction steps. Non-specific (e.g. blocking) and specific (effective immunoreaction) bindings were clearly distinguished. Together with the data about lateral nanostructure (from AFM) and protein surface density (from ARXPS), the experimental results provided a coherent picture of the biomolecules attachment and distribution onto silicon surfaces during the performance of immunoassays. In particular, it was found that the average thickness of organic overlayer predicted based on protein surface density calculated by analysis of ARXPS data correlates well with the average height of surface features determined by AFM, signifying the complementarily of these two methods for complex surfaces characterization. In addition, the data from time-of-flight secondary ion mass spectrometry (ToF-SIMS) revealed two separate processes taking place during the blocking step, i.e. BSA adsorption on the free surface sites complemented by desorption of IgG from the surface.

5.3 Materials and methods

5.3.1 Biosensor surface preparation for model immunoassay

The silicon substrates used are silicon wafers purchased from Montco Silicon Technologies, Inc. (Spring City, PA, USA). 3-Aminopropyl(triethoxysilane) (APTES), rabbit (rIgG; globulins Cohn Fraction I, II) and mouse (mIgG; globulins Cohn Fraction I, II) gamma-globulins, affinity purified polyclonal anti-rabbit IgG and anti-mouse IgG antibodies produced in goat against the whole molecule, and bovine serum albumin (BSA; Cohn Fraction V) were purchased from Sigma Chemical Co., St. Louis, MO, USA.

Silicon nitride (Si_3N_4) surfaces were obtained by deposition of a 1000-nm thick thermally grown silicon dioxide layer followed by deposition of a 150-nm thick silicon nitride layer. Cleaning and hydrophilization of the substrates were performed with oxygen plasma (using a reactive ion etcher) applied for 30 s under pressure of 10 mTorr and power of 400 W. The hydrophilized Si_3N_4 surfaces were then modified by immersion in 0.5% (v/v) aqueous APTES solution for 2 min, gentle washing with distilled water and curing for 20 min at 120 °C.

Model immunosensor surfaces were prepared in successive steps as follows: (a) coating with rabbit (rIgG) or mouse (mIgG) gamma-globulins through incubation with a 660 nM IgG solution (in addition, a 33 nM rIgG solution was used to complete the ToF-SIMS data) in 0.05 M phosphate buffer, pH 7.4, for 1 h at room temperature (RT), followed by washing with 0.05 M phosphate buffer, pH 7.4, and distilled water,

and drying under nitrogen stream; (b) blocking of free-protein binding sites of the surface via immersion in a 10 mg/ml BSA solution in 0.05 M phosphate buffer, pH 7.4 (blocking solution), for 1 h at RT, followed by washing and drying as previously. The surfaces were then reacted with anti-IgG specific antibodies through incubation with anti-rabbit IgG or anti-mouse IgG antibody solutions (respectively for surfaces coated with rabbit or mouse IgG) in 0.05 M phosphate buffer, pH 7.4, containing 10 mg/ml BSA, for 1 h at RT. The surfaces were then washed with 0.05 M phosphate buffer, pH 7.4, containing 0.05% (v/v) Tween 20, and distilled water and dried under nitrogen stream.

The stability of gamma globulins adsorption onto APTES-modified silicon nitride surface, as well as the stability of immunocomplexes formed through reaction with antibodies against rabbit or mouse gamma globulins have been tested using fluorescently labelled reagents and submitting the surfaces to extensive washing and/or to chaotropic solutions. Other results indicate that both the immobilization of rabbit or mouse gamma globulins through adsorption and the subsequent coupling of species specific antibodies are extremely stable (data not shown).

5.3.2 AFM surface characterization and image analysis methods

The AFM imaging of silicon nitride surfaces corresponding to the different steps of model immunoassays has been performed in air using an Agilent 5500 microscope working in non-contact mode. AFM cantilevers (probe type PPP-FMR, Nanosensors) with force constant of 2 N/m, resonant frequency of 75 kHz, and AFM tips with standard beam shape and small radius (<7 nm) were used. The set point and gains were adjusted to obtain minimal noise and clear images of the analysed surfaces. For each sample, topography and phase images were acquired simultaneously at several randomly chosen locations.

Surface vertical nanostructures were specified using the parameters of height distribution in a topographic AFM image, such as the average height, $\langle h \rangle$ (the distribution's mean), the root mean square (RMS) roughness, R_q (the distribution's spread), and the skewness, R_{sk} (the distribution's asymmetry). In addition, lateral nanostructures were also described based on autocorrelation and Fourier analysis of topographic and phase images. The relevant parameters of surface features were provided by the doubled width-at-half-maximum, 2whm, of radial averaged autocorrelation function (the feature's mean size) as well as the reciprocal of wave vector (1/k) at the maximum of radial averaged 2-dimensional fast Fourier transform (dominant spacing between the features). The vertical and lateral parameters were determined from AFM micrographs using the WSxM scanning probe microscopy software provided by Nanotec Electronica S.L. [12] (http://www.nanotec.es).

5.3.3 XPS and ARXPS surface characterization

X-ray photoelectron spectroscopy measurements were performed using a VSW Manchester spectrometer equipped with an Al Kα radiation source (1486.6 eV, 200 W). Angle-resolved XPS spectra were collected for three different values (0°, 60° and 70°) of photoelectron take-off angle Θ, which is defined as an angle between normal to the surface and the axis of the XPS analyser lens. The operating pressure in the analytical chamber was less than 5×10^{-8} mbar. All XPS peaks were charge referenced to the neutral (C-C) carbon C1s peak at 284.6 eV. Spectrum backgrounds were subtracted using the Shirley method. The

aminosilane-organic bilayer model used to determine the thickness of APTES film and the amount (effective XPS thickness) of immobilized proteins has been described in details in Section 2.2.3.3.2 and our earlier publications [13].

5.3.4 ToF-SIMS surface characterization

To examine with ToF-SIMS the effect of blocking procedure as a function of initial surface coverage with rIgG, the samples were analysed using the TOF.SIMS 5 (ION-TOF GmbH) instrument, equipped with a 30 keV bismuth liquid metal ion gun. Bi_3 clusters were used as the primary ions and the ion dose density was kept at levels lower than 10^{12} ion/cm^2 to ensure static mode conditions. High mass resolution spectra were acquired from sample spots corresponding to areas of 100 μm $\times$ 100 μm. For all spectra the minimal mass resolution (m/Δm) at C_4H_5+ (m/z = 53) peak was above 7400. Mass calibration was based on the H+, H_2+, CH+, C_2H_2+ and C_4H_5+ peaks.

5.4 Results

All surfaces of Si_3N_4 substrate modified with (3-aminopropyl)triethoxysilane (APTES) were examined prior to and after each step of the model immunoassays involved in this study by AFM and ARXPS. The surfaces were coated with rabbit (or mouse) gamma-globulins (IgG), and non-specific binding was blocked with bovine serum albumin (BSA). Then the surfaces were exposed to solutions of anti-IgG antibody to allow for specific binding with the immobilized IgGs. In case of rabbit IgG/anti-rabbit IgG different concentrations of anti-IgG antibody (0.3 nM $\leq$ c $\leq$ 330 nM) have been used, whereas in case of mouse IgG/anti-mouse IgG a single antibody concentration (c $=$ 330 nM) was applied. If not otherwise stated, the results for the two complementary pairs are presented in the same plots as solid and open symbols for the rabbit and mouse IgG, respectively.

5.4.1 Protein surface coverage reflected by XPS and determined from ARXPS

The multilayer structure silicon/APTES/protein of the silicon oxide and silicon nitride surfaces coated with IgG has been studied in Chapter 4 using XPS and ARXPS to examine the surfaces prior to and after both blocking with BSA and immunoreaction with anti-IgG antibody. The mesoscopic uniformity of the protein overlayer has been also confirmed by near-field scanning optical microscopy (see Section 4.4.2). Here, photoelectron spectroscopy was applied to evaluate, along with XPS, and determine in combination with ARXPS, surface coverage with protein of silicon nitride surfaces modified with an APTES film.

The XPS spectra of N1s core-level consist of both the signals characteristic for the Si_3N_4 substrate (binding energy of 397.5 eV) and for amine groups (NH_2, 399.8 eV, and protonated NH_3^+, 401.4 eV) present in the APTES/protein bilayer (see Section 4.4.1) and [13]. Therefore, the ratio of overlayer (NH_2 and NH_3^+) to total nitrogen concentration, N_{amine}/N, determined from XPS can be used as a measure of surface coverage by the bilayer. With the N_{amine}/N value for pure APTES film (6.8%) in mind, this ratio reflects also protein coverage. The N_{amine}/N ratio is plotted in Figure 5.1a (left scale) as a function of secondary

antibody concentration and compared with the situation prior to immunoreaction (labelled '+BSA' on the axis of abscissa) and just after adsorption of gamma globulins (labelled 'IgG').

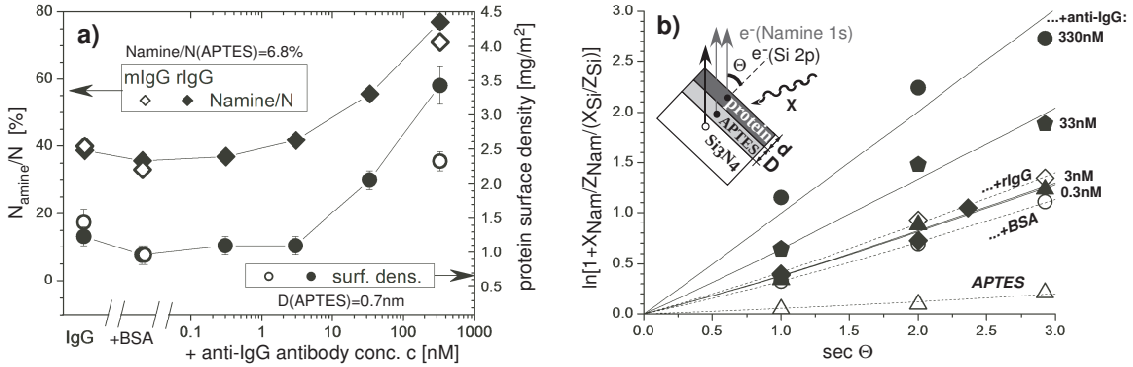

Figure 5.1: (a) Protein coverage of silicon nitride surfaces expressed as the ratio of amine to total nitrogen concentration derived from the XPS N1s spectrum (diamonds, left scale), and determined from ARXPS as protein surface density (circles, right scale) plotted against the anti-IgG antibody concentration c and compared with surfaces after IgG adsorption (labelled 'IgG') and blocking with BSA (labelled '+BSA'). Solid and open symbols are for the series with rabbit and mouse IgG, respectively. (b) The ARXPS ratio of normalized intensities of photoelectrons characteristic for amino-organosilane/protein bilayer (N1s from NH_2 and NH_3^+) and Si_3N_4 (Si2p) plotted versus the take-off angle function $\sec\Theta$. Lines mark results of linear regression analysis yielding XPS thickness of APTES and protein layer (D and d, respectively, marked in the inset). The latter, multiplied by protein density, yields protein surface density. The error bars for protein surface density (a) are given by the fitting procedure described in (b).

The ARXPS spectra depend on photoelectron take-off angle Θ, that modifies sampling vertical depth, and on XPS thicknesses of APTES film (D) and protein layer (d), that justify the effective attenuation of photoelectrons (see the inset to Figure 5.1b). The XPS thickness d, which is equivalent to a protein layer with uniformly distributed mass, is directly related (after being multiplied by protein density, 1.37 g/cm^3) with the density of proteins covering the surface.

The structural features of the APTES/protein bilayer are revealed by the ratio of intensities X_i of the photoelectrons characteristic for the aminosilane-organic bilayer (N1s from amine groups) and silicon substrate (Si2p), that is plotted in a logarithmic form versus the take-off angle function $\sec\Theta$ (see Figure 5.1b) [13]. The intensities X_i, calculated using tabulated sensitivity factors [14, 15], are normalized with respect to molar fractions Z_i of the atoms emitting photoelectrons [13] (see the axis of ordinates on Figure 5.1b). The Z_i values for all used proteins (11%) have been determined in previous publication (see also Section 4.4.3.1), while that for APTES and Si_3N_4 is obtained from the ARXPS data for the surface with no protein overlayer [13].

The data points, marked in Figure 5.1b with different open and solid symbols, respectively, correspond to immunosensor-like surfaces after subsequent modification steps (silanization with APTES, immobilization of rabbit rIgG, blocking with BSA) as well as after exposure of those surfaces to solutions of different anti-rIgG concentrations (ranging from 0.3 nM to 330 nM). The slope of each individual data set, always

starting at the origin of coordinate axes, depends on the total bilayer thickness (D with d). The thickness D of the APTES film, as determined in separate ARXPS measurements, is equal to 0.7 nm (in accord with results presented previous Chapters). With the value of D known, the XPS thickness d of protein overlayer remains the only fitting parameter of the linear regression fitting equation (2.9) (see Section 2.2.3.3.2). The resulting values of protein coverage (surface density) are plotted in Figure 5.1a (right scale) as a function of anti-IgG concentration and compared with the values after IgG adsorption (labelled 'IgG') and blocking with BSA (labelled '+BSA'), respectively.

5.4.2 Immunosensor surfaces examined with AFM

The inner structure of the protein overlayers is revealed by topographic and phase AFM micrographs. Representative topography images recorded prior to and after the immunoreaction corresponding to the different concentrations of anti-rIgG antibody are shown in Figure 5.2. The imaged protein overlayers can be described as random sets of surface features. Similar conclusions can be drawn for phase images (not presented).

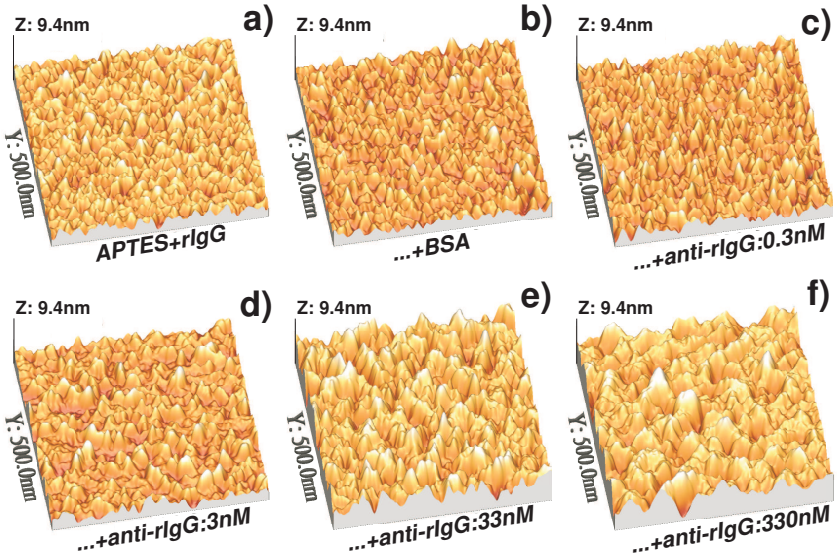

Figure 5.2: Representative AFM topographic micrographs recorded for silanized Si_3N_4 after adsorption of rabbit IgG (a), blocking with BSA (b), and specific binding of anti-rabbit IgG antibody from solutions of different concentration c (c-f).

5.4.2.1 Lateral nanostructure of protein overlayer

To examine quantitatively the lateral nanostructure of protein overlayer, autocorrelation and Fourier analysis was applied to the AFM micrographs, as suggested in Section 4.4.4 of previous Chapter. The double of width at half-maximum, 2whm, of radial averaged autocorrelation provides a measure of the mean size of topographic surface features. In addition, the reciprocal of wave vector at maximum, (1/k), of radial averaged power spectrum provides a measure of the dominant spacing of the features observed in the topography and phase AFM images. The determined values of lateral measures of the inner structure

of protein overlayer are presented in Figure 5.3 (left scale for (1/k), right scale for 2whm) vs. the anti-IgG antibody concentration and in relation with the situations prior to immunoreaction (labelled '+BSA' on the axis of abscissa) and just after adsorption of gamma globulins (labelled 'IgG').

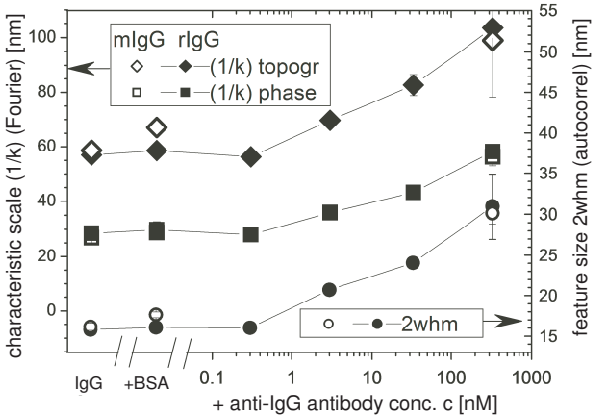

Figure 5.3: Lateral nanostructure parameters of biomolecule modified Si_3N_4 surfaces. Characteristic spacing (1/k) (left scale) and mean size of surface features 2whm (right scale) determined from topography and phase contrast AFM images plotted as a function of antibody concentration c (solid and open symbols are for the series with rabbit and mouse IgG, respectively). The initial values correspond to IgG coated surface, while those labelled '+BSA' to the blocked surface. Error bars are standard deviations, each determined from 5 images of the same surface.

5.4.2.2 Vertical nanostructure of protein overlayer

The vertical structure of surfaces examined with AFM is best described by the distribution of height in topographic images. Representative height histograms of AFM micrographs recorded prior to and after immunoreaction are shown (with their individual height scales) in Figure 5.4a-c. The contributions from the molecules used for silanization and coating (IgG on APTES, Figure 5.4a), blocking (BSA, Figure 5.4b) and imunnoreaction (anti-IgG antibody, Figure 5.4c) are illustrated schematically with separate Gaussian curves centered at different heights. These contributions change the overall height distribution in terms of its mean value, spread and asymmetry. Therefore, to characterize rigorously the vertical nanostructure of immunosensor-like surfaces, these three parameters are determined for each histogram: average height $\langle h \rangle$, standard deviation from $\langle h \rangle$ given by root mean square roughness R_q, and asymmetry specified by skewness R_{sk} (positive or negative for the longer histogram tail on its right or left side, respectively).

The mean values of these parameters as determined from the AFM height histograms are plotted in Figures 5.5a and 5.5b against the anti-IgG antibody concentration and with respect to the situations prior to immunoreaction. In addition, the average height (left scale of Figure 5.5a), RMS roughness (right scale of Figure 5.5a) and skewness (Figure 5.5b) can be also compared with the values corresponding to the silanized substrate with $\langle h \rangle = 0.83$ nm, $R_q = 0.22$ nm and zero R_{sk}, respectively.

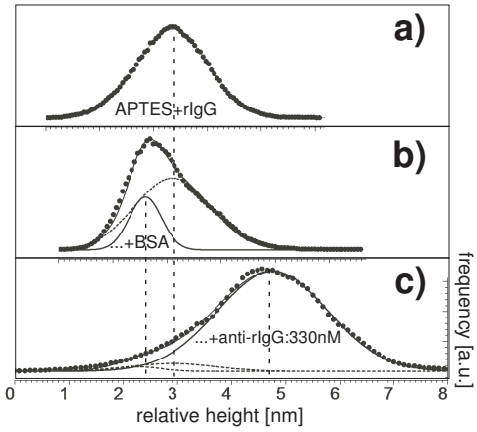

Figure 5.4: Representative height histograms (with individual height scales) from AFM micrographs of Si_3N_4 substrates silanized with APTES after coating with rabbit IgG (a), blocking with BSA (b) and immunoreaction with anti-rabbit IgG antibody (330 nM) (c). Contributions due to rabbit IgG and APTES, BSA and anti-rabbit IgG antibody are illustrated schematically with separate Gaussian curves. Deviations from flat surfaces are characterized by average height $\langle h \rangle$, standard deviation from $\langle h \rangle$ (RMS roughness R_q), and asymmetry (skewness R_{sk}, positive or negative for longer right or left side tail of histogram, respectively).

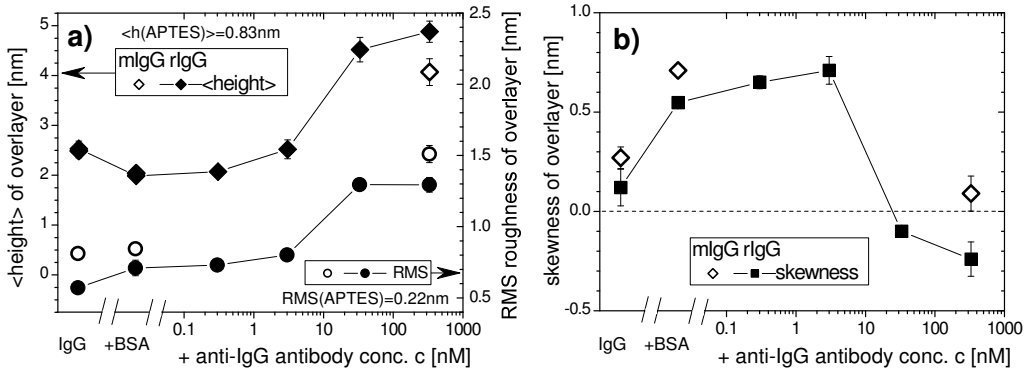

Figure 5.5: Vertical nanostructure parameters of biomolecule modified Si_3N_4 surfaces as determined from AFM height histograms (see Figure 5.4). Mean values of average height $\langle h \rangle$ (left scale in (a)), root mean square roughness R_q (right scale in (a)) and skewness R_{sk} (b) are plotted as a function of anti-IgG antibody concentration and compared with the initial value of IgG coated surface, and that corresponding to the blocked surface ('+BSA'). Error bars are standard deviations, each determined from 5 images.

5.5 Discussion

5.5.1 Biosensor surface prior to immunoassay

The surface modification with proteins through adsorption of gamma globulins to Si_3N_4 modified with APTES was quantified taking into account the substrate composition as specified by the molar fractions of silicon in the substrate, Z_{Si} =33.6($\pm$1.3)%, and amine nitrogen in APTES film, Z_{APTES} =1.7($\pm$0.3)%, determined by ARXPS. For the adsorbed rabbit and mouse IgG, the protein area density values determined

by ARXPS were 1.25($\pm$0.15) mg/m^2 and 1.4($\pm$0.2) mg/m^2, respectively (Figure 5.1a). These values are comparable with the value of 1.1($\pm$0.1) mg/m^2, determined in a previous Chapter for rabbit IgG adsorbed to SiO_2 silanized with APTES, with Z_{APTES} =2.6($\pm$0.4)% and Z_{Si} =32.5($\pm$1.4)%, respectively. This finding confirms earlier conclusions that the silicon substrate composition, either Si_3N_4or SiO_2, has small impact on immunoglobulin adsorption (see Chapter 4). The determined surface densities of adsorbed rabbit and mouse IgG (1.25-1.4 mg/m^2) are lower than the value expected for an area covered by singular immunoglobulin with side-on orientation (2.6 mg/m^2), while the other orientations (end-on, head-on) would result in even higher surface densities. This suggests partial but sizeable surface coverage with adsorbed IgGs with a side-on orientation that results in low surface coverage [16, 17].

Adsorbed gamma globulins (rabbit or mouse IgG) form surface nanostructures (Figure 5.2a), described as randomly distributed features corresponding to a topographic extent 2whm of 16 nm (Figure 5.3), comparable with the apparent IgG radii of 14 and 12 nm, respectively. These values are the adsorbed IgG radii predicted due to the broadening caused by the AFM tip (with 7 nm radius) for spherical [11] and half-spherical [9] molecular shapes (with 'real' radius of 7 nm [10]). For the F_c (or F_{ab}) subunits of IgG ('real' radius of 4 nm [18]) the radii expected from both models are somewhat smaller (11 and 8 nm, respectively). On the other hand, the spacing (1/k) between the features (Figure 5.3), obtained from topography (57-59 nm) is two times larger than that calculated from the phase images (27-29 nm). This suggests that topography AFM images show modulated height of immobilized IgG molecules, in accord with previous conclusions (see Section 4.4.4). In addition, the spacing (1/k) determined by the phase images doubles the topographic size 2whm. If the latter is related with the radius of IgG, then a picture of the surface with partial but sizeable coverage emerges in accord with the conclusion from surface coverage analysis.

The blocking procedure, which involves incubation of the surfaces coated with IgG with a high concentration BSA solution, reduces the surface coverage with proteins. This effect, visible already in the amine to total nitrogen concentration (Figure 5.1a), is quantified based on ARXPS data (Figure 5.1b) as a 33% and 22% reduction of the initial coverage of 1.4 mg/m^2 (mouse IgG) and 1.25 mg/m^2 (rabbit IgG), respectively. Taking into account previous results (see Section 4.4.3.2) that show hardly any change of total protein area density for surfaces with lower initial coverage (1.1 mg/m^2 of rabbit IgG), this finding suggests that the outcome of blocking with BSA depends on initial surface coverage with IgG. To further analyse this issue, we examined with ToF-SIMS surfaces modified with rabbit IgG through adsorption from solutions of two different concentrations (33 and 660 nM), both prior to and after blocking with BSA. The results are presented in Figure 5.6 as uniform (after adsorption) and hatched (after blocking) columns, respectively, and correspond to the normalized intensities of specific secondary ions, characteristic for the amino acids [19, 20] present both in IgG and BSA. While the surfaces with high rIgG coverage (obtained using a 660 nM solution for coating) show again blocking-induced reduction of total protein surface density, the surfaces with much lower initial coverage (obtained using a 33 nM rIgG solution for coating) manifest a huge increase of protein coverage upon exposure to BSA solution. This indicates two dominant processes taking place during blocking, BSA occupying mainly the free surface sites at surfaces with low coverage, and additionally replacing part of adsorbed IgG molecules at surfaces with higher protein density.

Recent experiments show that proteins can change their adsorption from irreversible to reversible, when a critical surface coverage is reached [21]. Similar behaviour of IgG molecules in the presence of

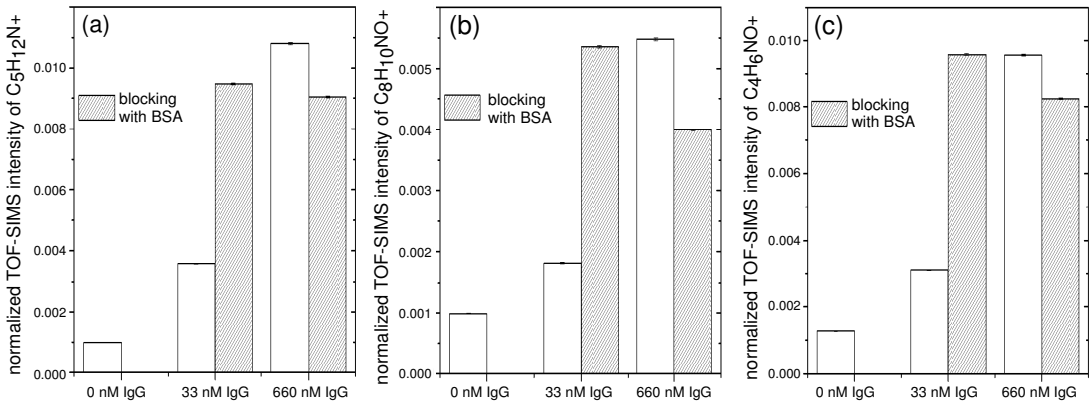

Figure 5.6: ToF-SIMS intensities of secondary ions characteristic for proteins: (a) $C_5H_{12}N+$ (from Ile and Leu [19, 20]), (b) $C_8H_{10}NO+$ (from Tyr [19, 20]) and (c) C_4H_6NO+ (from Glu and Gln [20]), normalized to the total ion intensity, as determined for Si_3N_4 surfaces silanized with APTES (reference values for 0 nM concentration) after rIgG adsorption from 33 nM and 600 nM solutions (uniform columns), respectively, and subsequent blocking with BSA (hatched columns). Error bars are standard deviations determined from the ToF-SIMS intensities.

BSA solution is suggested for a critical coverage value of $\sim$ 1.1 mg/m^2 . Above this value, the surface left by desorbed IgG molecules can be populated by BSA. IgG molecules (with nominal dimensions of 14.5 nm $\times$ 8.5 nm $\times$ 4 nm [10]) and BSA (with nominal dimensions of 14 nm $\times$ 4 nm $\times$ 4 nm [5]) can form monolayers of adsorbed molecules with side-on orientation and experimental thickness of 5 nm [5, 17] and 4 nm [5], respectively. Since IgG and BSA are comparable in size except for one dimension, their partial exchange should lead to a visible reduction of total protein coverage accompanied by less distinct (vertical) change in surface nanostructure. In fact, hardly any effect on the three lateral structural scales is observed (see Figure 5.3). Both the mean size 2whm of topographic surface feature, and dominant spacing (1/k) of the features visible on topography and phase AFM images are not altered during blocking. However, the three parameters ($\langle$h$\rangle$, R_q, R_{sk}) of vertical nanostructure, determined from AFM histograms of height distribution (cf. Figure 5.4a and b) are affected by blocking. In particular, the average height $\langle$h$\rangle$ is reduced (Figure 5.5a, left scale), the distribution's spread (RMS roughness R_q) slightly increased (Figure 5.5a, right scale), and the skewness R_{sk} increased from zero to positive values (Figure 5.5b) - reflecting histograms with longer right-hand tails. The reason for all these changes in vertical nanostructure is the incorporation of smaller BSA molecules into IgG overlayer. The height distribution determined for immobilized BSA by surfaces coated directly with BSA is symmetric, with lower mean and spread values as compared to IgG. The schematic illustration of the BSA and IgG contributions in Figure 5.4b explains their impact on height distribution after blocking. Intriguing relation between AFM height distribution, protein structure and surface coverage with proteins is discussed below in the Section 5.5.3.

5.5.2 Immunoassay on biosensor surface

Specific binding between immobilized IgG and anti-IgG antibody from solutions with increased concentration is manifested as a raise in protein coverage as it is presented in Figure 5.1a with respect to the situation prior to immunoreaction (zero anti-IgG antibody concentration). Surface coverage with proteins, as detected by the changes in XPS (N1s core level) signal ratio of N_{amine}/N, builds up with concentration c. These changes are visible for anti-rIgG concentrations equal to or higher than 3.3 nM. The ARXPS data, relying on angle-dependent ratio of XPS signals from different elements, seem less sensitive, since increase is observed for concentrations c equal to or higher than 33 nM. Nevertheless, the ARXPS data can provide the absolute values of protein area density which cannot be determined by XPS measurements [13] (see also Sestion 2.2.3.3.2). For the rabbit IgG/anti-rabbit IgG antibody pair, the surface density of proteins increases from 1.1($\pm$0.1) mg/m^2 to 3.4($\pm$0.3) mg/m^2 as the antibody concentration increases from 0.3 nM to 330 nM. It should be noted that an area density of 2.4 mg/m^2 (reached at c $\sim$ 100 nM) corresponds to a monolayer of densely packed (92% density) gamma globulin molecules with side-on orientation.

This monotonic increase of surface coverage with antibody concentrations equal to or higher than 3.3 nM (Figure 5.1a) is accompanied by a similar increase of lateral nanostructure parameters (see Figure 5.3). The mean size 2whm of randomly distributed topographic features increases during immunoassay from 16.0($\pm$0.2) nm to 30.9($\pm$4.0) nm. In addition, the spacing (1/k) of the features, grows from 28.1($\pm$0.7) nm to 58.3($\pm$2.3) nm as determined by the phase AFM micrographs, and from 56.3($\pm$1.5) nm to 103($\pm$25) nm as determined by topography images. This approximately two-fold increase of the 2whm value of surface features reflects a progressive formation of antigen-antibody complexes. Also, the characteristic scales (1/k) of both phase and topography images are roughly twice larger after immunoassay. Apparently, some of the imaged surface features must correspond to BSA or gamma globulins with orientations blocking or limiting the specific binding.

Immunoreaction of immobilized IgG with the anti-IgG antibody results also in drastic changes of vertical nanostructure. These changes are reflected in the parameters of the AFM height histograms which are clearly modified after immunoreaction with antibody concentrations higher than 3.3 nM (Figure 5.5). Such changes in the vertical structure are expected, since the antigen-binding sites of adsorbed gamma globulins (with preferred side-on orientation) are located above the silanized silicon level (see sketch in Figure 5.7b). In addition, the attached anti-IgG antibody molecules, in contrast to adsorbed immunoglobulins, are less prone to conformational modifications. There are two stages in the immunoassay-induced variation of vertical structure parameters (Figure 5.5). First, the region of antibody concentration c up to 33 nM corresponds to a distinct increase in both the mean value ($\langle$h$\rangle$) and spread (R_q) of height distribution accompanied by skewness R_{sk} reduced to zero. Second, for antibody concentrations equal to or higher than 33 nM a somewhat halted growth of both average height $\langle$h$\rangle$ and roughness R_q, and negative skewness are observed. The height histogram of AFM micrograph recorded for the rIgG modified surfaces after reaction with an anti-rIgG antibody solution of 330 nM is presented in Figure 5.4c. We notice that the height distribution is dominated by the anti-IgG antibody contribution, with very small input from the adsorbed IgG and BSA (see outlined schematically Gaussian curves), resulting in longer left distribution's wing. This height histogram reveals also the critical point at which the AFM tip stops to penetrate the deeper regions of

protein/APTES overlayer. This suggests complete formation of a continuous protein layer, expected from ARXPS to take place around c $\sim$ 100 nM, when a side-on orientation of immobilized gamma globulins is assumed.

5.5.3 Nanostructure vs. protein coverage

New insight into a model immunoassay on silicon nitride surfaces can be gained when the surface nanostructures, with their lateral and vertical parameters determined from AFM images and AFM height distributions, respectively, are analysed as a function of surface coverage with proteins, evaluated by ARXPS. The results of such an analysis are presented in Figure 5.7a for surfaces coated with rabbit (circles) or mouse IgG (diamonds). The plotted values of the mean size of surface features 2whm (open symbols, right scale) show a monotonic albeit scattered relation with protein coverage, reflecting (except for two data points) progressive build up of antigen-antibody complexes. The high spread of values is mainly due to the two points with the lowest feature size, corresponding to adsorbed rabbit and mouse IgG, which upon blocking are shifted to the respective points with reduced abscissa (protein surface density) but almost the same ordinate (2whm).

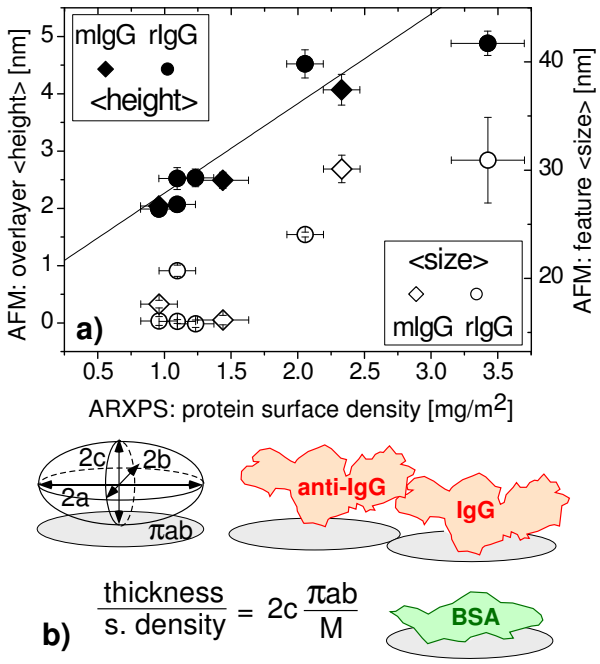

Figure 5.7: (a) Vertical (average height $\langle h \rangle$, left scale) and lateral (mean feature size 2whm, right scale) nanostructure parameters (from AFM) of Si_3N_4 surfaces coated with rabbit (circles) or mouse IgG (diamonds) plotted against protein surface density (from ARXPS). Solid line marks the average overlayer thickness expected from the model depicted in (b). Error bars are standard deviations, specified in Figure 5.1 and Figure 5.3.

More revealing is the relation between the average AFM height $\langle h \rangle$ and the surface coverage with proteins. Therefore, for more accurate analysis model described in Section 3.4.3 have been applied. The

observed monotonic dependence in Figure 5.7a with solid symbols (left scale) can be correlated with the protein structure, i.e. the weight M of a single molecule and the dimensions 2a $\times$ 2b $\times$ 2c of ellipsoid describing the immobilized molecules shape. The ratio of globular thickness to molecular surface density is expressed as 2c (πab/M) (see Figure 5.7 b). Please note that this formula is independent of immobilized protein orientations, as all ellipsoid dimensions are in its numerator. In addition, the ratio of thickness to area weight density calculated for immunoglobulin (IgG and anti-IgG, with 150 kDa molecular weight), 1.69 nm.m^2/mg, is almost the same as that of BSA (with 66.4 kDa molecular weight), 1.73 nm.m^2/mg. Therefore, practically one value characterizes all types of biomolecules present at the silicon surface. This ratio multiplied by the surface density corresponding to the area covered with a single protein (with given orientation) would provide the relevant globular thickness. In addition, this ratio multiplied by the actual surface coverage with proteins yields the average thickness of the protein layer. The predicted values, after the addition of the APTES film thickness (known from ARXPS) are presented as a solid line in Figure 5.7a. This line matches quite well with the average AFM height $\langle$h$\rangle$ data (solid symbols), except for the last point which corresponds to anti-rIgG antibody concentrations higher than 100 nM, where AFM tips stops to penetrate the continuous protein/APTES overlayer.

5.6 Conclusions

To conclude, combined local microscopic (AFM) and global spectroscopic (XPS, ARXPS) analysis of biosensor-like surfaces (silicon modified with amino-organosilane APTES) has been extended to all the steps of an immunoassay, using antibody concentrations extending over four orders of magnitude (0.3 nM $\leq$ c $\leq$ 330 nM, for two complementary IgG/anti-IgG antibody pairs).

AFM detection of specific binding at biosensor-like surfaces with large number of biomolecules can be quantified by autocorrelation and Fourier analysis of AFM topography and phase images in terms of lateral nanostructure parameters. Following this approach, the formation of antigen-antibody complexes is detected for antibody concentrations equal to or higher than 3.3 nM. Similar sensitivity was demonstrated by XPS. ARXPS seems less sensitive (signals statistically different from zero antibody concentration are obtained for concentrations c $>$ 33 nM) but on the other hand it can provide information about absolute surface coverage (area density) with proteins that the other two methods cannot.

In addition, the AFM height distribution parameters (mean-average height $\langle$h$\rangle$, spread - roughness R$_q$ and asymmetry - skewness R$_{sk}$) provide complete, often neglected, information on vertical nanostructure that enables additional analysis of the biosensor-like surfaces prior to and after immunoreaction. These parameters resolve non-specific binding, due to blocking with BSA, from specific binding due to antigen-antibody interactions for concentrations higher than 1 nM.

Synergic examination of nanostructure and protein coverage, especially the relation of average AFM height vs. the protein surface density, enables surface analysis involving protein dimensions but also weight of a single molecule. The average protein layer thickness determined taking into account both the protein structure and surface coverage is in accordance with average AFM height.

Spectroscopic examination (ToF-SIMS) of biosensor-like surfaces prior to immunoassay indicates that BSA not only blocks free surface sites but in addition replaces some adsorbed IgGs especially at the

surfaces with high protein coverage.

Bibliography

[1] Cui, Y., Wei, Q., Park, H., and Lieber, C. M. *Science* **293**(5533), 1289–1292 (2001).

[2] Raiteri, R., Grattarola, M., Butt, H.-J., and Skládal, P. *Sensors and Actuators, B: Chemical* **79**(2-3), 115–126 (2001).

[3] Meskini, O., Abdelghani, A., Tlili, A., Mgaieth, R., Jaffrezic-Renault, N., and Martelet, C. *Talanta* **71**(3), 1430–1433 (2007).

[4] Schipper, E. F., Brugman, A. M., Dominguez, C., Lechuga, L. M., Kooyman, R. P. H., and Greve, J. *Sensors and Actuators, B: Chemical* **40**(2-3), 147–153 (1997).

[5] Jeyachandran, Y. L., Mielczarski, J. A., Mielczarski, E., and Rai, B. *Journal of colloid and interface science* **341**(1), 136–142 (2010).

[6] Kitsara, M., Petrou, P., Kontziampasis, D., Misiakos, K., Makarona, E., Raptis, I., and Beltsios, K. *Microelectronic Engineering* **87**(5-8), 802–805 (2010).

[7] Yuk, J. S., Trnavsky, M., McDonagh, C., and MacCraith, B. D. *Biosensors and Bioelectronics* **25**(6), 1344–1349 (2010).

[8] Li, L., Chen, S., Oh, S., and Jiang, S. *Analytical Chemistry* **74**(23), 6017–6022 (2002).

[9] Lv, Z., Wang, J., Chen, G., and Deng, L. *International journal of biological macromolecules* **47**(5), 661–667 (2010).

[10] Lee, K.-B., Park, S.-J., Mirkin, C. A., Smith, J. C., and Mrksich, M. *Science* **295**(5560), 1702–1705 (2002).

[11] Ouerghi, O., Touhami, A., Othmane, A., Ben Ouada, H., Martelet, C., Fretigny, C., and Jaffrezic-Renault, N. *Biomolecular engineering* **19**(2-6), 183–188 (2002).

[12] Horcas, I., Fernández, R., Gómez-Rodríguez, J. M., Colchero, J., Gómez-Herrero, J., and Baro, A. M. *Review of Scientific Instruments* **78**(1) (2007).

[13] Awsiuk, K., Bernasik, A., Kitsara, M., Budkowski, A., Rysz, J., Haberko, J., Petrou, P., Beltsios, K., and Raczkowska, J. *Colloids and Surfaces B: Biointerfaces* **80**(1), 63–71 (2010).

[14] Scofield, J. H. *Journal of Electron Spectroscopy and Related Phenomena* **8**(2), 129–137 (1976).

[15] Briggs, D. *Surface analysis of polymers by XPS and static SIMS*. Cambridge University Press, (1998).

[16] Urano, H. and Fukuzaki, S. *Journal of Bioscience and Bioengineering* **90**(1), 105–111 (2000).

[17] Tronin, A., Dubrovsky, T., and Nicolini, C. *Langmuir* **11**(2), 385–389 (1995).

[18] Buijs, J., Lichtenbelt Th., J. W., Norde, W., and Lyklema, J. *Colloids and Surfaces B: Biointerfaces* **5**(1-2), 11–23 (1995).

[19] Dubey, M., Emoto, K., Takahashi, H., Castner, D. G., and Grainger, D. W. *Advanced Functional Materials* **19**(19), 3046–3055 (2009).

[20] Wang, H., Castner, D. G., Ratner, B. D., and Jiang, S. *Langmuir* **20**(5), 1877–1887 (2004).

[21] Rabe, M., Verdes, D., Rankl, M., Artus, G. R. J., and Seeger, S. *ChemPhysChem* **8**(6), 862–872 (2007).

Chapter 6

Immobilization of capture oligonucleotide probes on silicon biosensor surfaces using biotin-streptavidin system examined with microscopic and spectroscopic techniques

6.1 Abstract

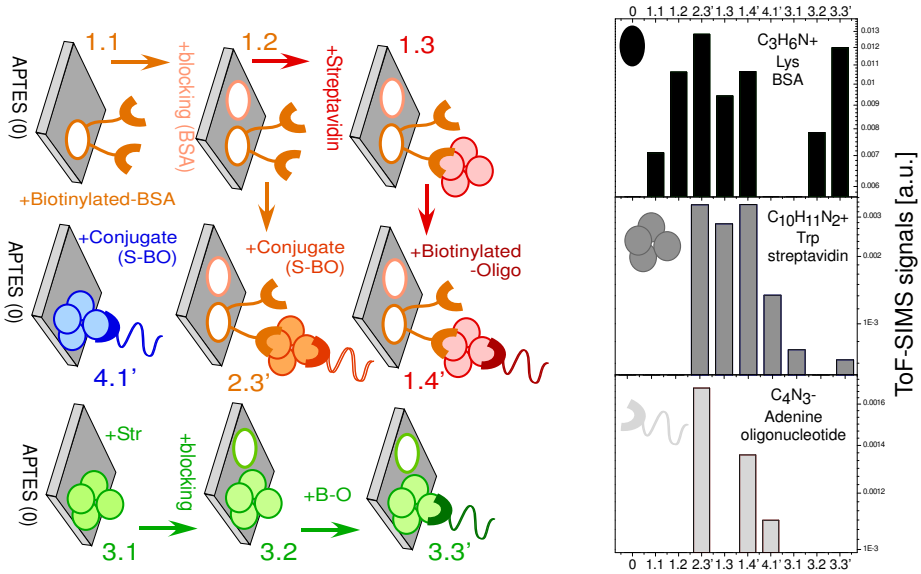

A strategy to immobilize capture oligonucleotide probes on silicon biosensor surfaces, based on streptavidin-biotin system, is examined with Atomic Force Microscopy, Angle-Resolved X-ray Photoelectron Spectroscopy and Time-of-Flight Secondary Ion Mass Spectrometry for four immobilization approaches applied to SiO_2 modified with (3-aminopropyl)triethoxysilane. The first approach involves: adsorption of biotinylated bovine serum albumin BSA, blocking free surface sites with BSA, reaction with streptavidin, final immobilization of biotinylated oligonucleotide. Alternatively, in second approach the last

two steps are exchanged with immobilization of (streptavidin-biotinylated oligonucleotide) conjugate. The third approach consists of adsorption of streptavidin, blocking with BSA and immobilization of biotinylated oligonucleotide. Whereas the fourth approach involves a direct immobilization of (streptavidin-biotinylated oligonucleotide) conjugate. Surface coverage with biomolecules, determined rigorously from ARXPS, accords with average AFM height of organic overlayer, and is anti-correlated with intensity of Si+ secondary ions. These measures show also the highest surface density of biomolecules for the last two steps of first and last step of second approaches. These surfaces with proteins, larger than other biomolecules, anchored to other pre-adsorbed proteins exhibit also higher surface roughness. The effectiveness of oligonucleotide immobilization is indicated by phosphorus ARXPS atomic concentration equal to 0.7%, 0.4%, $\sim$ 0%, 0.2%, for the first, the second, the third and the fourth approach, respectively. Positive and negative secondary ions, characteristic for oligonucleotide (Ade-H-), streptavidin (Trp), BSA (Lys) and all proteins (Ala), allow additional insight into overlayer composition. They verify the ARXPS results and show the superiority of the first two approaches in terms of streptavidin and oligonucleotide concentrations.

Highlights

• 4 approaches immobilize biotinylated oligonucleotide using biotin-streptavidin system. • Methods applying pre-adsorbed biotinylated BSA show superior by ARXPS and ToF-SIMS. • ToF-SIMS gives multimolecular (proteins, oligonucleotide, substrate) composition. • Composition accords with molecular coverage (ARXPS) and average height (AFM).

Keywords

oligonucleotide probes; streptavidin-biotin system; Time-of-Flight Secondary Ion Mass Spectrometry; Angle-Resolved X-ray Photoelectron Spectroscopy

6.2 Introduction

Immobilization of detecting biomolecules to biosensor or microarray surfaces is generally a multi-step process. Supervision of effectiveness of each step of surface modification and functionalization is a key factor to obtain a required amount of detecting molecules immobilized to the surface.

To enable detection of different genetic mutations a proper immobilization of oligonucleotide probes to biosensor transducer or microarray surface is necessary. To this end different immobilization approaches were tested. Most of them are based on modification of 5'-end of oligonucleotides by attaching different chemical groups, especially thiol- or amine- groups. Such terminated oligonucleotides are covalently bounded directly to gold surface or to silicone-based surface modified with different organo-silanes [1–4]. Alternatively, some approaches exploit modification of 5'-end with biotin and their strong affinity to streptavidin or avidin [5–8]. Mir et al. reported that streptavidin underlayer minimizes non-specific binding when exposed to solution of negatively charged nanoparticles or streptavidin. It imposes surface anti-fouling characteristics in comparison to thiolated DNA brushes [6]. However, orientation of streptavidin molecules has to be controlled due to their influence on oligonucleotide probes orientation and density [5].

Testing different approaches as well as examination of the quantity of immobilized oligonucleotide probes is a key point to improve sensitivity of microarrays and biosensors. The most popular method to characterize the amount of immobilized oligonucleotide probes before and after hybridization is based on fluorescence tagging [1,3,7–9]. However, in multi-steps procedures it is extremely important to examine surface after each step of surface modification and, finally, after oligonucleotide probe immobilization. Therefore, many experimental methods are used to evaluate surface properties after successive biomolecules immobilization. The most popular method providing insight into surface arrangement of immobilized biomolecules is Atomic Force Microscopy (AFM). However, to evaluate changes on the surface and to discern different immobilized biomolecules after each successive step of surface modification, spectroscopic methods are very helpful.

Time of flight secondary ion mass spectroscopy (ToF-SIMS) and X-ray photoelectron spectroscopy (XPS) are two commonly used methods to characterize biomolecular layers. XPS and angle resolved XPS (ARXPS) measurements yield information about atomic composition. Especially, they enable to determine phosphorus signal characteristic for nucleic acids [1, 2, 9]. Additionally, biomolecular surface density can be estimated by tracking characteristic signals from substrate and biomolecular overlayer [2, 10]. However, atomic composition of proteins is similar and XSP measurements do not provide possibility to distinguish them. To this end ToF-SIMS method can be employed to detect characteristic fragments originating from different proteins as well as oligonucleotides [9, 11]. Proteins are composed of the same 20 amino acids but their sequence and amount are different. ToF-SIMS yields information about the molecular structure. Therefore, signals of secondary ions allow to distinguish amino acids [12, 13]. Since the concentration and arrangement of amino acids in protein molecules are not the same, characteristic signals are commonly observed for different proteins.

In this Chapter, evaluation of four different approaches to immobilize oligonucleotide probes to silicone surface using streptavidin-biotin system is presented. Different micro- and spectro-scopic methods are used to examine surface after each step of multi-step procedures. Insight into local arrangement of biomolecules immobilized to modified silicon substrate as well as information (average height and surface roughness) about biomolecular layer are provided by AFM micrographs. ARXPS measurements yield information about atomic composition of the surface. This allows to estimate biomolecules surface density. The insight into multi-molecular composition is provided by ToF-SIMS signals characteristic for substrate, different proteins and oligonucleotide probe. Different micro- and spectro-scopic methods of surface analysis provide complementary data that accord with each other. Finally, all obtained results enable to compare various methods for oligonucleotide probe immobilization.

6.3 Materials and methods

6.3.1 Materials

Silicon wafers were purchased from Montco Silicon Technologies, Inc. (Spring City, PA, USA). 3-Aminopropyl(triethoxysilane) (APTES), N-[2-hydroxyethyl]piperazine-N'2-ethanesulfonic acid] and bovine serum albumin (BSA; Cohn fraction V, RIA grade) were purchased from Sigma Chemical Co., St.

Louis, MO, USA. 6-((Biotinoyl)amino)hexanoic acid sulfo-succinimidyl ester (sulfo-NHS-LC-biotin) and streptavidin were from Pierce (Rockford, IL, USA). Sodium dodecyl sulfate and ethylenediaminetetracetic acid were from Fluka Chemie (Buchs, Switzerland). Biotinylated oligonucleotide probes were obtained from VBC Biotech (Vienna, Austria). Biotinylated BSA (b-BSA) was prepared according to a published method [14, 15].

6.3.2 Biosensor surface preparation

Silicon substrates on which a 1000-nm thick silicon dioxide (SiO_2) layer was thermally grown by low pressure chemical vapour deposition were cleaned and hydrophilized by immersion in Piranha solution (1:1 (v/v) H_2O_2/H_2SO_4) for 20 min, followed by washing with distilled water and drying with nitrogen stream. Next, the hydrophilized SiO_2 surfaces were modified by immersion in a 0.5% (v/v) aqueous APTES solution for 2 min, gently washed with distilled water and cured at 120°C for 20 min. Four different approaches to immobilize oligonucleotides on silanized SiO_2 surfaces, which are illustrated schematically in Figure 6.1, have been implemented to prepare oligonucleotides modified surfaces. The first one involved: (1.1) adsorption of b-BSA from a 100 μg/mL b-BSA solution in 50 mM phosphate buffer, pH 7.0 (coating buffer) at room temperature (RT), (1.2) blocking the free surface sites by immersion in a 1% (w/v) BSA solution in coating buffer for 1h at RT, followed by washing and drying, (1.3) reaction with a 100 μg/mL streptavidin solution in coating buffer for 1h at RT and then washing, and finally (1.4') immobilization of biotinylated oligonucleotides through incubation for 1 h with a 5 μM biotinylated oligonucleotide solutions in coating buffer. Finally, the surfaces were rinsed with coating buffer and distilled water, and dried by N_2.

In the second approach, the last two steps were replaced by a single step (2.3') including immobilization of pre-incubated streptavidin-biotinylated oligonucleotides conjugates. The conjugates were prepared through reaction of an 88 μg/mL streptavidin solution (1.67 μM) with a 5 μM of biotinylated oligonucleotide solution both diluted in coating buffer for 10 min at RT prior to application onto the surface.

The third approach consisted of (3.1) direct adsorption of streptavidin on the silanized substrates from a 25 μg/mL solution in coating buffer for 1h at RT, followed by washing with coating buffer and distilled water, (3.2) blocking with BSA and (3.3') immobilization of biotinylated oligonucleotides performed as described above. Finally, the forth approach (4.1') involved direct adsorption of pre-incubated streptavidin-biotinylated oligonucleotide conjugates to the silanized silicon substrates.

In all approaches oligonucleotide with the biotin-5'-TTAAAACTAAATGTAAGAAAAATC-3' sequence was used.

6.3.3 AFM surface characterization

Atomic Force Microscopy (AFM) measurements were performed in non-contact mode using an Agilent 5500 AFM microscope system. AFM probes with spring constant about 2 N/m, tip radius below 10 nm and resonant frequencies about 70 kHz were used. The set point and all gains were adjusted to obtain minimal noise and clear image of the examined surface. For each sample, topography images were acquired at several different randomly chosen locations. The measurements were performed in air at room temperature. AFM micrographs were analysed with PicoImage software.

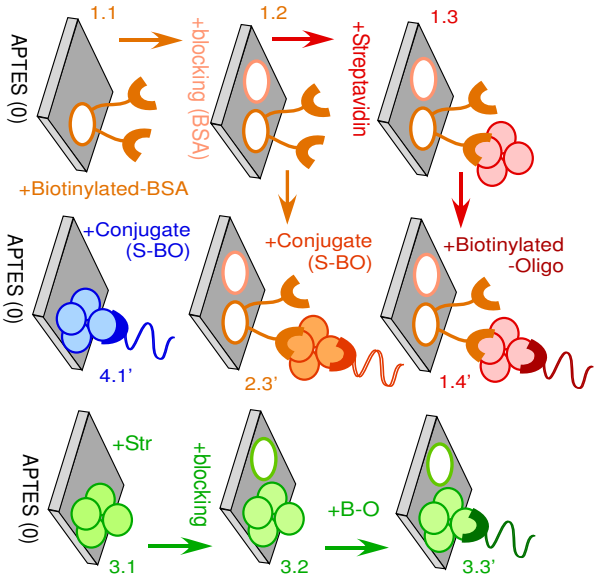

Figure 6.1: Schematic representation of different approaches to immobilize capture oligonucleotide probes on silicon pre-modified with (3-aminopropyl)triethoxysilane APTES surfaces based on streptavidin-biotin system. The first approach involves: (1.1) adsorption of biotinylated bovine serum albumin (b-BSA), (1.2) blocking free surface sites with BSA, (1.3) reaction with streptavidin, and finally, (1.4') immobilization of biotinylated oligonucleotides. Alternatively, the last two steps are exchanged with immobilization of streptavidin-biotinylated oligonucleotide conjugate (2.3'). The third approach consists of adsorption of streptavidin (2.1), blocking with BSA (2.2), and immobilization of biotinylated oligonucleotides (2.3'). A direct immobilization of streptavidin-biotinylated oligonucleotide conjugate is a last alternative (4.1').

6.3.4 ARXPS surface characterization

X-ray photoelectron spectroscopy (XPS) measurements were performed using a VSW Manchester spectrometer equipped with Al Kα radiation source (1486.6 eV, 200 W). Angle-resolved XPS spectra were collected for three different values (0°, 60° and 70°) of photoelectron take-off angle Θ. The operating pressure in the analytical chamber was less than 5×10^{-8} mbar. All XPS peaks were charge referenced to the neutral (C-C) carbon C1s peak at 284.6 eV. Spectrum backgrounds were subtracted using the Shirley method.

6.3.5 ToF-SIMS surface characterization

The surfaces after each step of preparation were analysed using the TOF.SIMS 5 (ION-TOF GmbH) instrument, equipped with 30 keV bismuth liquid metal ion gun. The Bi_3^+ clusters were used as the primary ions, with the ion dose density lower than 3.5×10^{12} ion/cm^2, rastered randomly over a region of 100 μm $\times$ 100 μm area. Pulsed low energy electron flood gun was used for charge compensation. For positive spectra mass resolution m/Δm > 7000 (at C_4H_5+ (m/z=53) peak) and for negative spectra m/Δm > 4000 (at C_2H+ (m/z=25) peak) were maintained.

6.4 Results and discussion

6.4.1 Biomolecular layer uniformity examined with AFM

Performed AFM measurements enable an insight into the 3-D structure of biomolecular overlayer after each successive step of the four approaches used to immobilize oligonucleotide probes (Figure 6.1). Representative topographic micrographs (Figure 6.2) confirm lateral uniformity of biomolecular layer. However, molecules are more densely packed for adsorbed biotinylated BSA as compared to adsorbed streptavidin.

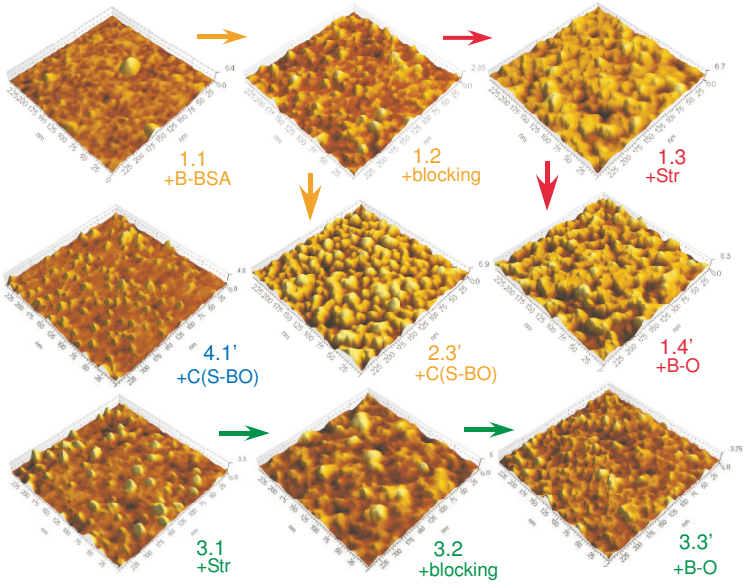

Figure 6.2: Representative topographic AFM micrographs recorded from SiO_2 biosensor surfaces after the successive steps of the different approaches followed for the immobilization of the capture oligonucleotides (cf. Figure 6.1).

Furthermore, vertical evolution of organic layer after successive preparation steps can be described using the parameters of height distribution in topographic AFM images (Figure 6.3), such as average height $\langle h \rangle$ (the distribution's mean) and the root mean square (RMS) roughness (the distribution's spread). The APTES layer formed on SiO_2 substrate is characterized by average height of 0.72($\pm$0.08) nm and relatively small height fluctuations with RMS roughness of 0.39($\pm$0.04) nm. Obtained results accord with the values reported in previous Chapters for APTES modified silicone based substrates (SiO_2 and Si_3N_4) and are typical for monomolecular APTES layer [16].

The 1st and the 2nd immobilization approach involved specific binding between streptavidin and pre-adsorbed biotinylated BSA. Successive steps of biotinylated BSA adsorption and blocking procedure result in slight increase of average AFM thickness to 1.02($\pm$0.04) nm and 1.18($\pm$0.19) nm and RMS roughness to 0.72($\pm$0.04) nm and 0.64($\pm$0.11) nm, respectively. In turn, vertical structure of organic overlayer changes considerably after biotin-streptavidin binding. Average AFM height increases significantly to 3.57($\pm$0.08) nm after immobilization of the conjugate of streptavidin-biotinylated oligonucleotide (step 2.3') and to 3.85($\pm$0.10) nm and 4.35($\pm$0.03) nm after successive steps of streptavidin immobilization (step 1.3) and reaction with biotinylated oligonucleotide (step 1.4'), respectively. Moreover, these surfaces exhibit

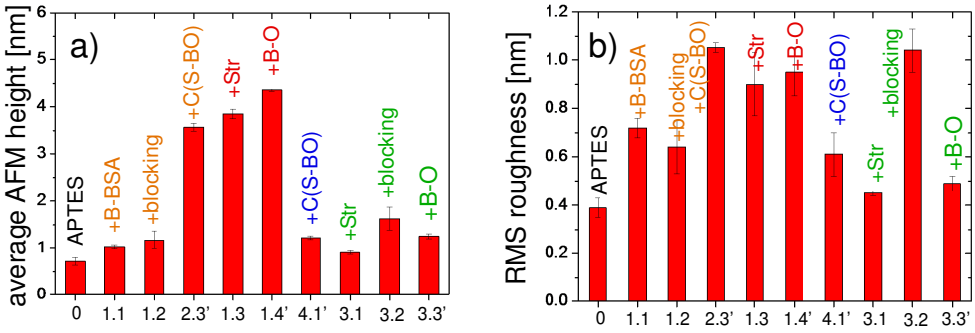

Figure 6.3: Mean values of (a) average AFM height and (b) RMS roughness of organic layer formed on silicon nitride after the successive steps of the different immobilization approaches. Higher values are due to anchorage of streptavidin molecules to pre-adsorbed biotinylated BSA (2.3', 1.3, 1.4') in a-b and adsorption of singular BSA clusters during the blocking procedure (3.2) in b. Error bars are Standard Error of the Mean each determined from 3-6 images of the same surface.

also higher RMS roughness (close to the 0.9-1.0 nm).

The 3rd and 4th immobilization approach used physical adsorption of streptavidin to form suitable platform to anchor biotinylated oligonucleotide probes. Compared to APTES modified substrate average AFM height increased to 1.23($\pm$0.04) nm and surface roughness to 0.61($\pm$0.09) nm after adsorption of the streptavidin-biotinylated oligonucleotide conjugate. In turn, both values are lower for adsorbed streptavidin with 0.91($\pm$0.4) nm and 0.45($\pm$0.01) nm for $\langle h \rangle$ and RMS, respectively. The next step of the 3rd immobilization approach induces increase of both average AFM height (to 1.62($\pm$0.24) nm) and RMS roughness (to 1.04($\pm$0.02) nm). This is due to the BSA clusters deposited on the surface. However, these clusters are removed during the incubation in biotinylated oligonucleotide solutions (compare step 3.2 and 3.3' in Figure 6.2). As a result both average AFM height and RMS decrease to 1.26($\pm$0.05) nm and 0.49($\pm$0.03) nm, respectively.

The final organic layers resulting from the 3rd and 4th approach (steps 3.3' and 4.1') reveal similar average AFM height and comparable RMS roughness. However, these results differ from the final values characteristic for the 1st and 2nd approach (steps 1.4' and 2.3'), with $\langle h \rangle$ three times thinner and less coarse surface.

6.4.2 Atomic concentrations and biomolecular surface coverage revealed by ARXPS

Effective attenuation of photoelectrons by organic layer on silicon substrate is observed in ARXPS measurements and described within a monolayer model [10] (equation (2.10)) by the XPS thickness D of the overlayer. Photoelectron intensities characteristic for the substrate (element B) and the organic layer (element A) are recorded as a function of photoelectron take-off angle Θ that modifies sampling vertical depth. The intensities recalculated using tabulated sensitivity factors are normalized with respect to molar fractions (Z_B for the substrate and Z_{AB} for the organic layer) of the atoms emitting photoelectrons. These molar fractions are determined from atomic concentrations (Section 6.4.2.1). Finally, XPS thickness D

of organic layer allows to estimate surface coverage with different biomolecules by taking into account different biomolecular densities (Section 6.4.2.2).

6.4.2.1 Atomic concentrations

SiO_2 wafers are well defined substrates with Si atomic concentration equal to 33.3%. This value is taken for the stoichiometric molar fraction Z_B of the element characteristic for the substrate. Such a value accords with our earlier measurements for SiO_2 yielding 32.7($\pm$0.6)% [10] and 32.5($\pm$1.4)% (Section 4.4.3.1).

A more challenging is the evaluation of molar fraction of the element(s) characteristic for the organic layer. This is due to multi-molecular composition. Organic materials, especially biomolecules, are composed mostly of carbon, hydrogen (not detected by XPS), oxygen and nitrogen. In some cases slight amount of other elements, like phosphorus or sulphur, is present. Atomic concentration of every present element was determined from ARXPS measurements taking into account the XPS signals from the C1s, N1s, O1s, P2p and Si2p core levels. Next, molar fraction (Z_{AB}) of nitrogen and carbon (Figure 6.4b,c), used to characterize the organic layer, was calculated from atomic concentrations of all elements present in the layer (C, N, excess O and P) averaged for Θ angle values between 0° and 70°:

$$Z_{AB} = \left\langle \frac{C_{AB}}{\sum_i C_i} \right\rangle_\theta \tag{6.1}$$

Oxygen atomic concentration in excess of that given by the SiO_2 stoichiometry (and silicon concentration) was taken as related with the layer. The Θ-averaged molar fraction of nitrogen and carbon in APTES layer is equal to 2.5($\pm$0.6)% and 92.6($\pm$4.5)%, respectively, and accords with the values determined earlier [10] and reported in Chapters 3, 4 and 5 that indicate adventitious carbon incorporated in the layer. Further steps of surface preparation increase molar fraction of nitrogen reflecting successive immobilization of biomolecules. Among these values the lowest increase to 3.4($\pm$0.6)% and 3.9($\pm$0.4)% is observed (Figure 6.4b) for physical adsorption of streptavidin (step 3.1) and streptavidin-biotinylated oligonucleotide conjugate (step 4.1'), respectively.

Finally, molar fraction of phosphorus in the organic layer (Figure 6.4a) can be used as a measure of the effectiveness of oligonucleotide immobilization. The P atomic concentration, determined by ARXPS, equals to 0.7($\pm$0.1)%, 0.4($\pm$0.1)%, $\sim$ 0%, 0.2($\pm$0.1)%, for the first, second, third and fourth immobilization approach, respectively. Very low efficiency of the third and fourth approach to immobilize oligonucleotide, with phosphorus concentration around XPS detection limit, is related with small adsorption of streptavidin or its conjugate, as mentioned earlier when discussing nitrogen molar fraction.

6.4.2.2 Biomolecular surface coverage

As a first step to evaluate surface coverage with biomolecules, the XPS thickness D of the organic layer is determined for two pairs of XPS signals C1s/Si2p and N1s/Si2p characteristic for the layer/substrate geometry. The analysis is shown here for the C1s/Si2p signal pair. The ratio of normalize photoelectron intensities is plotted in logarithmic form versus the take-off angle function $\sec\Theta$ in Figure 6.5. The data points marked with different symbols correspond to different immobilization approaches. The slope of each

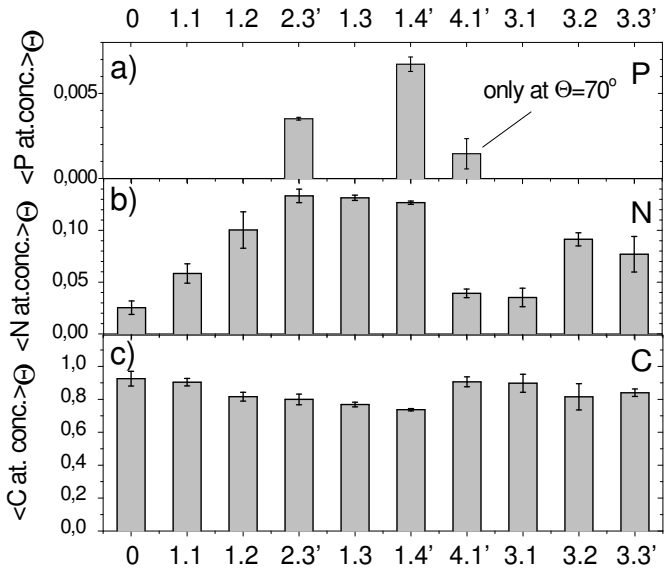

Figure 6.4: Atomic concentration of (a) phosphorus, (b) nitrogen, and (c) carbon in organic layer averaged for take-off angle Θ between 0° and 70°. Error bars are Standard Error of the Mean.

individual data set, always starting at origin of coordinate axes, depends on the XPS thickness D of organic overlayer.

The data sets, plotted for both pairs C1s/Si2p and N1s/Si2p versus the take-off angle function $\sec\Theta$, were used for regression analysis to yield the XPS thickness D of the organic layer (Figure 6.6).

The ARXPS results for silanized substrate yield the APTES film thickness D equal to 0.78($\pm$0.08) nm and 0.82($\pm$0.05) nm for the C1s/Si2p and N1s/Si2p pair, respectively. This accords with average AFM height 0.72($\pm$0.08) nm reported in the previous Chapter. In addition for all examined samples, their thickness D determined for the XPS signal pair C1s/Si2p hardly differs from that yielded for the pair N1s/Si2p (Figure 6.6). For further analysis, the layer XPS thickness D, weighted average of the C1s/Si2p and N1s/Si2p values, is considered. An increase in D between successive steps within each of four oligonucleotide immobilization approaches (Figure 6.1) is a token of a new biomolecule present on the surface. The increase ΔD, divided by specific biomolecular density, would yield the surface density increment caused by this molecule.Density values equal to 1.37 g/cm^3, 1.54 g/cm^3 and 1.39 g/cm^3 for proteins (streptavidin, BSA and biotinylated-BSA), biotinylated-oligonucleotide and streptavidin-biotinylated oligonucleotide conjugate, respectively, were assumed.

The first two steps for the 1st and 2nd approach (steps 1.1 and 1.2) yield surface coverage of BSA and biotinylated BSA equal to 0.43($\pm$0.11) mg/m^2 and 0.66($\pm$0.12) mg/m^2, respectively, that accord with our previous results (see Figure 4.5 in Chapter 4). Reaction with streptavidin-biotinylated oligonucleotide conjugate (step 2.3') and streptavidin (step 1.3) increases total surface coverage with biomolecules to 1.31($\pm$0.22) mg/m^2 and 2.23($\pm$0.24) mg/m^2, respectively. Lower amount of immobilized streptavidin conjugate (step 2.3') as compared to bare streptavidin (step 1.3) might be due to the fact that some of the conjugate binding sites have already been occupied by biotinylated oligonucleotide probes. Consequently, probability to be attached to biotinylated BSA decreases. The final step of the 1st approach (step 1.4') yields

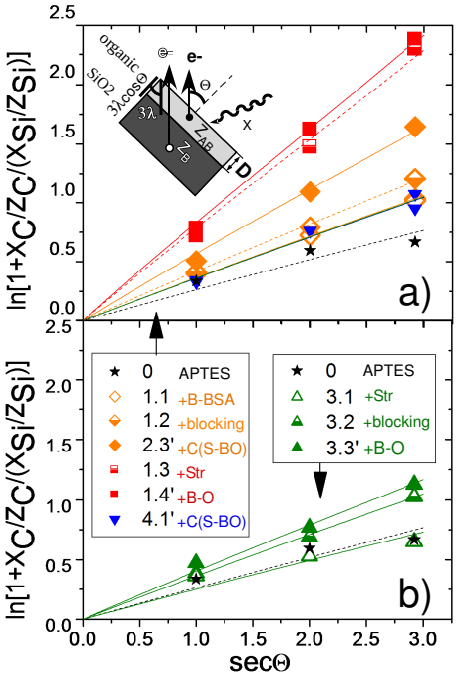

Figure 6.5: The ratio of normalized ARXPS intensities corresponding to photoelectrons characteristic for the organic (silane/protein/oligonucleotide) overlayer (C1s for this data set, or N1s not presented) and silicon substrate (Si2p) plotted versus the take-off angle function $\sec\Theta$. Lines mark results of regression analysis yielding XPS thickness D of organic layer (marked in the inset) formed after the successive steps of oligonucleotide immobilization procedures.

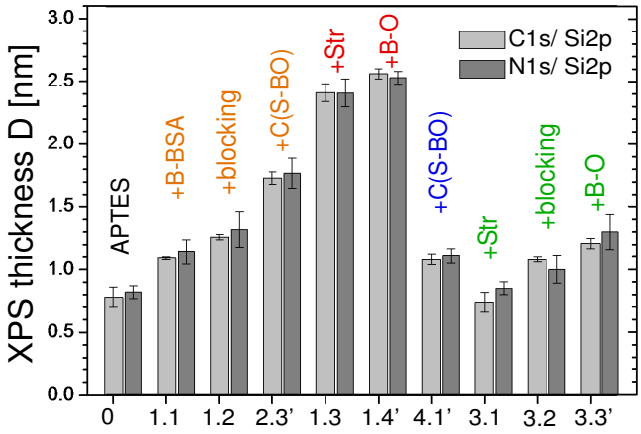

Figure 6.6: XPS thickness D of organic layer determined for signal pairs C1s/ Si2p (see Figure 6.5) and N1s/ Si2p. Error bars are given by the fitting procedure described in Figure 6.5.

the total surface coverage with biomolecules equal to 2.45($\pm$0.38) mg/m^2.

The ARXPS measurements show only a negligible amount of streptavidin adsorbed to APTES modified SiO_2 substrate (step 3.1) with protein surface density equal to 0.03($\pm$0.12) mg/m^2. Such a low amount accords with the AFM results. The final biomolecule surface coverage for the 3rd approach, after blocking

procedure and oligonucleotide immobilization, equals to 0.58($\pm$0.20) mg/m^2. It is comparable with the value for BSA adsorbed to APTES modified SiO_2 surface.

Finally, direct adsorption of streptavidin-biotinylated oligonucleotide conjugate to APTES modified substrate (step 4.1') provides surface coverage of 0.41($\pm$0.11) mg/m^2 of biomolecules.

6.4.3 Multi-biomolecular composition revealed by ToF-SIMS

The ToF-SIMS method has been applied to reveal multi-biomolecular composition through detection of the signals characteristic for each of the biomolecules used during multi-steps preparation process. Characteristic fragments (positive and negative secondary ions) of amino acids and nucleic acids have been examined and reported previously [9, 11–13]. To choose adequate ToF-SIMS signals, both streptavidin and BSA were examined, with respect to amino acids composition [12].

The amino acids most frequently presented in streptavidin are threonine (16.08%) and tryptophan (9.25%). In turn, glutamic acid (12.13%) and lysine (11.35%) are the most frequently met in BSA. On the other hand, concentration of lysine and tryptophan is relatively low in streptavidin (3.96%) and BSA (0.03%), respectively. Therefore, the ToF-SIMS signals from tryptophan (Trp): C_9H_8N+ (m/z=130), $C_{10}H_{11}N_2$+ (m/z=159), $C_{11}H_8NO$- (m/z=170) and lysine (Lys): C_3H_6N+ (m/z=56), $C_5H_{10}N$+ (m/z=84) characteristic for streptavidin [12, 17, 18] and BSA [19–21], respectively, were chosen to detect these proteins after successive preparation step. Normalized intensities of these ToF-SIMS signals are presented in Figure 6.7a-e.

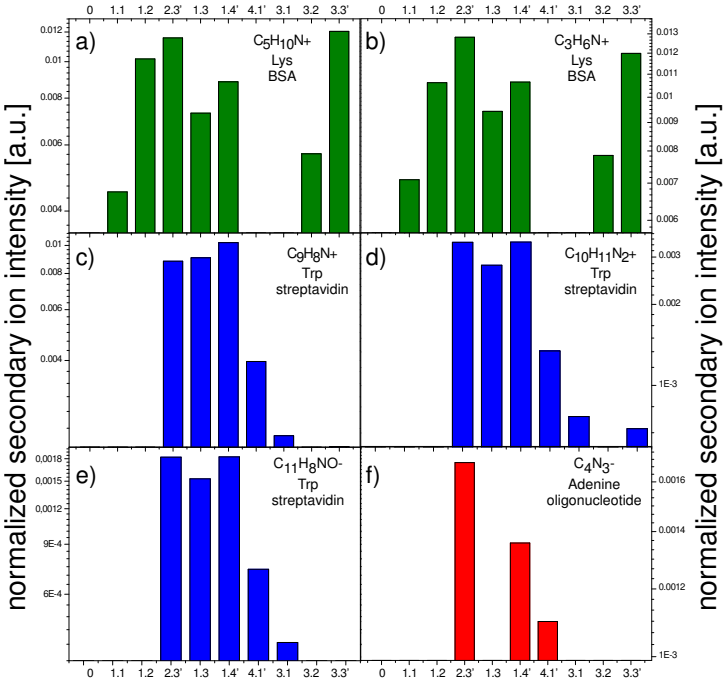

Figure 6.7: Normalized ToF-SIMS intensities of secondary ions characteristic for BSA: (a) $C_5H_{10}N$+ (m/z=84) and (b) C_3H_6N+ (m/z=56) from lysine; streptavidin: (c) C_9H_8N+ (m/z=130), (d) $C_{10}H_{11}N_2$+ (m/z=159) and (e) $C_{11}H_8NO$- (m/z=170) from tryptophan; oligonucleotides: (f) C_4N_3- (m/z=90) from adenine recorded for the SiO_2 surfaces after the successive steps employed for capture oligonucleotides immobilization (cf. Figure 6.1).

The signals characteristic for BSA (Figure 6.7a, b) suggest efficient adsorption of biotinylated BSA as well as blocking the free surface sites with BSA for all approaches. On the other hand, ToF-SIMS measurements (Figure 6.7c-e) reveal also that the streptavidin immobilization is more effective utilizing specific binding with pre-adsorbed biotinylated BSA (the 1st and 2nd approach) rather than direct adsorption to SiO_2 substrate modified with APTES (in the 3rd and 4th approach). Protein composition revealed by ToF-SIMS measurements accords very well with the results obtained from AFM and ARXPS measurements.

In addition, the efficient immobilization of oligonucleotide probe is indicated by the presence of C_4N_3- (m/z=90) signal from adenine [11] in ToF-SIMS spectra of negatively charged secondary ions (Figure 6.7 f). The adenine signal is higher for the second and the first approach as compared with the remaining two methods to immobilize oligonucleotide probes. ToF-SIMS results compared with phosphorus concentration from ARXPS point to the first two approaches as the most efficient. Such conclusion accords with ToF-SIMS results for streptavidin, which provides anchorage platform for biotinylated oligonucleotide probes.

6.4.4 Complementarity of different surface characterization methods

Figure 6.8 shows comparison of the results yielded by different experimental methods. The first two graphs (Figure 6.8a, b) present normalized secondary ion intensities of Si+ (m/z=28) and C_2H_6N+ (m/z=44) characteristic for substrate and alanine (presented in proteins), respectively. Signal from alanine is related to the amount of immobilized proteins and its anti-correlation with the Si+ signal is observed. In addition, the average AFM height of organic layer (Figure 6.8c) and surface coverage with biomolecules determined from ARXPS (Figure 6.8d) correlate with each other and accords with C_2H_6N+ and Si+ ToF-SIMS signals.

These results show that different surface characterization methods provide complementary information enabling better insight into the structures formed after successive steps of biosensor surface modification and functionalization. Especially, here the micro- and spectro-scopic results provide also complementary information about effectiveness of different immobilization approaches.

6.5 Conclusions

To summarize, four different approaches of oligonucleotide probes immobilization exploiting biotin-streptavidin system to functionalize biosensor surface have been examined. To this end AFM and different spectroscopic methods (ARXPS and ToF-SIMS) were applied. All experimental methods indicate that using pre-adsorbed biotinylated BSA (the first and second approach) leads to the more efficient streptavidin immobilization as compared to direct adsorption. More specifically, AFM average height of biomolecular layer as well as biomolecular surface density estimated by ARXPS significantly increase after streptavidin immobilization utilizing biotin-streptavidin binding. Furthermore, ToF-SIMS examination of the surfaces reveals higher intensity of tryptophan fragments for the streptavidin immobilized via interaction with biotinylated BSA. To the contrary, all these parameters indicate rather poor streptavidin immobilization through physical adsorption to APTES modified substrate.

Large variety of employed experimental methods allows to suggest the most effective approaches for

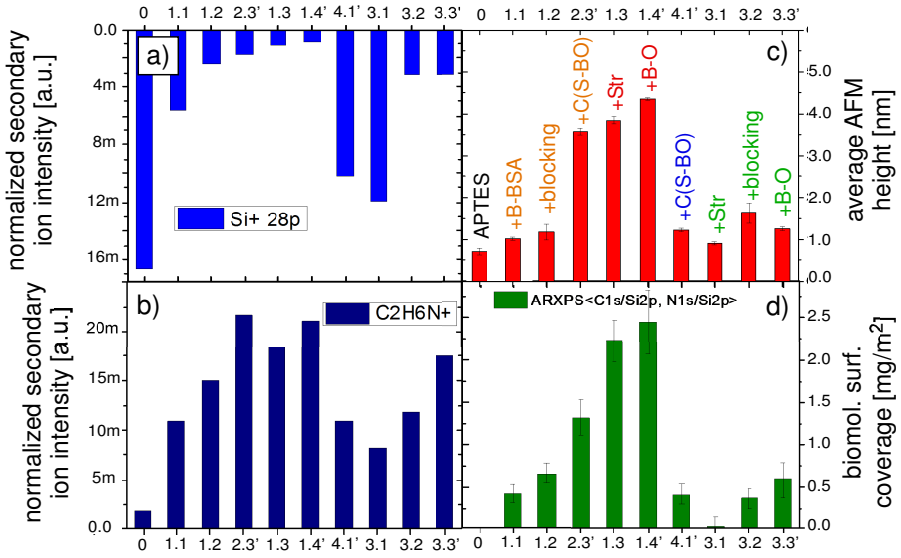

Figure 6.8: Normalized ToF-SIMS intensities of secondary ions characteristic for (a) the silicon substrate (Si+, m/z=28) and (b) of adsorbed proteins (C_2H_6N+, m/z=44, from alanine). (c) Average AFM height of organic overlayer and (d) total surface density of biomolecules determined from ARXPS. Please note accordance between AFM (c), ARXPS (d) and ToF-SIMS data (correlation with (b), anti-correlation with (a)) reflecting molecular coverage of biosensor surfaces after the successive steps employed for immobilization of capture oligonucleotides with the approaches described in Figure 6.1.

oligonucleotide probes immobilization. The highest phosphorus signal from ARXPS and intensity of C_4N_3-ions characteristic for adenine from ToF-SIMS indicate that the first and the second approaches utilizing pre-adsorbed biotinylated BSA provide the most effective immobilization of oligonucleotide probes.

The faint phosphorus ARXPS signal (only for $\Theta = 70°$) above and below detection limit for the 4th and 3rd approach suggests their low applicability to immobilize oligonucleotide probes into biosensor surface. This is related with poor streptavidin immobilization due to physical adsorption, providing a platform for reaction with biotinylated oligonucleotide.

Finally, comparison of the data provided by different experimental methods reveals correlation or anticorrelation between them and points to the complementarity of applied microscopic and spectroscopic techniques.

Bibliography

[1] Gong, P., Harbers, G. M., and Grainger, D. W. *Analytical Chemistry* **78**(7), 2342–2351 (2006).

[2] Petrovykh, D. Y., Kimura-Suda, H., Tarlov, M. J., and Whitman, L. J. *Langmuir* **20**(2), 429–440 (2004).

[3] Charles, P. T., Vora, G. J., Andreadis, J. D., Fortney, A. J., Meador, C. E., Dulcey, C. S., and Stenger, D. A. *Langmuir* **19**(5), 1586–1591 (2003).

[4] Herne, T. and Tarlov, M. *Journal of the American Chemical Society* **119**(38), 8916–8920 (1997).

[5] Su, X., Wu, Y. J., Robelek, R., and Knoll, W. *Langmuir* **21**(1), 348–353 (2005).

[6] Mir, M., Cameron, P. J., Zhong, X., Azzaroni, O., Álvarez, M., and Knoll, W. *Talanta* **78**(3), 1102–1106 (2009).

[7] Malainou, A., Petrou, P. S., Kakabakos, S. E., Gogolides, E., and Tserepi, A. *Biosensors and Bioelectronics* **34**(1), 273–281 (2012).

[8] Escorihuela, J., Banuls, M. J., Puchades, R., and Maquieira, A. *Chemical Communications* **48**(15), 2116–2118 (2012).

[9] Lee, C.-Y., Harbers, G. M., Grainger, D. W., Gamble, L. J., and Castner, D. G. *Journal of the American Chemical Society* **129**(30), 9429–9438 (2007).

[10] Awsiuk, K., Bernasik, A., Kitsara, M., Budkowski, A., Rysz, J., Haberko, J., Petrou, P., Beltsios, K., and Raczkowska, J. *Colloids and Surfaces B: Biointerfaces* **80**(1), 63–71 (2010).

[11] May, C. J., Canavan, H. E., and Castner, D. G. *Analytical Chemistry* **76**(4), 1114–1122 (2004).

[12] Dubey, M., Emoto, K., Takahashi, H., Castner, D. G., and Grainger, D. W. *Advanced Functional Materials* **19**(19), 3046–3055 (2009).

[13] Samuel, N. T., Wagner, M. S., Dornfeld, K. D., and Castner, D. G. *Surf.Sci.Spectra* **8**, 163–184 (2001).

[14] Kakabakos, S. E., Christopoulos, T. K., and Diamandis, E. P. *Clinical chemistry* **38**(3), 338–342 (1992).

[15] Petrou, P. S., Chatzichristidi, M., Douvas, A. M., Argitis, P., Misiakos, K., and Kakabakos, S. E. *Biosensors and Bioelectronics* **22**(9-10), 1994–2002 (2007).

[16] Kim, J., Seidler, P., Wan, L. S., and Fill, C. *Journal of Colloid and Interface Science* **329**(1), 114–119 (2009).

[17] Kim, Y. P., Hong, M. Y., Shon, H. K., Moon, D. W., Kim, H. K., and Lee, T. G. *Applied Surface Science* **252**(19), 6801–6804 (2006).

[18] Kim, Y. P., Hong, M. Y., Shon, H. K., Chegal, W., Cho, H. M., Moon, D. W., Kim, H. S., and Lee, T. G. *Applied Surface Science* **255**(4), 1110–1112 (2008).

[19] Bretagnol, F., Sirghi, L., Mornet, S., Sasaki, T., Gilliland, D., Colpo, P., and Rossi, F. *Nanotechnology* **19**(12), 125306 (2008).

[20] Iguerb, O. and Bertrand, P. *Surface and Interface Analysis* **40**(3-4), 386–390 (2008).

[21] Wilhelmi, M., Müller, C., Ziegler, C., and Kopnarski, M. *Analytical and Bioanalytical Chemistry* **400**(3), 697–701 (2011).

Chapter 7

Summary

The aim of this work was to evaluate immobilization of biomolecules to model biosensor surfaces. To this end different microscopic and spectroscopic methods have been implemented. As model detecting biomolecules gamma globulins (Chapter 3, Chapter 4 and Chapter 5) or oligonucleotide probes (Chapter 6) have been chosen.

In the Chapter 3 comparison of IgG immobilization via physical adsorption or covalent bonding to Si_3N_4 surface modified with amino- or epoxy-silane, respectively, has been presented. Correlated data from implemented spectroscopic methods, ARXPS and ToF-SIMS, yield protein surface density. Moreover, obtained results reveal that protein surface coverage is higher and develops faster for adsorption than covalent bonding. Finally, model combining data from AFM, ARXPS and ToF-SIMS has been presented. This model allows for an insight into vertical structure in relation to surface coverage of protein overlayer. Implementation of this model to IgG immobilized via physical adsorption or covalent bonding reveals that adsorbed IgG molecules are more densely packed compared to covalent bound ones but their conformation is more flattened.

Next, results of complex characterization of model biosensor surface after each subsequent step of preparation procedure have been presented in Chapter 4. Two different substrates (SiO_2 and Si_3N_4) have been modified with amino-organosilanes, and rabbit IgG has been used as a model detecting molecule. Lateral nanostructure of protein overlayer, examined with AFM, is not affected due to blocking procedure (with BSA) but rises considerably after immunoreaction (with anti-IgG antibody). Additionally, similar observations are made for protein surface coverage, which increases significantly after antigen-antibody binding. Moreover, preferential orientation of protein polar functional groups towards substrate has been revealed for all protein layers by ARXPS measurements.

Observed changes in protein layer morphology after immunoreaction have been studied in details for model immunoassay described in Chapter 5. Immunoassay has been performed for immobilized gamma globulins (IgG) reacting with anti-IgG antibody for two (mouse and rabbit) complementary pairs at various concentrations of antibody. AFM and XPS measurements allow to detect formation of antigen-antibody complexes for antibody concentrations equal to or higher than 3.3 nM. On the other hand, ARXPS is less sensitive but enables estimation of protein surface coverage which increases monotonically for anti-IgG antibody concentrations higher than 1 nM. In addition, the model introduced in Chapter 3 allows here

to determine average protein layer thickness based on protein structure and surface coverage provided by ARXPS. Obtained results are in accord with average height of protein layer determined from AFM.

Moreover, surface analysis prior to and after blocking procedure (Chapter 4 and Chapter 5) revealed that BSA molecules not only block free surface sites but also replace loosely bounded IgG molecules.

The last part of this Thesis (Chapter 6) focuses on examination of four different approaches of oligonucleotide probes immobilization based on streptavidin-biotin system. Multi-biomolecular overlayer composition was revealed by characteristic fragments of BSA, streptavidin and oligonucleotide reflected in the ToF-SIMS spectra. Moreover, all implemented experimental methods reveal more effective streptavidin immobilization via reaction with pre-adsorbed biotinylated BSA rather than due to physical adsorption. Finally, ARXPS phosphorus signals as well as ToF-SIMS secondary ions characteristic for adenine also point out that the most effective immobilization of oligonucleotide probes is provided by the methods using biotinylated BSA.

List of Abbreviations

2whm	doubled value of width-at-half-maximum
ACF	autocorrelation function
AFM	Atomic Force Microscopy
APTES	(3-Aminopropyl)triethoxysilane
ARXPS	Angle Resolved XPS
b-BSA	biotinylated BSA
B-O	biotinylated oligonucleotide
BSA	bovine serum albumin
C(S-BO)	streptavidin-biotinylated oligonucleotide conjugate
DNA	deoxyribonucleic acid
d-SIMS	dynamic Secondary Ion Mass Spectrometry
EGFP	enhanced green fluorescent protein
ELISA	enzyme-linked immunosorbent assay test
FET	Field effect transistors
FFT	Fast Fourier transform
GOPS	(3-Glycidoxypropyl)trimethoxysilane
IgG	gamma globulins, immunoglobulins
JEV	Japanese encephalitis virus
LFM	lateral force microscopy
Lys	lysine
mIgG	mouse gamma globulins
MZI	Mach-Zehender interferometer
NHS	N-Hydroxysuccinimide
NSOM	Near-field Scanning Optical Microscopy
OTFT	organic thin film transistors
PC	Principal Component
PCA	Principal Component Analysis
PCR	Principal Component Regression
pI	isoelectric point
rIgG	rabbit gamma globulins
RMS	Root-mean-square

RNA	ribonucleic acid
RT	room temperature
SPM	Scanning Probe Microscopy
SPR	Surface plasmon resonance
s-SIMS	static Secondary Ion Mass Spectrometry
Str	streptavidin
ToF-SIMS	Time-of-Flight Secondary Ion Mass Spectrometry
Trp	tryptophan
XPS	X-ray Photoelectron Spectroscopy

List of Tables

List of Figures

Relevant papers and conference contributions of the author

Papers:

P1 Awsiuk K., Budkowski A., Psarouli A., Petrou P., Bernasik A., Kakabakos S., Rysz J., Raptis I., Protein adsorption and covalent bonding to silicon nitride surfaces modified with organo-silanes: comparison using AFM, angle-resolved XPS and multivariate ToF-SIMS analysis, submitted

P2 Marzec M.M., Awsiuk K., Bernasik A., Rysz J., Haberko J. Luzny W., Budkowski A., Buried polymer/metal interfaces examined with Kelvin Probe Force Microscopy, Thin Solid Films 531 (2013) 271-276

P3 Awsiuk K., Budkowski A., Petrou P., Bernasik A., Marzec M. M., Kakabakos S., Rysz J., Raptis I., Model immunoassay on silicon surfaces: Vertical and lateral nanostructure vs. protein coverage, Colloids Surf. B 103 (2013) 253-260

P4 Stetsyshyn Y., Zemła J., Zolobko O., Fornal K., Budkowski A., Kostruba A., Donchak V., Harhay K., Awsiuk K., Rysz J., Bernasik A., Voronov S., Temperature and pH dual-responsive coatings of oligoperoxide-graft-poly(N-isopropylacrylamide): Wettability, morphology, and protein adsorption, J. Colloid Interface Sci. 387 (2012) 95-105

P5 Zemła J. , Rysz J., Budkowski A., Awsiuk K., Proteins grouped into a variety of regular micro-patterns by substrate-guided domains of self-assembling poly(ethylene oxide)/polystyrene blends, Soft Matter 8 (2012) 5550-5560

P6 Awsiuk K., Bernasik A., Kitsara M., Budkowski A., Petrou P., Kakabakos S., Prauzner-Bechcicki S., Rysz J., Raptis I., Spectroscopic and microscopic characterization of biosensor surfaces with protein/amino-organosilane/silicon structure, Colloids Surf. B 90 (2012) 159-168

P7 Budkowski A., Zemła J., Moons E., Awsiuk K., Rysz J., Bernasik A., Björström-Svanström C.M., Lekka M., Jaczewska J., Polymer blends spin-cast into films with complementary elements for electronics and biotechnology, Journal of Applied Polymer Science 125 (2012) 4275–4284

P8 Awsiuk K., Psarouli A., Petrou P., Budkowski A., Kakabakos S., Bernasik A., Rysz J., Raptis I., Spectroscopic and microscopic examination of protein adsorption and blocking of non-specific binding to silicon surfaces modified with APTES and GOPS, Procedia Engineering 25 (2011) 334-337

P9 Awsiuk K., Bernasik A., Kitsara M., Budkowski A., Rysz J., Haberko J., Petrou P., Beltsios K., Raczkowska J., Protein coverage on silicon surfaces modified with amino-organic films: A study by AFM and angle-resolved XPS, Colloids Surf. B 80 (2010) 63-71

P10 Budkowski A., Bernasik A., Moons E., Lekka M., Zemła J., Jaczewska J., Haberko J., Raczkowska J., Rysz J., Awsiuk K., Structures in multicomponent polymer films: Their formation, observation and applications in electronics and biotechnology, Acta Physica Polonica A 115 (2009) 435-440

Conferences:

- 14/12/2012 Chorzów, XI Seminarium Krakowsko-Katowickie
  Oral presentation: "Fizysorpcja vs chemisorpcja immunoglobulin G do powierzchni krzemowych modyfikowanych silanami"
- 3–6/07/2012 Warszawa, III Krajowa Konferencja Nano i Mikromechaniki
  Oral presentation: "Methods using biotin-streptavidin system to immobilize oligonucleotide probes on biosensor surfaces evaluated with microscopy and spectroscopy"
- 27/05-1/06/2012 Kraków, 3rd International Symposium on Surface Imaging/Spectroscopy at the Solid/Liquid Interface
  Poster: "Covalent bonding and physical adsorption of immunoglobulin on silicon nitride modified with organo-silanes: comparison using AFM, angle-resolved XPS and multivariate TOF-SIMS analysis"
- 18–19/11/ 2011 Kraków
  Organization and participation in the 30th months meeting of EU project PYTHIA.
- 7–8/09/2011 Athens, Greece, 4th International Workshop on Multianalyte Biosensing Devices
  Poster: "Immobilization of oligonucleotide probes on silicon surfaces using the biotin-streptavidin system examined with microscopic and spectroscopic techniques"
- 20–21/05/ 2011 Kraków, X Katowicko-Krakowskie Seminarium pt. "Fizyka Fazy Skondensowanej"
  Oral presentation: "Spektroskopowa i mikroskopowa charakteryzacja powierzchni biosensora o strukturze białko/warstwa amino-organiczna/krzem"
- 5–8/07/2010 Montpellier, France, MOLMAT2010 Conference
  Poster: "Protein coverage on silicon surfaces modified with amino-organic films: A study by AFM and angle-resolved XPS"
- 11–12/06/2010 Rychwałd, IX Katowicko – Krakowskim Seminarium Fazy Skondensowanej
  Oral presentation: "Analiza AFM/ARXPS struktury jednorodnych i niejednorodnych nanowarstw białek"
- 3–4/06/2010 Kraków, NanoMeasure2010 scientific symposium
  Poster: "Uniform and non-uniform protein nanolayers on modified silicon surfaces: integral geometry approach to AFM and XPS data"

- 8/05/2009 Kraków, VIII Katowicko – Krakowskim Seminarium Fazy Skondensowanej.
  Poster: “Badanie własności powierzchni czynnej biosensorów metodami mikroskopii skaningowej i spektroskopii fotoelektronów”

Acknowledgements

During my PhD studies and preparation of this Thesis I have experienced support from many People. I would like to take the opportunity to express my deepest gratitude to all of them for thir knowledge, advice and help. It is my pleasure to acknowledge:

- Prof. dr hab. Budkowski, my supervisor, who gave me the opportunity to work in the fascinating field of macromolecular nanofilms, for his scientific guidance and the inspiring discussions
- dr Panagiota Petrou, from N.C.S.R. 'Demokritos' in Athens, for sample preparation
- dr hab. eng. Andrzej Bernasik, from AGH-University of Science and Technology, for XPS measurements and help with data analysis and results interpretation
- dr Jakub Rysz, from Macromolecular Nanofilms Group, for discussions and his support in ToF-SIMS measurements
- My other colleagues from Macromolecular Nanofilms Group, especially, dr Joanna Raczkowska, dr Joanna Zemła and M.Sc. eng. Mateusz Marzec - for help, cooperation and the pleasant working atmosphere in the group.
- My wife and parents for patience and great support in good and bad times

I acknowledge that during the work on my thesis I have been a scholarship fellow of the "Doctus - Małopolski fundusz stypendialny dla doktorantów" project cofounded by EU funds within European Social Fund.

This work was supported by the EU funded project "PYTHIA" (FP7-ICT2-224030). The research was partly carried out with the equipment purchased thanks to the financial support of the European Regional Development Fund in the framework of the Polish Innovation Economy Operational Program (contract No. POIG.02.01.00-12-023/08).